Applications of a Nonlinear Wing Planform Design Program

by

B. Matthew Knapp

Submitted to the Department of Aeronautics and Astronautics
in partial fulfillment of the requirements for the degree of

Master of Science

at the

MASSACHUSETTS INSTITUTE OF TECHNOLOGY

August 1996

Author .....
Department of Aeronautics and Astronautics
August 9, 1996

Certified by .....
Eugene E. Covert
T. Wilson Professor
Thesis Supervisor

Accepted by...
Jaime Peraire
Chairman, Department Graduate Committee

Applications of a Nonlinear Wing Planform Design Program

by

B. Matthew Knapp

Submitted to the Department of Aeronautics and Astronautics
on August 9, 1996, in partial fulfillment of the
requirements for the degree of
Master of Science

Abstract

The Wing Aero and Structures Program (WASP) uses a sequential quadratic solver to optimize the full wing and tail planform over a range of flight conditions. The program is able to adjust both the wing and tail geometry to find minimum weight and maximum range. This capability provides an opportunity to look at the effect of specific design variables not just on a local operating point, but on the full wing planform. An initial baseline design case was created from which trade studies were done on each of the six following parameters: airfoil C_{m_0}, the ratio of maximum allowable stresses in the upper and lower wing skins, spar box material density, viscous drag from skin roughness, wave drag, and cruise Mach number. These parameters were given a range of values and the full optimization procedure repeated. The final planforms were then compared for performance and wing planform geometry. The results often revealed more about the process of nonlinear wing planform optimization than about wing planform design. The data was less consistent than expected and on several occasions the optimizer followed a logical but unexpected path in configuration space. There was an interesting bifurcation in the optimization which would lead to two separate families of planforms. The cause of this bifurcation is not clear and will need more investigation. Also, the optimizer is prone to finding solutions which are logical but not desirable. Constraints can be used to force the proper result, but this approach is less desirable than building better physics into the models. With attention to constraints, and by providing a well posed problem to the optimizer, several of the trade studies were able to show interesting trends in both the geometry and the performance variables which would not normally be apparent from the standard fixed planform optimization approach. Thus, while the nonlinear optimization process continues to display the potential to be a very effective design tool, but it is also clear that a lot of work needs to be done on modeling the problem.

Thesis Supervisor: Eugene E. Covert
Title: T. Wilson Professor

Acknowledgments

This thesis is the final product of an Engineering Internship Program (EIP) with the Massachusetts Institute of Technology and the *BOEING* Aircraft company in Seattle, Washington. I would like to thank the people I worked with at *BOEING* for taking the time and interest to help out a summer intern. A big thanks to John Bussoletti for finding a good project and serving as my mentor in my second summer at *BOEING*. Many thanks to the High Speed Aero Research group under Wen-Hui Jou with whom I worked for the second half of 1995. Thanks very much to Doug McLean who served as my mentor for this project, and to Tim Purcell for assistance with UNIX, technical matters and good coffee.

Back on the East coast, a very large thank you to my advisor, Professor Eugene E. Covert, who is retiring as I finish up this endeavor. His wisdom and experience have been a saving grace on more than a few occasions. I will remember always that it is the physics that is fundamental – the numbers come later.

Last and hardly least, a big thank you to my parents and siblings for supporting me in my 5 year journey through the perils of MIT. Thanks to my smiling friends and Rosanna who have lent support and persuaded me not to jump off the dome, with or without a hang glider. And thanks most recently to Stacy with bb2k for support in the final countdown.

Contents

List of Figures

List of Tables

Introduction

The purpose of computing is insight, not numbers – R. Hamming

Aircraft wings are complex structures which need to be strong yet light, with low drag in cruise, yet able to fly slowly enough to land safely. The design of an optimum wing is inevitably a set of compromises. This problem would seem to be a prime candidate for computer optimization. However, there are two primary complications: planform optimization is a nonlinear problem, and constructing accurate but fast models for the optimizer is very difficult.

For a fixed planform, the approach to optimizing planform variables such as twist distribution, is linear and relatively fast. However, once the optimizer is allowed to vary the wing planform by modifying span, sweep, aspect ratio, the problem becomes nonlinear. While several nonlinear optimization algorithms exist, the mathematics are considerably more difficult than simple linear analysis. This thesis is based on the Wing Aero and Structures Program (WASP)[1] written at Stanford. The optimizer chosen for the code is Sequential Quadratic Programming (SQP) which attempts to strike a balance between speed and stability.[1]

The second problem is that a detailed computer model of any one aspect of wing design can take hours or sometimes even days to run a single simulation. During an optimization run, these models may be called several thousand times before finding a satisfactory optimum. In order to obtain a run time of less than a week, only simple models for the aerodynamics and the structure of the wing may be used. Short turn around time is especially important because a code run is never perfect. Variables need scaling, minimum step sizes need adjusting, initial guesses need improvement, constraints need adjusting, and so even a full planform optimization code is still an iterative process.

Thus the models need to be fast, but at the same time, they must be able to accurately model the physics involved with the large number of design variables which affect the optimum design point. Of course, the optimizer knows nothing of airplanes and the optimum is simply wherever the optimizer finds the best "performance" out of these models. If the models have holes or don't accurately reflect the physical processes involved, the optimizer will happily exploit these weaknesses and produce a completely unrealistic wing. Constraints may be applied to keep the optimizer from straying too far off track, but too many constraints limit the ability of the optimizer to find any sensible minimum.

Despite all the drawbacks, the process of multidisciplinary optimization of a full wing planform is an intriguing one which promises to offer new insight into the planform optimization problem. At the current time, the WASP program is the most comprehensive single code written with the intent of optimizing the entire wing and tail planform in one big whack. Simple aero and structural models are combined with a gradient based optimizer which satisfies constraints over a combination of up to 14 flight conditions while searching for a minimum, usually either minimum weight or maximum $\frac{C_L}{C_D}$. Available design variables include the quarter chord sweep, wingspan, incidence angles, tail moment arm, and thickness distribution among others. The aero model is based on a simple lifting line method with enhancements to add in high lift, viscous and wave drag effects. The structural model

[1] A commercial version of the quadratic optimizer called NPSOL and marketed by Stanford is commonly used by industry for nonlinear optimization problems. The WASP version of the optimizer was written with the same algorithms but modified convergence criteria [1, A.5]

was based on a single cell beam which was sized according the the worst case of bending stress or buckling. There were also enhancements to find leading and trailing edge weights.

The initial work on this code was done during an internship at the *BOEING* Company. Naturally, *BOEING* was only interested in the code if it could first duplicate their current deign codes and methodologies. Thus, the focus of the work during that period was an attempt to modify the existing structural and aerodynamic models in order to get better agreement with *BOEING* codes. Chapters 1 and 2 will describe in detail the code models and the modification made, in particular to the structural model.

BOEING was also interested as to whether the code could be sufficiently modified from an "academia in-house code" to a production engineering code. The "user interface" for the code is somewhat cryptic, but much more of a problem for trying to package the code for general consumption is the actual optimization process. Unlike linear optimization algorithms which either converge or don't, nonlinear algorithms have a large nebulous zone in the middle. As will be explained in 1.3, the way a nonlinear optimizer deals with design variables and constraints is quite different from a conventional optimizer. Also, the choice of design variables, variable scaling, and minimum variable step size become critical to finding a good optimization path. The result is that it is not possible to simply plug in a starting planform and set of desired flight conditions and turn on the optimizer. Many code runs and re-runs are required to find the correct weights, scalings and combination of design variables and constraints to finally produce a well converged result. To even approach "packaged code" status for design engineering would require large amounts of pre and post-processing routines to prompt the user, and the results would still be quite questionable if the user was not familiar with the optimization process.

This thesis is based on applications of the modified WASP code (using the modifications done for *BOEING*). A solid baseline optimization case was set up and tested to a satisfactory convergence. This case was then used as the starting point for a series of trade studies on various aerodynamic parameters such as the airfoil C_{m_0}, and the mach drag rise point of the foil (wave drag). These parameters were given a range of values around the baseline value and then the full optimization procedure (a total of 6 passes at the optimizer) is run again.The set of final planforms were then analyzed to look at the quantitative and qualitative effect that parameter had on the optimized planform. Also of interest was the sensitivity of the design to the tested parameter.

Chapter 1 will present an overview of the code, SQP optimization, the code models, the flight conditions used during optimization, and a discussion of the code's assumptions and limitations. Chapter 2 goes into detail on the new structural model. Chapter 3 will discuss the step by step optimization procedure, the design variables, used, and the importance of variable scaling. Chapter 4 presents a detailed description of the optimization of the baseline case starting from a generic "initial guess" wing planform. Chapter 5 will discuss the trade studies done for the thesis, the parameters varied, why the parameters were chosen and any code related problems with those parameters. Chapter 6 will present the results of the trade studies, and chapter 7 has the conclusions and recommendations.

Nomenclature

Note: Abbreviations for coefficients such as $C_D$and $C_d$follow the convention that a capital subscript indicates a three-dimensional flow coefficient while the lower case subscript indicates that the coefficient is for two-dimensional flow.

α	wing angle of attack in degrees from zero lift line
δ	horizontal tail angle of attack in degrees from zero lift line
C_D	coefficient of drag (planform)
C_{D_i}	inviscid drag coefficient
$C_{D_{tot}}$	total coefficient of drag (includes all contributions from viscous, inviscid and compressible drag)
C_{D_v}	viscous drag coefficient
C_{D_c}	compressible drag coefficient
C_d	section drag coefficient
C_f	flat plate turbulent coefficient of skin friction
C_L	coefficient of lift (planform)
$\frac{C_L}{C_D}$	lift to drag ratio
C_l	section lift coefficient
$\overline{C_l}$	non-dimensional section lift coefficient (see equation 4.1 for the definition)
C_{m_0}	airfoil section zero lift coefficient of pitching moment
C_m	section coefficient of pitching moment
$C_{m_\perp}$	section coefficient of pitching moment perpendicular to the sweep axis of the wing
$c_{l_{max}}$	Maximum section coefficient of lift
I_{xx}	area moment of inertia around x axis
I_{xz}	cross area moment of inertia, x and z axis
I_{zz}	area moment of inertia around z axis
K_{cf}	flat plate $C_f$multiplicative factor to account for surface roughness
M_∞	free stream Mach number
M_{cc}	Mach number at the thickest portion of the airfoil, the "crest critical Mach number"
R_e	Reynolds number
σ_y	Skin stress in Pa, y direction (along the wing span from bending loads)
$\frac{t}{c}$	airfoil geometry thickness to chord ratio
$\frac{x}{c}$	airfoil geometry, percentage chord

Chapter 1

Code Description and Overview

This Chapter will present an overview of the wing planform design problem and the "Wing and Aero Structures Program" (WASP) used for this thesis. Practical and theoretical aspects of the code will be discussed including, the optimization algorithm, the physical models, and the flight conditions used for optimization. The chapter closes with a discussion of the potential capabilities and limitations of the code.

1.1 Problem Definition

As was stated in the introduction, optimization of an aircraft planform is inevitably a set of compromises. There are a large number of design variables and an even larger number of constraints. The conventional method for design optimization is to pick one of these design variables and leave all others constant. The "independent variable" is tested over a range of values with the goal of finding a curve showing an optimum point. While each variable is being tested, all other variables are left fixed so as the isolate the effects of the independent variable. This approach has the benefit of being very controlled with a clear input and output. However, the method shows several disadvantages when it comes time to apply these isolated studies towards a full planform. Once a set of parameters has been tested in this way, it is up to the designer to figure out how to combine all the optimum curves. Some of them will most likely conflict and so decisions must be made as to which parameter is compromised. The design is modified and the process repeated. However, since changing one parameter in a vacuum is generally not realistic, the modified design will not be an optimum either and so the whole cycle iterates until time, budgets and design engineers are exhausted.

The solution to this of course is to simply take the entire design process and throw it at a super robust optimizer which can handle modifying all the design variables simultaneously to track down the final optimum planform. To a certain extent, this is what the WASP program attempts to do. However, as was also mentioned in the introduction, this approach has problems with modeling the problem well enough to get a good solution without needing weeks of computation time. The WASP code contains very simple models; a box beam for the spar and a lifting line for the wing. These are enhanced with numerical routines to provide for some low speed handling and compressible drag effects.

1.2 Optimization Code Procedures

There are three major sections to an optimization code: The optimizer, the physical models and the operating conditions. A short summary of each follows:

The Optimizer uses a set of design variables to create a "design space" which is an n-dimensional map of the second derivatives of the goal with respect to each design variable. The optimizer takes steps in the direction of the steepest gradient until reaching a minimum. Constraints can be imposed to block off parts of the design space and impose outside conditions on the optimization.

The Physical Models are the mathematical representation of what is being optimized. In this case, lift and induced drag are by simple lifting line, the structures model relies on basic cell beam theory, and both models are enhanced to account for other factors, such as wave drag, flap lift and drag.

The Operating Conditions attempt to define the full envelope of performance demands on a wing and tail planform. Take off, climb out, cruise, maximum maneuvering load and other flight conditions are all applied to the design. Thus, while the optimizer may be attempting to minimize cruise drag, these conditions ensure that the wing will also be strong enough to maneuver, big enough to take off at a low velocity and otherwise satisfy all desired corners of the flight envelope.

Each of these sections can be written as a more or less independent code. To combine the three into a functional optimization routine requires one more section which controls what conditions and models are evaluated when and how this information is passed along to the optimizer. The next section explains the difference between "internal iteration" and "optimizer directed iteration" and presents an outline of the overall flow process through the code.

1.2.1 Code Flow Overview: Internal and Optimizer Directed Iteration

Optimization is a fundamentally iterative process. As the code starts, the existing condition is some starting guess, usually with constraints violated and lousy performance. Figure 1-1 shows an example of a starting planform with the elements and panels labeled. After an iteration the optimization process becomes a steady repetition of the following cycle:

1. Calculate the performance of the current planform at all required flight conditions
2. Find an optimization path based on improvement of performance and resolution of violated constraints.
3. Take a "step" in this direction. This is accomplished by the optimizer picking new values for all of the design variables
4. If a step can not be found, check for convergence. If converged, exit. Otherwise repeat from step 1.

This is the outer optimization loop. Nested inside this loop can be numerous small iteration loops related to skin sizing, aerodynamic influence coefficients etc. The problem with these internal loops is that they also converge to some tolerance, with a convergence

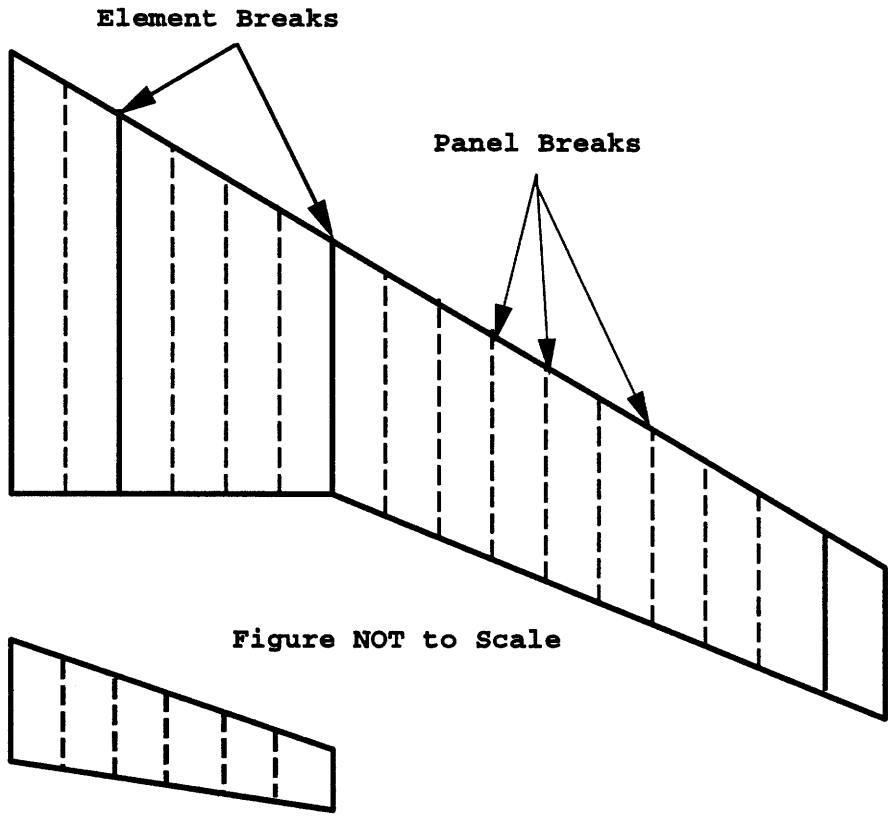

Figure 1-1: Sample starting planform with elements and panels labeled

derivative which can be significant and so are a considerable source of noise in the larger iteration scheme.[1, 3.3]

An alternative to nested iteration loops is to simply remove them. This is done by taking the variables from the internal loops and making them design variables which are then calculated in the outer optimization loop (optimizer directed iteration). This does remove the noise problem, but applying this approach to too much of the code would mean a large number of design variables and an even larger number of constraints. After some experimentation, it was found that the best approach was to make the structural design variables optimizer directed and leave the other internal loops [1, 3.3.2]. This leads to the introduction of an end load design variable for the root and tip of each element, where the end load is defined as: σt_s where σ is skin stress and t_s is the smeared skin gauge. Figure 1-2 shows a diagram of the overall code flow, and section 1.4.2 will detail the optimizer directed structural design process.

1.3 Fundamentals of Sequential Quadratic Programming

As with any optimization, the goal is to pose a problem which consists of a parameter to minimize, a set of design variables which will affect the minimization goal, and, if necessary, a set of constraints on the design variables. For example, a very simple optimization would be for minimum wing weight with a fixed planform. The optimizer would be allowed to adjust twist distribution, wing α and tail δ and the wing skin endloads (structural design variables which will be explained in section 1.4.2).

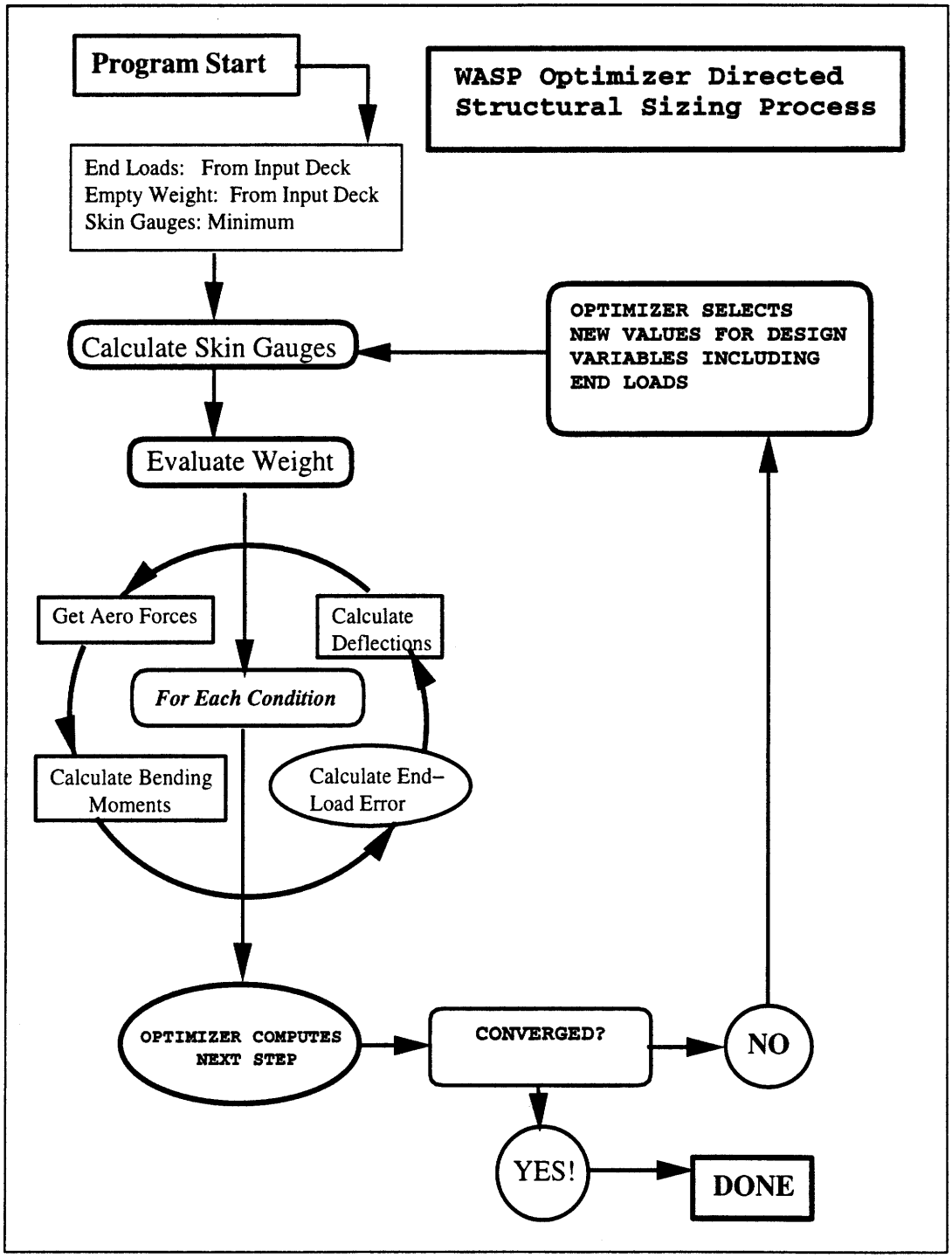

Figure 1-2: WASP Structural Sizing Flow Chart

Constraints could be placed on the maximum and minimum wing twist values as well as maximum allowable endloads. Other constraints to consider would be minimum skin thickness, maximum allowable deflection etc. The optimizer then takes the second order derivatives of the goal with respect to these design variables and constructs a design space. This space can be viewed as an "n-dimensional" topography in which the optimizer is searching for a local minimum. The constraints effectively serve to put boundaries on sections of the design space, or, to force the optimizer to find an optimum on the path of a specific constraint (for example: minimum weight for $C_L = 0.4$).

Important Note: A linear optimization will first satisfy all the constraints, and then optimize within these constraints. Thus, even a non-converged solution could still be within the constraint bounds. However, with non-linear optimization, the optimizer will work on improving the most active constraint while moving towards the goal. In the process, the optimizer will make sure that any other active constraints don't get worse, but won't actually work to improve the other constraints until they in turn become most active. Thus, if the optimizer hasn't found a fully converged solution there are probably several active constraints remaining.

1.3.1 SQP Specifics and Procedure

This section is distilled down from [1, Chapter 3]. The basic elements in the optimization are the matrix of constraints, matrix of design variables, Hessian matrix, and the Lagrange multipliers. The Hessian is an approximate second derivative matrix based on information computed over the course of several iterations. The second derivative of the goal with respect to the design variables forms a gradient design space which the optimizer will use to find a step towards the local minimum. (Note: this means that the design variables *must* be second order smooth.) The optimization then proceeds in this sequence:

1. Initialize Hessian to identity matrix, compute the objective and the constraints from the current location.

2. Find a step to satisfy constraints

3. Use the SQP methods to find a step direction towards the goal

4. Execute a line search in this direction in order to minimize a merit function.

5. Depending on the success of the line search algorithm the code will now either re-set the Hessian and start from step 2, or continue by calculating the difference gradients.

6. Update the Hessian. If the new approximation is not positive definite, reset the matrix to the I matrix. If the matrix is positive definite but doesn't pass a more strict check, the updates are bypassed. The newly calculated point now becomes the current location.

7. When the optimizer can no longer find improvement, check for convergence and exit if converged.

The merit function checks the relative improvement in satisfying constraints through a summation of Lagrange multipliers, constraints at the present location and constraints at the projected location. See [1, section A.7] for details.

Convergence is checked for with the following formula:

$$\begin{bmatrix} I & A_{act}^T \\ A_{act} & 0 \end{bmatrix} \begin{Bmatrix} p \\ \lambda \end{Bmatrix} = \begin{Bmatrix} -g \\ c_{act} - c \end{Bmatrix} \tag{1.1}$$

Where A_{act} are the gradient constraints in the working step, λ are the Lagrange multipliers, I is the identity matrix, p is the step vector, g is the objective gradient and c and c_{act} are vectors of working constraints. Since the optimizer is required to set the Hessian to the I matrix before checking for convergence, the I takes the place of the approximate Hessian. The Kuhn-Tucker conditions for convergence are:

$$-p = g + A_{act}^T \lambda \tag{1.2}$$

Which means that ideally at convergence the Lagrange multipliers are 0 and there are no more steps indicating that the minimum has been found.

1.3.2 Optimizer Design Space and Variable Scaling

The quadratic optimizer works by constructing a "design space" which is an n-dimensional surface composed of the second derivatives of the goal with respect to the design variables. In order for this approach to yield good results, all variables in the design space need to be scaled to be of order 1. If the variable slope is to small, the optimizer will have difficulty in finding a step on the shallow gradient. If the variable slope is too large, the steep slope will obscure other variables and alter the step direction. For a variable which directly affects the goal, this scaling should be calculated from the second order derivative. For the indirect variables, which are variables which do not directly affect the goal but which influence constraints, the scaling is a bit more complicated and needs to be done with the Lagrange multipliers. [1, p 69].

The constraints also have a scale factor, however this factor is much less critical than the design variable scaling. In this case, the scaling acts more like a weighting factor increasing or decreasing the penalty for violating that particular constraint.

The importance of the design variable scalings and step sizes can not be over emphasized. On a full optimization run there are 50 to 60 design variables and on the order of 600 constraints. Very rarely does the optimizer actually find a fully converged solution. Much more often the final solution is when the optimizer can not find another search direction and quits. If the error is small enough at this point, the code is called done. One of the factors output at this point is which particular design variable could not be improved. By modifying the scaling and or step size of this variable and re-running the last stage of optimization, the solution will often advance several more steps which can lead to significant changes in wing weight and less significant changes in the wing span, sweep etc.

1.4 Original Code Models

The primary physical models are the structural model for wing weight calculation and the aerodynamic model which uses lifting line and Treffetz plane to calculate the primary lift and drag. A full airplane wing consists of considerably more than a spar box and a set of horseshoe vortices. However for a lot of the calculations, these simple models will adequately represent the physics of the problem. The structural model can be enhanced with

multiplicative factors to take into account "other weight" such as high lift systems, access hatches etc. Much more difficult to model and not included in the code is additional weight necessary to eliminate flutter. A simple aerodynamic model is only a valid approximation to a wing at cruise, and the validity of lifting line on highly swept wings is also questionable. The code needs to account for wave drag, flap and slat drag, flap and slat lift, and viscous drag so these are patched in with empirical functions which are sometimes built into the code and sometimes user input.

1.4.1 Original Structural Model

The structural model was changed significantly from the original WASP code. This section will give a summary of the original model and the problems found. The next section will summarize the changes made and chapter 2 will go into detail on the new structural model. For a complete description of the original structural model, see [1, sections 2.2,2.3].

1.4.1.1 Model Assumptions

The WASP code is meant to size just about everything on the wing including $\frac{t}{c}$, chord, dihedral and sweep. If all of these variables were treated independently, the code would gain significant complexity in variable storage and handling. A better approach for this level of design is to find a way to scale and modify a basic wing cross section over the full length of the wing. This approach requires several major assumptions:

1. There is only one generic airfoil cross section
2. The upper and lower skins of the spar box can be represented by parabolas fit to three points which were supplied by the user.
3. The smeared skin gauge is constant around the foil so that once the inertial properties, I_{xx}, I_{zz}, $I_{xz}$are calculated, they can also be scaled to the local $\frac{t}{c}$and chord.
4. This airfoil can then be scaled to fit local $\frac{t}{c}$and chord.
5. The maximum or minimum z coordinate with reference to the z centroid is the location of maximum stress and sizes the wing skins.

The assumption that there is only one foil cross section for the entire wing is not valid aerodynamically, but from a structural standpoint, the variations in the actual spar box dimensions can be kept quite consistent along the wing so this approach is reasonable. Likewise, the skins over the length of the spar box are relatively flat so a parabolic approximation is reasonable. Carefully picking which three coordinates the curve will be fit on can help improve this approximation.

The constant smeared skin gauge all the way around the spar box is *not* a valid assumption. In almost all cases, the spar box is sized by bending, and bending is driven by I_{xx}so that the upper and lower skins offer most of the resistance to bending in the vertical plane, while the front and rear spar make almost no contribution (in this direction). Thus, a spar box with this assumption will end up significantly heavier than necessary. See section 2.2 for a description of the fix applied to this problem.

From an aerodynamic standpoint, supercritical foils do not scale simply with $\frac{t}{c}$. Instead, the airfoil is changed to match scaled pressure distributions. However, the code is already

assuming a single airfoil cross section and so the geometry behind scaling the structural properties can be worked out. This can actually be a bit tricky and and is derived in appendix B.

1.4.2 Skin Sizing by Optimizer Directed Iteration

Bending, Shear and Torsion moments are all calculated along the length of the wing. The skins are then sized to by the most critical of these loads. At this point the integration with the optimizer starts to become apparent. As was briefly mentioned in 1.2.1, the skin sizing problem has been placed in control of the main optimization loop. The function takes the current end loads from the optimizer and sizes the skin gauges to withstand the load simply by constraining the calculated structural end load to be less than the applied end load. There are two end loads for each element, one for the root and one for the tip. These are design variables which are always necessary when the optimizer is sizing the structure. The optimizer directed iteration makes the skin sizing process proceed as follows:

1. Initialize the skin to minimum gauge
2. Calculate foil properties (I_{xx}etc.)
3. Call the function to size the skin gauges and then calculate the resulting wing weight.
4. Call the aerodynamic models to calculate the lift and drag forces
5. find the resulting bending moments
6. Use the bending moments to find the actual end loads on each element.
7. compare these end loads to the end loads the skins were sized with in step 3
8. Use constraints to force the optimizer end loads to be greater than the actual calculated end loads
9. Based on the violated constraints, the optimizer picks a new set of end loads.
10. repeat

This is diagrammed in figure 1-2. This approach to skin sizing works quite well most of the time but will occasionally produce very heavy wings. Constraints are applied to make sure the optimizer end loads exceed the actual end loads which keeps the wing from failing. However, making a structure twice as strong as necessary will satisfy the constrains just fine while carrying around a lot of extra weight. The optimizer is quicker to satisfy constraints than to shave off weight. Constraining the end loads to be very close to the actual end loads (not just greater than) will make for very shallow gradients in optimization space and the optimizer will have difficulty finding a search path. The result is that the wing will sometimes end up with some extra structure, especially in regions of discontinuity (sweep or taper change).

In the original MassEval function the skin gauges are calculated using a number of buckling equations which had been solved for skin gauge. The optimizer end loads were used in the calculation and the resulting skin gauge was then multiplied by the scaled unit area of the spar box and the panel width to get the volume of Al for that panel, and hence the weight. [1, sections 2.3.5 – 2.3.8] explains the assumptions, and equations used for the

skin thickness sizing. This set of criteria almost always defaulted to the bending load as the most critical. For that matter, since the spar box had assumed constant smeared gauge on all sides the code would be unable to re-size the shear webs to resolve a torsional wing sizing problem. This approach would generally find a reasonable[1] skin thickness. However, applying the same thickness to the entire spar box would result in a total spar box weight several times higher than necessary. Chapter 2 will give a detailed discussion of the new weight model implemented to solve this problem.

1.4.3 Other Structural Parameters

The code calculates a Structural Influence Coefficient matrix for bending and twist, and also takes into account aeroelastic effects. These models were given a standard *BOEING*planform as a validation test. The aeroelastic effects came out quite well, however the wing deflections under load were about $\frac{1}{3}$ of the *BOEING*deflections. The routines which did these calculations were not changed so this holds true for all cases done in this thesis.

1.4.4 Weight Calculation

There are three major components to aircraft weight: Structural weight, fuel weight and all other weights.

Structural weight This is the weight calculated from the wing and spar boxes when sized to meet all structural design loads. Using the new weight method, the spar box structure is modeled as four skins with parabolic upper and lower skins and vertical webs. The webs stay at a pre-set thickness, while the optimizer varies the upper and lower skins to meet design loads. The effect of stringers is incorporated into the wing by using a "smeared skin gauge" which is the average thickness of the skin and stringers combined.

Fuel weight The fuel weight is the difference between the Maximum take off weight and the maximum zero fuel weight. Both of these parameters are user entered and are constant. Thus the fuel mass is constant and the optimizer will have to design a wing to contain the desired fuel volume. The relevant variable here measures the fraction of total available fuel volume actually occupied by fuel. This is constrained to ≤ 1.

Other Weights There are actually 3 sub-categories of this section, calculated, scaled and flat weight. The only calculated weights were the leading and trailing edges which were sized to withstand a fixed pressure load [1, Section 2.3.7]. These weights were not considered necessary for the purpose of this study and the pressure loads were left constant for all cases.

The scaled weights were simply empirical factors multiplied by the wing area to get various add-on weights such as inspection hatches, rib to spar joint weights etc. These factors only add an offset to the final weight and do not affect the design in any way.

Flat weights are simply for anything else the user wants accounted for in the total weight. Major items include landing gear and fuselage, both of which were set to zero. If the engines were on the wings, the code did have provisions for attaching a fixed

[1] "Reasonable" as defined by comparing the output of WASP with *BOEING*preliminary design codes. The actual numbers are proprietary

mass on a specific wing panel to simulate the engine. The effects of engine thrust on wing structure would not be included.

1.4.5 The Aerodynamic Model

The aero model is a simplified version of LINAIR, which is a vortex lattice code written by Professor Ilan Kroo.[2] In WASP, a single lifting line at the quarter chord is used for lift calculation with induced drag calculated in the Treffetz plane. This code does model the full wing to allow for asymmetric effects of aileron deflection. However, there is no correction for a fuselage and lift is assumed continuous across the center of the wing. Another problem is that the panel widths in WASP tend to be quite large, on the order of 1 meter in width. This makes it very difficult for the code to accurately model the lift towards the wing tip where the lift distribution is changing very quickly.

1.4.6 Drag Calculations

The original code had three options for calculating C_{D_v} and a fourth was added for use at *BOEING*. These applied during cruise and additional corrections are necessary when using the high lift devices for take off and landing as will be briefly explained in section 1.4.7.

The standard method for finding C_{D_v} is to use the local R_e number to calculate the flat plate turbulent skin friction coefficient (C_f).

$$C_f = K_{cf} \frac{0.455}{(log_{10} R_e)^{2.584}} \tag{1.3}$$

where K_{cf} is a multiplicative constant to account for "surface roughness". This was set to 1.0 for most code runs. The other two methods depend on user inputs. The first asks the user for an array of C_f values to use instead of calculated values. The second asks the user for the first and second order coefficients for a $C_l - C_d$ drag polar.

To increase the accuracy of finding both C_{D_v} and C_{D_c}, the ability to reference user input drag polars was added. The user enters as many polars as desired along the wing span. The code then interpolates and scales the polars to local $\frac{t}{c}$ as described in appendix B. During aero model evaluation, the code scales the polars to account for local sweep and Mach number. Polars from a generic *BOEING* airfoil[3] for a small transport were used for most of the code runs done in this thesis.

The rest of the parasite drag for the aircraft (nacelles, fuselage, etc.) is accounted for with the user input f_{fus} parameter, which is an equivalent drag area. This scales as:

$$C_{D_{fus}} = \frac{f_{fus}}{S_{ref}} (1 + 0.38 C_L^2)$$

Where the 0.38 is a purely empirical correlation, again for a small transport[1, page 44]. *NOTE:* For this thesis, the $C_{D_{fus}}$ was left at zero.

[2] Professor Ilan Kroo teaches Aeronautics at Stanford University and was the thesis advisor for the WASP program

[3] the actual polars are proprietary

1.4.6.1 Wave Drag

The Wave Drag model uses the Shevell Crest Critical Mach Number, M_{cc} method[1, section 2.4]. This method determines the minimum Mach at which supersonic flow would occur at the thickest point of the foil:

$$M_{separation} = [known\ value] \geq \frac{M}{M_{cc} + M_{cc_{offset}}} \tag{1.4}$$

Simple sweep is then used to correct $M_\infty$to $M_\perp$. The M_{cc} is a function of $\frac{t}{c}$and C_L. Drag is found from an empirical correlation [1, figure 2.16]. The attractive part of this model is that it is quick and changes with $\frac{t}{c}$so that the optimizer will have to balance $\frac{t}{c}$based on drag and weight. However, in validation tests, the drag tended to be excessively high.

1.4.7 High Lift Devices

A lifting line model does not predict stall behavior or separation drag, therefore the aerodynamic model needs a set of adjustments to handle the effects of the high lift devices during take-off and landing. The code needs to be able to predict the wing stall speed, stall α, maximum lift clean wing, and maximum lift with high lift devices.

Clean Wing Stall Is found from the lifting line model and the user input $C_{L_{max}}$ for each element. When any one panel is determined to be at $C_{L_{max}}$, the wing is stalled

Lift From Flaps and Slats As explained in [1, section 2.5.2], the extra lift and increased $C_{L_{max}}$ from the flaps is calculated using $C_L$increments multiplied by the flap deflection angle. The actual maximum lift is found by calculating an equivalent panel incidence increment and adjusting the lifting line accordingly so that maximum lift and stall can be calculated as in the previous method. Lift from slats is also an empirical adjustment. [1, section 2.5.3]

Drag for the high lift devices is purely empirical. A drag increment is added to the total $C_D$for flaps and slats. The slat calculation is very simple - when the slat is down, add .006 to the total C_D. The flaps are very slightly more sophisticated with the drag increment depending on the flap deflection angle. [1, pp 47,48]

1.4.8 Flap Induced Flow Corrections

One item which is treated in some detail in the thesis is the application of an incidence correction to the panels which border panels which have flaps deployed. Since the flaps modify the incidence of the neighboring panels, and thus the stall α of those panels, the critical section approach to maximum lift could be in error if this effect is ignored. The computed correction depends on local geometry, C_l and a set of empirical correlations calculated in LINAIR (in full Vortex Lattice Mode) [1, pp 51–56].

1.5 Flight Conditions

There are a total of 14 available flight conditions which can be used for the planform optimization. Each condition has a number of attributes which can be set by the user. These include the options which should be calculated for that flight condition (high lift

drag, compressible drag and other options), the operating conditions and some geometry factors. For example, at the take off condition, the altitude, velocity, load factor, slat and flap deflections, slat $C_L$increments, and aileron deflections can all be specified with the options including "calculate high lift drag and proximity to stall". The take off condition also has pre-defined attributes in the code regarding the need for the elevator to rotate the fully loaded aircraft to take off and trim to climb out etc.

Definitions: MTOW = Maximum Take Off Weight and MZFW = Minimum Zero Fuel Weight.

1.5.1 Structural Conditions

There are a total of six structural conditions. Usually the critical structural condition is the high load maneuver at MTOW. The abbreviation after each condition is the reference label used for that condition in the code.

1. Cruise at MTOW, aft CG (Cr)
2. Vertical Gust, forward CG, MZFW (Gt)
3. Horizontal Gust, forward CG, MZFW (Sd)
4. Maneuvering Condition forward CG, MZFW (Mn)
5. Maneuvering Condition forward CG, MTOW (Mf)
6. Another Cruise Condition at forward CG, MZFW (St)

1.5.2 Tail Sizing Conditions

The tail planform is designed simultaneously with the wing, which requires an additional series of flight conditions. Generally the tail will turn out much too small unless the optimizer has to meet requirements for maximum tail pitch authority. The conditions used primarily to size the tail and elevator are:

1. Take-off rotation, forward CG, MTOW (TO)
2. Landing Approach mis-trim. Condition assumes flaps down, 1.8 V_{stall}, stabilizer trim set for approach, and elevator only can be used to trim the aircraft. (sizes the elevator) (FM)

Some of the other high lift conditions in the next section may also influence horizontal tail sizing.

1.5.3 High Lift Conditions

In order to size the wing properly for take off and landing several high lift conditions can be specified along with the desired flap and slat settings and speeds to try to fly.

1. Take-off Rotation (see previous section)
2. Take-off Maximum lift forward CG, MTOW, check stall speed (HL)
3. Take-off climb, forward CG, MTOW, 1.3 V_{stall} from previous condition (HC)

4. Landing maximum lift, forward CG, MZFW, calculate landing stall speed (FD)

5. Landing approach, forward CG, MZFW, 1.3 V_{stall} (from FD), sets trim setting for the FM condition. (FA)

1.5.4 Other Conditions

The weight model includes the effects of inertial bending relief that wing fuel tanks supplies. The optimizer found it could take advantage of this by moving fuel outboard to the extent of trying to create tip tanks. To penalize this approach, a Taxi Bump (Tx) condition was added which is some load imposed with zero airspeed so the wing has to take the mass imposed bending moments.

The last condition, which is not critical to overall planform design, is the Rolling Moment Check (HR). This condition is used to size the ailerons, usually to meet the maximum hinge torque constraint. One visible effect of including this option is that the outboard wing trailing edge will have a reduced sweep in order to get the aileron hinge line closer to being perpendicular to freestream.

1.6 Code Assumptions and Limitations

The code was written for optimizing planforms for mid-sized subsonic commercial transports and should be applicable to aircraft in the 100-300 passenger range. Larger of smaller aircraft have changes in construction methodology which reduce the accuracy of the weight analysis.

The simple lifting line will not tolerate sharp breaks in chord along the span or other unusual geometries. Furthermore, there are internal code limits to the total number of panels which can be set for the wing, somewhere in the range of 35. Since the paneling is fixed width instead of a cosine distribution, the errors introduced at the tips of long, high aspect ratio wings become considerable. Also, *the paneling in the tail must line up exactly with any panels in the wing which the tail overlaps* (due to the code methodology in LINAIR).

The empirical increments used for the flaps and slats are only good for a fairly generic set of flap and slat deflections so more efficient high lift systems would be unnecessarily penalized.

The crest critical mach number method produced excessively high drag values when run with a standard aft loaded, highly cusped supercritical airfoil. The M_{cc}offset can be used adjust this drag down to much more reasonable values but finding the exact required offset is difficult.

The code does not model a fuselage, account for loss of lift in fuselage carry-over fashion or account for vortex drag at the fuselage-wing intersection. These parameters are sensitive to flight velocity and would affect planform outcome.

The use of drag polars allows a much more accurate drag assessment, but this is only good provided that the optimized planform has ended up quite close to the design the polars were originally meant for. Designs which stray too far from the original foil size and operating point will probably leave the valid range of the polar.

Chapter 2

Modifications to the WASP Code

Several modifications were made to the WASP code while working at *BOEING*. The addition of drag polars to the list of methods for calculating C_{D_v} and C_{D_c} was a simple addition to the capabilities of the code. A correction was made to how the code handles the section C_{m_0}. Major modifications were made to the skin thickness calculation part of the structural model.

2.1 Pitching Moment Correction

During code evaluation trials at *BOEING*, the tail span loading profile was consistently incorrect even though the wing spanload was reasonably accurate. In [1, B.2] there is a lengthy discussion of how to handle the section pitching moments. The section describes two derivations for C_{m_0}, one for a "swept wing" and the other for a "sheared wing". The results of the derivation are that the "swept" case corrects with $cos^3\lambda$ while the "sheared" case corrects with a $cos\lambda$ (where λ is the local quarter chord sweep). According to comments in the code, this correction was intended to be applied to a C_{m_0} from a streamwise foil section.

Most C_{m_0} data available is from MSES[1] or similar programs and is $C_{m_\perp}$. The following equations are from Doug McLean [7] and are used in a pre-processing program that modifies the MSES $C_{m_\perp}$ to be a streamwise C_{m_0}.

Definitions:

$$\begin{aligned} V &= \texttt{Freestream Velocity Vector} \\ c &= \texttt{freestream chord} \\ q &= \texttt{freestream dynamic pressure} \end{aligned} \tag{2.1}$$

Basic Conversions: to convert each of the above freestream values to the equivalent vector perpendicular to the quarter chord:

$$\begin{aligned} V_\perp &= V\cos\lambda \\ c_\perp &= c\cos\lambda \end{aligned}$$

[1]MSES is a multi-element airfoil design optimization and analysis code written by Professor Drela at MIT

$$q_\perp = q\cos^2\lambda \tag{2.2}$$

C_{m_0}Definition For the quarter chord pitching moment:

$$C_{m_{\frac{c}{4}}} = \frac{M_{\frac{c}{4}}}{qSc} \tag{2.3}$$

Using the above relations, the conversion is simply:

$$\begin{aligned} C_{m_{\frac{c}{4}_\perp}} &= \frac{M_{\frac{c}{4}_\perp}}{q_\perp S c_\perp} \\ &= \frac{M_{\frac{c}{4}}\cos\lambda}{q\cos^2\lambda Sc(\cos\lambda)} \\ &= \frac{C_{m_{\frac{c}{4}}}}{\cos^2\lambda} \end{aligned} \tag{2.4}$$

And since the input data is the $C_{m_\perp}$:

$$C_{m_{\frac{c}{4}}} = C_{m_{\frac{c}{4}_\perp}}\cos^2\lambda \tag{2.5}$$

and

$$M = C_{m_{\frac{c}{4}_\perp}}\cos^2\lambda qSc \tag{2.6}$$

Which is obvious on inspection since $C_{m_{\frac{c}{4}_\perp}} = \frac{C_{m_{\frac{c}{4}}}}{\cos^2\lambda}$ and substituting this back into equation 2.6 simply gives: $M = C_m qSc$ which is correct by definition.

From [1, Section B.2] :

$$M = q\cos\lambda C_{m_\perp} c_\perp S + q\cos^2\lambda C_{l_\perp}\frac{b\tan\lambda}{2}S \tag{2.7}$$

The second half of the term is from the integration of the pitching moment across the span of the wing and can be re-derived. The first term is also the same once the $c_\perp$ is converted back to c, and again, on inspection, the first term reduces to the definition of C_m. However, there seems to have been a disconnect between this section and the actual coding. The code expects a streamwise C_{m_0} (according to comments in the code), and the chord was already streamwise, but the $\cos\lambda$ term stayed in anyway. The code was changed to use a $\cos^2\lambda$ correction and so the C_{m_0} in the input deck should be a $C_{m_\perp}$. This fix greatly improved the agreement of the horizontal tail loading.

2.2 Spar Box Skin Sizing and Weight Calculation

The previous chapter contained a discussion of the optimizer directed iteration and the original code model. As was discussed in section 1.4.1.1 the original model made several simplifying assumptions which significantly reduced the accuracy of the weight predictions. This new weight model was written using *BOEING* preliminary design code structural methods as a guide. The intention was both to provide a more realistic spar box structure and try to match the output of *BOEING* preliminary design codes.

A number of attempts were made to completely change the structural model. However, documentation on the code was very limited, as were time and resources. The initial attempts to replace the skin sizing routine met with severe optimization instabilities and were abandoned. Eventually a new method was patched together that would work with the panel end loads which were the already existing design variables. However, since the previous structural model had assumed a more or less symmetric spar box with even skin thickness distribution, there was only one set of end loads for each element. Since it was desirable to optimize the upper and lower skins independently, a brief attempt was made to double the number of skin end load design variables. This also meant doubling the number of constraints, which is a much larger number since there is one constraint for each panel. The attempt also ended in optimizer instability problems and was abandoned. The following procedure was finally adopted as being the best method that could be applied with the existing design variables.

2.2.1 Background Information

The codes this method is based on requires the maximum material stress, σ_y as a user input. The method works by calculating the actual stress in the foil at several points - usually the front and rear spars and the middle of the sparbox. The skin thickness is then corrected based on the ratio of actual to allowable stress and this process iterates until actual skin stress matches maximum skin stress. The maximum skin stresses are a user input parameter with one value for each element. In the WASP code the internal iteration has been removed so that for each time the optimizer calls the structural model, new skin gauges are calculated from the stress ratio and simply returned.

From Rivello [6, section 7.3] the governing set of equations for a box beam are:

$$\sigma_{yy} = \frac{P}{A} - \frac{M_z I_{xx} - M_x I_{xz}}{I_{xx} I_{zz} - I_{xz}^2} x - \frac{M_x I_{zz} - M_z I_{xz}}{I_{xx} I_{zz} - I_{xz}^2} z \tag{2.8}$$

The $\frac{P}{A}$ term is for loads along the axis of the beam (loading a beam in compression) and is zero in this case.

2.2.1.1 Compression and Tension Allowables

There is an added complication to this method which is due to the fact that the maximum compression stress allowable in a material is a function of end load. The maximum stress under tension does not change with end load so these values can be entered in a short array in the input deck. However, a table of compression allowable vs. end load must be supplied for the calculation of skin thicknesses for surfaces in compression. The code will interpolate the maximum compression allowable from the existing end load. In case the end load falls above or below the limits of the table, the maximum value will be used. There is no extrapolation.

There was also insufficient time to tie in a torsional sizing model to calculate the thicknesses of the front and rear spar webs. Instead of assuming a constant thickness these values have also been made a user input parameter. The web thicknesses used for this thesis were approximated from a similar sized transport wing[9].

2.3 Skin Gauge Sizing by Stress Ratio

Since this method works with only one set of end loads for each element, a relationship must be found between the upper and lower skins as compared to the stresses in the upper and lower skins. The following method depends heavily on one assumption: *the ratio of maximum stress in the upper skin compared to the lower skin, $\frac{\sigma_{max_u}}{\sigma_{max_l}}$ is specified for all points on the wing.* Also necessary as input is the the maximum allowable upper skin stress in compression and tension as described in the preceding section.

The concept of using a ratio of upper to lower skin stresses is based on a study done at *BOEING*. The primary objective was to find methods for comparing the structural effectiveness of airfoil spar box shapes. Airfoil shapes can vary widely around a spar box of similar strength but vastly different weights depending on the efficiency of the box. One parameter investigated in the study was the relationship between the maximum stresses in the upper and lower skins and whether it was preferable to have both skins at maximum stress, only one maximally stressed etc. The upper skin tends to have less curvature, is loaded in compression and subjected to less curvature change than the lower skin. The lower skin needs a higher tensile strength and undergoes a substantial amount deformation in flight as the wing bends, and so needs good low cycle fatigue qualities. In practice, this means that the "7-series" of aluminum alloys are used on the upper surface and the "2-series" on the lower surface. The 7-series is considerably better in strength to weight compared to the 2-series, even when comparing tension in the 2-series with compression in the 3-series. Thus, for the standard *BOEING* wing the result turned out to be

$$Stress\ Ratio = \frac{\sigma_{u_c}}{\sigma_{l_t}} = 1.36$$

where σ_{u_c} is compression yield on the upper skin and σ_{l_t} is ultimate tensile on the lower skin.[4] NOTE: This methodology is based at the mid-span of the wing where upper surface buckling is not a failure mode so that the normal compression yield strength of the material is used. This will tend to find lighter than actual wings out at the wing tips, but a minimum gauge can be specified to help avoid this problem.

The basic methodology works as follows:

1. Start with the Optimizer end load values in Nm
2. By simple definition: (End Load)=$\sigma_{max} \times t_s$. Since the code asks the user to specify σ_{max}, the code can simply solve for the smeared skin gauge, t_s
3. relate the ratio of $\frac{\sigma_{max_u}}{\sigma_{max_l}}$ to the ratio of $\frac{t_{s_u}}{t_{s_l}}$ to find the lower skin smeared gauge
4. Calculate the actual stress from bending moments for the upper skin with standard structural equations[6], continue with the optimization as in the original code

Step 3 is not implicit and requires a short iterative sizing process.

2.3.1 Relating Stress ratios to Skin Gauge Ratios

To start the procedure, the area moments of inertia for a generic upper and lower skin need to be defined. This is fairly simple since the skins are approximated with parabolic coefficients:

$$z = A + Bx + Cx^2 \tag{2.9}$$

The code has user inputs for three (x,z) coordinates on the upper and lower surface and a utility to calculate the parabolic coefficients. Since those coordinates are for a generic airfoil, scaling will need to be done to adjust for the local $\frac{t}{c}$. A straight geometric scaling would imply multiplying all of the z coordinates by the ratio of $\frac{t}{c_{local}}/\frac{t}{c_0}$. However, in the case of transonic airfoils, the airfoils tend to keep the upper surface relatively constant and modify the t/c for the lower surface. Thus, for a spar defined with the coordinates z_u and z_l for some arbitrary coordinate system with the x axis roughly in the middle of the spar box, the z_{l_s} (scaled) would be adjusted by :

$$z_{l_s} = z_l - (z_u - z_l)\left(\frac{\frac{t}{c_{local}}}{\frac{t}{c_0}}\right) \tag{2.10}$$

With z as a function of x, the following integral forms can be used for the moments of inertia:

$$I_{xx} = t_s \int_0^{x_{rs}} z^2 dx \tag{2.11}$$

$$I_{xz} = t_s \int_0^{x_{rs}} xz dx \tag{2.12}$$

$$I_{zz} = t_s \int_0^{x_{rs}} x^2 dx \tag{2.13}$$

Where x_{rs} is the x coordinate of the rear spar. Since the calculation is going to assume that the only bending moment is M_x, the I_{zz} moment will not actually be used and will be left out of the rest of the calculations.

The original intent was to calculate three generic moments of inertia and scale them appropriately during the iterative loop to find the correct skin gauge ratio. This is easy if the skin thickness is constant around the spar box. However, with independent skin thicknesses it was easier to simply re-calculate the centroid and moments of inertia than to scale the original numbers.

During the actual sizing process the panel end loads are set by the optimizer. The upper skin gauge can be found from the σ_{max_u} and the following process then needs to be done to find the lower skin gauge:

1. Assume a skin gauge ratio, $\frac{t_{s_u}}{t_{s_l}}$
2. Calculate the (x, z) coordinates of the centroid for the foil section
3. Calculate the area moments of inertia around the centroid airfoil $\frac{t}{c}$ and current skin ratio.
4. Find the location of maximum stress on the upper and lower skins
5. Calculate the stress at this point for unit bending moment, upper and lower skins
6. Compare the calculated stress ratio with the desired stress ratio.
7. Use the secant method to find the skin gauge ratio which will yield the desired stress ratio

That skin gauge ratio will then work for all foil sections with this geometry. Thus, this ratio will only have to be calculated once for each time the code is run, unless $\frac{t}{c}$ is being optimized.

For reference, the equations for the location of the centroid, starting from an arbitrary coordinate system:

$$x_{cg} = \frac{(A_{fs}x_{fs} + A_{rs}x_{rs}) + t_{s_u}\int_{x_{fs}}^{x_{rs}} x ds_u + t_{s_l}\int_{x_{fs}}^{x_{rs}} x ds_l}{A_{total}} \tag{2.14}$$

$$z_{cg} = \frac{(A_{fs}z_{fs} + A_{rs}z_{rs}) + t_{s_u}\int_{x_{fs}}^{x_{rs}} z ds_u + t_{s_l}\int_{x_{fs}}^{x_{rs}} z ds_l}{A_{total}} \tag{2.15}$$

Where the subscript $_{fs}$ is for front spar and $_{rs}$ is rear spar. The formula can be simplified by assuming that the area of the skin is simply $t_s(x_{rs} - x_{fs})$ instead of doing the full integration.

Step 4 is only simple and straight forward if there is no cross term, $I_{xz} = 0$. This is almost always not the case, so the location of maximum stress is *not* simply the maximum z value for the foil. However,because the skin is described with a parabola, this location can be found in closed form. By simplification of equation 2.8 we get:

$$\sigma = \frac{M_x I_{xz}(x - x_{cg}) - I_{xx}(z - z_{cg})}{I_{xx}I_{zz} - I_{xz}^2} \tag{2.16}$$

Assume a unit M_x and take the derivative with respect to x to find the location of maximum stress. The Inertial values are constants so the denominator drops out. The $x - x_{cg}$ and $z - z_{cg}$ will simply be referred to as x and z, but it is important to keep track of the coordinate origin.

$$\frac{d\sigma}{dx} = I_{xz} - I_{xx}\frac{dz}{dx} \tag{2.17}$$

setting the slope of the maximum stress to zero and rearranging:

$$\frac{dz}{dx} = \frac{I_{xz}}{I_{xx}} \tag{2.18}$$

Assuming that we found numerical values for the moments of inertia based on the current airfoil $\frac{t}{c}$ and the current guess for the skin gauge ratio, we now have a numerical expression for the slope of the skin of the airfoil at the location of the maximum stress. Take the derivative of the parabola for the wing skin and the equation reduces to a linear:

$$\begin{aligned} B + \frac{1}{2}Cx &= \frac{I_{xz}}{I_{xx}} \\ x &= 2C(\frac{I_{xz}}{I_{xx}} - B) \end{aligned} \tag{2.19}$$

The only task remaining is to put all the scaled moments of inertia and the (x,z) location for maximum stress back into equation 2.16 for the airfoil. The denominators cancel for a final ratio of :

$$\sigma = \frac{I_{xz}x_{upper} - I_{xx}z_{upper}}{I_{xz}x_{lower} - I_{xx}z_{lower}} \tag{2.20}$$

To make this compatible with the root finding algorithm, take the absolute value of the stress ratio (the ratio will generally be negative since the upper surface is in compression), and subtract the desired stress ratio. Now this routine can be interfaced with a root finding algorithm, in this case, Brent's method as coded in **zbrent.c** for Numerical Recipes in C. [8]

2.3.1.1 Problems With the Foil Shape

The procedure described above is not fully robust when applied to the typical supercritical airfoil spar box with parabolic upper and lower skins. Because of the proprietary nature of the foil, the shape can not be printed here. However, to clarify the "picture" a little: The parabolic skins are only over the spar box. For a supercritical airfoil the skins in this region are quite flat, especially on the upper surface. The cusp shape lies behind the spar box, so the curvature on the lower skin is also parabolic and does not have a slope reversal at any point.

A test foil was treated in the manner described above where the upper skin was kept constant and all of the $\frac{t}{c}$ scaling was done to the lower skin. Figure 2-1 shows a plot of stress ratio vs. skin ratio for several locations along the wing starting at the root and moving out to about mid span. The root foils are well behaved. However, for some of the significantly scaled down sections out towards the wing tip there was no root to the curve. Two curves in figure 2-1 show this behavior with no zero on the curve. This phenomenon is very dependent on geometry since straight skins showed no such problems.

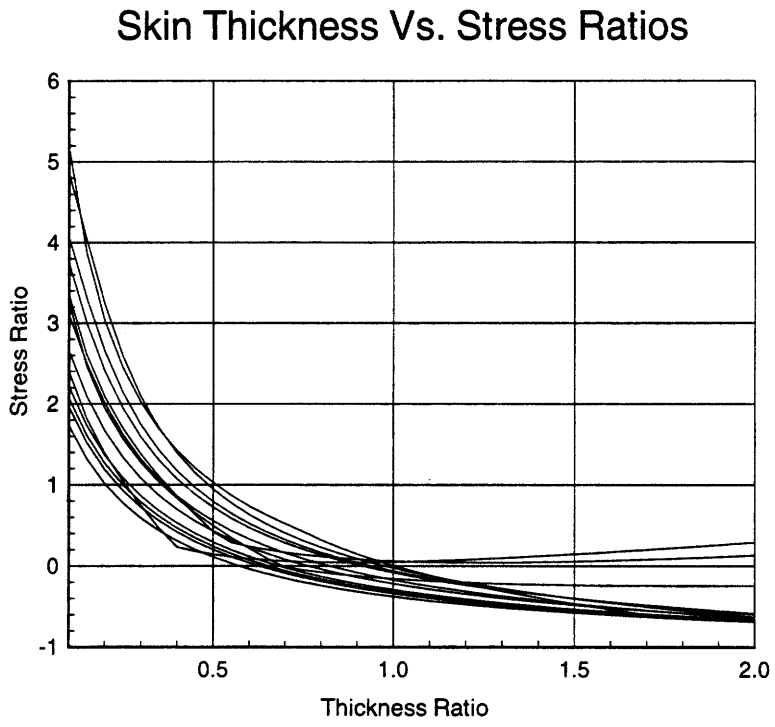

Figure 2-1: Plot of stress ratio vs. skin gauge ratio at several locations along the span starting at the root for parabolic skins

Additional plots and discussion of the stress ratio can be found in section 6.5 including figure 6-3 which plots the skin stress and thickness ratios from one of the near-final planforms.

Chapter 3

Optimization Procedure

Each wing design process actually requires five or six executions of the WASP code. The first three runs are concerned with finding an optimal case for the baseline planform and the stall speed velocities. No planform modification is done during these runs. The second set of three runs gradually adds design variables and constraints to hone in on the final design. Section 3.2 will present an outline of the full optimization procedure, and the following sections will discuss the specific design variables, constraints and goal used at each design stage. The next chapter will follow the baseline case through all six optimization steps with a description of what changes were made to the planform at each stage.

3.1 Starting Design

The optimization cycle needs an approximate geometry and a number of physical parameters to start the process. While the wing planform may change drastically over the course of the iterations, a poor initial planform "guess" will prevent the optimizer from finding a decent search path to any sort of converged solution. Especially important are the minimum and maximum weights for the aircraft. While the optimizer does try to minimize wing planform weight, the code assumes that the total aircraft weight is constant. While this may at first seem to limit the optimization process, it is actually a very reasonable method and prevents the problem of starting the optimization case for a 737 and ending up with a 777! (The code assumes the engines put out enough thrust for take off at maximum weight.)

3.1.1 Configuration Basics

The initial planform requires a number of physical parameters consistent with the desired weight class of aircraft. The initial wing loading, span and aspect ratio, the landing gear weight and position, empty weight, take off and landing speeds etc. need to be set by the user. Since the first two cases will not modify the planform at all, the wing should have a reasonable thickness and twist distribution along with a reasonable planform and area. The "aircraft" used for this study was given a basic profile as a short range transport of about 100 passenger capacity. The issue of passenger and payload weight is ignored and the entire entire useful load is considered to be fuel - if the fuel volume exists to contain it. For simplicity of optimization, the engines were assumed to be aft mounted, which is also

reasonable for the weight class.[1] The range for this type of aircraft should be on the order of 4000 km, however since fuselage and excrescence drag are not included, the ranges given by the code are about twice that value.

With this profile in mind, the maximum aircraft weight was set to 488,000 N (about 109,000 lbs) and the zero fuel weight was set to 380,000 N (about 85,000 lbs) for a mass fraction of 0.77. This weight class is on par with the DC9-32 and the 737-500, which seat about 100 passengers and are usually used on runs of less than 3000 km. The specific fuel consumption was set to 0.8, again consistent with the lower bypass ratio engines used with aft mounted engines. Lastly, the drag polars used were from an airfoil designed for a 100 seat aircraft[9].

Figure 4-1 shows a planform view of the starting geometry, a simple swept trapezoid with an average $\frac{t}{c}$ of about 12%. The details of this geometry are discussed in section 4.1. The symbols on the graph represent the element breaks. The optimizer can change most aspects of the geometry at these breaks - sweep, dihedral, $\frac{t}{c}$etc. Between the breaks all variable attributes scale linearly. The optimizer can also adjust the tail moment arm to control pitch (although there is no fuselage weight penalty for increasing the tail moment arm).

3.2 Outline of Full Optimization Procedure

A standard optimization case, starting from the described baseline and ending with a final planform design and reasonable convergence tolerance requires five or six executions of the code. The following is an outline of what happens at each execution. Details of each step are presented in the rest of this chapter.

1. Initial Structural Design, no planform modification at this stage.

   Goal: Minimum structural weight (wing and tail spar boxes)

   Design Variables: Skin end loads, wing α and tail δ for each design condition.

   Results: A well converged structural weight and skin thickness distribution.

2. Stall Speed Minimization

   Goal: High Lift condition stall speed

   Design Variables: High Lift condition velocity, wing α and tail δ for the high lift condition.

   Results: Minimum stall speed for a clean wing. Empirical methods are used to find the other low speeds used for take off and landing for the user input flap and slat deflections.

3. Secondary Structural Design

   Goal: Minimum Structural Weight

   Design Variables: Same as for step 1

[1] The optimizer does have a provision for putting engines on the wings in the form of introducing a point mass at the desired wing location. However, all previous work with the code had involved aft mounted engines and this work was used to formulate the baseline case.

Results: Structural variables converged to a higher tolerance than in step 1 using the new low speed velocities from step 2.

4. First Aerodynamic optimization

   Goal: Maximum Range

   Design Variables: Wing span and area, Sweep of wing root and tail, tail moment arm, wing incidence angles, and all design variables from step 1

   Results: Wing loading, span and area are all optimized close to final values, sweep is modified somewhat, $C_L$distribution approaches final values.

5. Second Aerodynamic Optimization

   Goal: Maximum Range

   Design Variables: All variables from Step 4 and $\frac{t}{c}$ ratios for the outboard wing elements, all chord ratios, and dihedral.

   Results: Wing thickness distribution optimized, chord ratios (taper modified), small modifications to span, sweep etc.

6. Final Aerodynamic Optimization

   Goal: Maximum Range

   Design Variables: Same as for step 5, Scaling factors are changed and the constraint penalty parameter is increased to force a tighter convergence.

   Results: Final design with tighter convergence criteria, small modifications to design variables.

Note: In some cases the optimizer reaches the limit of it's ability to improve the design in step 5. In this case, no steps are taken in step 6 and the output from 5 is considered the final design.

3.3 Initial Structural Design

The first and third code executions are nearly identical and deal only with sizing the structure. The minimization goal for these two runs is weight, so the lightest possible converged structure is produced without regard to aerodynamics. The second code execution is used to find the take off and landing velocities. The the high lift stall speed is calculated for a clean wing at maximum take off weight and minimizes velocity while avoiding stalling any panel of the wing.

3.3.1 Optimization Goal And Design Variables

For The first and third code executions, the goal and design variables are:

Goal: Total Weight This is the sum of the spar box weights for the wing and tail, leading and trailing edges and and miscellaneous weights as defined in section 1.4.4

Condition.Alpha wing angle of attack for the prescribed condition

Condition.Delta tail angle of attack for the prescribed condition

FFMF Fraction of available fuel volume actually occupied by fuel. This condition is constrained to ≤ 1 if there are no fuselage fuel tanks.

Tail Flap Deflection This effectively acts as the elevator trim tab and is used for elevator loads and (later) sizing.

3.3.2 Basic Constraints

The use of optimizer driven iteration (see section 1.4.2) requires large numbers of constraints - in some cases one for each panel or element of the planform. These constraints can take one of two forms: absolute and or error bound.

The absolute constraints, as the name indicates, simply place and upper and lower bound on a parameter. However, for many of the variables used in the internal iteration, defining a set maximum or minimum would be awkward so instead, an error parameter is calculated. For example, if the desired load factor for cruise is 1g, and after calculating the cruise condition for a given weight, the actual load factor is only 0.75g, the load factor error would be 0.25. This error is then constrained to zero. The basic constraints are:

Load Factor Error Constraint forces the optimizer to set wing α and tail δ to produce the desired load factor.

Pitching Moment Error Constraint Similar to the Load factor constraint, this constraint forces the tail to supply enough load to meet the target C_m. However, from the code, this is specified as:

$$C_{m_{target}} = ACWT\left(\frac{X_{gear} - X_{cg}}{qS_{ref}c_{ref}}\right) \tag{3.1}$$

Where the X coordinates are the location of the landing gear and the aircraft center of gravity, both of which were specified by the user. In the aircraft coordinates, the center of lift is at $X = 0$. This particular C_m seems only concerned with the pitch forces on rotation for sizing the tail.

Static Margin Constraint In theory, this constraint is needed to force the tail into a negative loading configuration. This is not a target constraint but an actual number. From the code, the formula for the Static Margin is:

$$SM = \frac{-\left(\frac{dC_m}{d\alpha}\right)}{\left(\frac{dC_L}{d\alpha}\right)} C_{ref} \tag{3.2}$$

Note that *this constraint has the units of length.* A more stadard definition of static margin is the ratio of the $C_m$and $C_L$slopes which is dimensionless. The usual value of this constraint was in the vicinity of 2.5 which produced a satisfactory down-load on the tail in the baseline configuration[9]. The actual function of this constraint is not clear. The user specifies the forward and aft CG location, the code is then allowed to modify the tail moment arm for the optimum pitch control. The indication from the code (although this was *not* documented) was that the center of lift for the wing would be at the $X = 0$ coordinate, and thus if the user specified CG values < 0, the tail should always need to supply a down load to trim the aircraft. However, without

this constraint specified, the optimizer will find a configuration with both surfaces providing positive lift (statically unstable configuration). This constraint proved to have a much greater effect on the entire planform design than had been considered, and the selection of the constraint value had to be changed several times during the trade studies to enforce static stability. Unfortunately, this large influence was not realized until quite late in the data collection, but there will be a full discussion of the effects of this constraint in sections 6.8.2 and 7.2

Fuselage Fuel Weight Constrained to 0.0 to force all necessary fuel volume into the wings.

Skin End Load Error Constrained to ≤ 0. This value is the difference of the actual and optimizer selected end loads. The actual end load is calculated from the bending moment. Constraining this error to less than zero for all panels and all structural sizing conditions ensures adequate wing structure.

The above constraints are necessary for all levels of optimization which involve the structure (all code runs except the low speed flap and slat deflection case).

3.3.3 Minimum Stall Speed

As explained in section 1.4.7 The code incorporates an add-on low speed model to calculate stall speed with and without flaps and slats. To find the initial clean wing stall speed for the aircraft one run of the code is done with the Velocity for the High lift condition as the goal for minimization. This condition is at maximum weight and clean wing and sets the stall speed for later use with flap and slat C_l increments. The only design variables for the case are the velocity, wing α and tail δ. The only constraints are error bounds on the maximum lift produced by each panel. With the error ≤ 0, each panel $C_l \leq c_{l_{max}}$. This method of finding stall speed is called the "critical section" method [1, 2.5.1] because when any panel is stalled, the entire wing is considered to be stalled. With the clean wing the high lift condition velocity was minimized to $\approx$ 63m/sec. This is for the starting geometry, which was less swept than the final geometry, but also had a higher wing loading. Repeating the high lift velocity optimization at later points in the aerodynamic design had adverse effects on final convergence. However, repeating this optimization step on the final wing as a check found a minimum velocity within a few m/sec of the original value so the generalization is not too bad.

3.3.4 Second Weight Run

From the clean wing stall speed the take off and landing speeds are calculated from empirical factors. These are plugged into the output from the first weight optimization and the case is run again with a higher penalty parameter to force a tighter convergence. All other parameters are the same as the initial weight optimization. When this case finishes, the convergence error should be on the order of 10^{-4} or smaller in order to proceed to the aerodynamic optimization. (A poorly converged weight solution will make it very difficult for the optimizer to find a search path for aerodynamic optimization)

3.4 Aerodynamic Optimization

The second set of code runs use the "Inverse Range" as the optimization goal (inverse because the goal is always *minimized*). The range is calculated from the standard Breguet Range Equation

$$Range = V\frac{C_L}{C_D}\frac{1}{TSFC}ln\frac{W_i}{W_f} \tag{3.3}$$

Where W_i is the initial weight and W_f is the final weight. In the code, the TSFC is held constant, and the velocity is set for each leg of the flight profile. The initial and final weights are set to the empty weight and the maximum weight and so are also constant. Thus the only changing variable is $\frac{L}{D}$ so the range optimization is actually a minimum drag optimization.

All aerodynamic parameters are now available for optimization, however adding degrees of freedom in stages rather than all at once provides a cleaner optimization and a better chance of finding a well converged solution.

3.4.1 Usable Design Variables

The following is a list of all the possible aerodynamic parameters used as design variables. Note: the design variables from the weight cases (1 and 3) continue to be used for all cases.

BaseSemiSpan Is the sum of the wing and tail semi-spans. As far as the code is concerned this is (total panels)*(panel width). Using this variable allows the panel width to change and hence the total wing and tail spans to change.

BaseSemiArea The area of one wing and tail (where a wing is half of a symmetric wing).

Sweep Allows the optimizer to vary the quarter chord sweep of the element.

Tail Moment arm Adjusts the distance between the wing and tail quarter chords.

Incidence Adjusts the local angle of incidence (angle between local airfoil zero lift line and the wing zero lift line for the root or tip of an element. This angle varies linearly along the element.

Thickness Adjusts the local $\frac{t}{c}$ at the element root or tip. Again, the thickness then varies linearly between the root and tip of the element. Usually only the tip values are used as design variables, the value from the preceding tip being carried to the root of the next element.

Chord Ratios To nondimensionalize the geometry as much as possible the wing is expressed as a set of chord ratios, quarter chord sweep and number of panels. These 3 values can be used to "build the wing" (given the total area in order to find the actual root chord). All chord ratios can be used as design variables which is how the optimizer can set the "taper".

Dihedral(n) This was initially set to 3° and included as a design variable. However, the optimizer did not find any gradient related to the dihedral so there was no change in this variable.

3.4.2 Aero Constraints

While the weight optimization cases were quite well behaved, the number of degrees of freedom introduced with the aero design variables opens a whole new set of possible directions the optimizer can take. Any weakness in the models not related to the physics of the problem will be used by the optimizer if they seem to provide an improvement. Since perfect models are not an option here, the easiest way to keep the optimizer within the realms of reason is with constraints.

Tip Chords The wing tip chord ratio had to be constrained to prevent a reverse taper in the last panel. Otherwise the optimizer would tend to add unloaded (lots of washout twist) wing area at the tip in an attempt to keep the tip $\frac{t}{c}$small yet have a thick wing for structures.

Wing $\frac{t}{c}$ The drag polars used for most of the runs were not sensitive to wing thickness changes. Without the wave and viscous drag penalties, the optimizer would find very thick (and light!) wings. Maximum wing $\frac{t}{c}$values were used to constrain the problem. However, with constraints of $\frac{t}{c} \leq 0.2$, the optimizer would fail to find a decent solution. Leaving out $\frac{t}{c}$as a design variable also led to difficulties in finding an optimization gradient, so the wing is thicker than would be practical. Even for the cases where the Wave Drag model (see section 1.4.6.1 was used instead of the polars the wing $\frac{t}{c} \approx 0.18$.

Landing Gear Constraint As explained in [1, 5.3.1], there is a landing gear constraint which basically forces the optimizer to allow a user specified amount of space behind the rear spar for landing gear placement. This usually has the effect of taking out a lot of the sweep on the inboard trailing edge, that is, adding a yehudi to the wing [2]

Static Margin Specifies the amount of static stability margin desired for the aircraft. Not constraining this will allow the optimizer to find the (aerodynamically preferable) configuration of positive, parabolic lift on the wing and tail, with the resulting instability problems. This constraint was imposed on the cruise and maneuvering conditions to ensure positive stability (negative tail load) at all times.

Element End Load Error Constraint Similar to the panel end load constraint, but in this case the parameter is $\frac{design\ end\ load}{actual\ end\ load}$ At sharp panel break points, such as a sweep change, the optimizer would sometimes find a divergent case of increasing load at the break point, increase the structural mass, which created and additional (unstable) load increase etc. Constraining the maximum excess structural loads carried helped reduce this problem but excessive constraints here made it very difficult for the optimizer to find any search path.

3.4.3 Initial Aerodynamic Optimization

With the output from the third code run as input, the code is ready to begin optimizing the planform. While it is possible to simply throw all the aerodynamic variables at the optimizer now, this usually results in the optimizer having difficulty finding a good search

[2] Boeing-ese for the straight section of inboard trailing edge, used to boost thickness at the wing root to provide for gear placement etc. without excessively increasing $\frac{t}{c}$.

path. For this reason, the first aerodynamic optimization is focused mostly on finding area, span and sweep and twist distribution. Chord ratio and $\frac{t}{c}$optimization are considerably more sensitive and will be added at the next step.

Some of the planform variables have an associated variable which governs their behavior at or between break points. For example, the panel incidence can be set to be continuous or discontinuous at element break points. It can also be set to vary linearly between the root of one element up to the tip of the next outboard element (across the break point). For this optimization run, the following transition values were set:

Incidence Continuity: Continuous between break points

Quarter Chord Sweep: Continuous across all break points except between the 3rd and 4th panels.

Note: Since only the root sweep is being optimized here, this means that outboard of the 3rd panel will continue to assume the values from the input deck. Several attempts were made at optimizing the entire wing continuously or letting the optimizer vary the sweep in multiple elements. All of these experienced stability problems and would tend to run towards a maximum or minimum sweep value.

The output from this optimization run is generally not very well converged, however any convergence error less than order one should be ok to use as input to the next stage.

3.4.4 Final planform optimization

This usually takes 2 code executions, although sometimes the second attempt does not find a step to take and so no optimization occurs. Added to the design variables from the last stage are the chord ratios for all elements and the $\frac{t}{c}$ratios for the outboard wing elements. Dihedral was also included as a variable, but was not modified. Both of these variables also had element transition variables attached and these were set as:

Thickness Continuity Set to vary linearly from the root of one element to the tip of the next outboard element.

Chord Continuity The first three breaks are continuous, outboard of the 3rd wing element chords vary linearly from the root of one element to the tip of the next outboard element. (These were set more by trial and error than by a set logical algorithm. In this case, this chord distribution produced the most "reasonable" and consistent output.)

The first code run with the full set of parameters will make small changes to the formerly optimized parameters.

Chapter 4

Baseline Optimization Case

This chapter will present the baseline case used for all of the optimization runs. Data and graphs showing the progress from the starting geometry to the final planform will be presented for each step as detailed in chapter 3

4.1 Starting Geometry

Figure 4-1 shows the basic starting geometry used for all the optimization cases. The units are in meters, the symbols on the plots are the locations of the element break points. Each element consists of 1 or more panels. Starting panel width is 0.75 m with 20 total panels in the wing and 7 in the tail. Changing the span of the wing thus changes the span of the tail since all panels are of constant width. See the next section for details on plot descriptions.

The geometry is very simply a tapered, swept block. Not shown is the Dihedral which is +3° for the wing and the -3° for the tail The initial $\frac{t}{c}$ distribution was roughly copied from a Boeing aircraft of the same size [9]. As explained in chapter 3, there is no geometry change during the first three code executions. The second code execution modifies the take off and landing speeds, the first and third executions size the structure. Table 4.1 shows these parameters. The physical dimensions do not change between runs but are included here for reference. Aerodynamic parameters are not currently being optimized and are omitted.

4.2 Plots Description

The basic geometry plots are more or less self explanatory. The upper graph is simply an "overhead" view of the wing and tail planform with the dimensions in meters and the plot symbols marking the break points for the elements. The lower graph of the geometry plots uses the same horizontal scale of of 1-25 m with a highly expanded vertical scale to show the $\frac{t}{c}$ distribution along the span. Again, the symbols are located at the element break points and the distribution is linear between these points.

The next set of plots contain a total of eight sub-plots on four pages. All of the plots use η for the horizontal axis. For these plots the symbols are located at the center of each panel. Proceeding from the upper left corner in a clockwise direction, the eight plots are:

1. **C_L Vs.** η Shows a plot of lift coefficient for each panel on the wing and tail

2. **Nondimensional C_L Vs.** η Where the nondimensional C_L, indicated by $\overline{C_l}$ is

Data for:	Initial Guess	Velocity	Final Structure
Convergence Error	5.02637e-03	3.30921e-06	3.53354e-04
Structural and Geometry Data			
Wing Semi-Span (m)	14.97945	14.97945	14.97945
Wing Area (m^2)	56.25	56.25	56.25
Wing Aspect Ratio	7.97809	7.97809	7.97809
Tail Volume	0.709333	0.709337	0.709337
Spar Box Mass (kg)	970.073	970.068	970.079
Total (half) Wing Mass (kg)	2126.37	2126.36	2124.94
Wing Root Sweep (deg)	24.6236	24.6236	24.6236
Takeoff speed (m/sec)	70.0000	70.0000	75.6418
Landing speed (m/sec)	54.8138	54.8138	54.8138
Performance Metrics			
Wing M.F. (spar box/total)	0.024966	0.024966	0.024966
(Fuel mass)/(wing mass)	11.368423	11.368584	11.368352

Table 4.1: geometry and weight summary data for Baseline case structural sizing and low speed optimization runs

defined as:

$$\overline{C_L} = \frac{(local\ chord) * (Panel\ C_L)}{MAC * C_{L_{condition}}} \tag{4.1}$$

In this way the lift coefficient is adjusted by chord length.

3. **Panel Incidence Vs.** η This is the angle of incidence (Free stream angle - zero lift angle) *including* aeroelastic deflection.

4. **Bending Moment** Wing bending moment calculated from the lift loading, units are N*m

5. **Actual and Optimizer Selected End Loads** As explained in section 1.4.2, the structural iteration depends on having the optimizer find end loads which are all $\geq$ actual end loads. This plot shows both. In all cases, the *optimizer* $\geq$ *actual* condition should hold, however in some cases the optimizer has erred on the side of a much higher load than needed. This most often happens towards the tip as the bending moment goes to zero and at breaks in the quarter chord sweep. Note that the vertical scale is logarithmic and the units are N*m

6. **Wing and Tail Smeared Skin Gauge** Shows the smeared skin gauge (average of skin thickness + stringer thickness) along the wingspan for the upper and lower skins.

7. **Wing and Tail Deflection Vs.** η Deflection calculated from shell beam theory and the *actual* bending moment load. Units are meters.

8. **Panel Mass Including Fuel** The mass of each panel in kg. The inboard panels carry fuel, which in many cases leads to a significantly higher mass on the inboard sections.

File Name conventions: Most of the graphs use the file names in the legend. While the file name itself is not important, there are several bits of relevant information contained in the filename. The format is:
Surface + Run_Name + Run_Number + Run_Name_Suffix + Case_Type
where the Run_Name and suffix are arbitrary but reflect the type of data. For the trade studies, the suffix contains the value of the independent variable for that run. For example:

`WingBase1FCr`

- The "Wing" of course means that this line is the wing data
- The "Base" is the (arbitrary) prefix to the filename (in this case, the Baseline run)
- The "1" is the code execution number. Due to a slightly illogical numbering scheme, the executions are, in order: 1,v,2,3,4 and 5. Since the "v" run is very short and only used to get information for low speed operations, data from this run is never plotted. Thus the mapping is:

  1 & 2 are structural optimizations

  3, 4 & 5 are aerodynamic optimizations.

- The "F" is the filename suffix (in this case, F= final)
- "Cr" is the condition, in this case "Cruise". See section 1.5 for a description of the possible flight conditions and abbreviations.

4.2.1 Data Table Description

Along with the graphics plots, there is also a standard data table of key geometric and performance figures which are useful for comparing different designs. Table 4.1 was a shortened version of this table (no aerodynamics parameters were shown). Most of the entries are self explanatory, however there are several performance metrics which should be defined.

NOTE: All geometric values such as wing span and area are for the *semi-span.* All masses given are also for a semi-span wing.

Wing Aspect Ratio or AR is the simple geometric aspect ratio defined by: $\frac{b_{wing}^2}{S_{wing}}$.

Tail Volume is a measure of the total leverage power of the tail and is defined as:

$$V_{tail} = \frac{tail\ moment\ arm \times S_{tail}}{MAC_{wing} \times S_{wing}} \tag{4.2}$$

Where the tail moment arm is the distance from the aircraft CG to the tail root quarter chord, S_{tail} is the tail area, and MAC is the geometric mean aerodynamic chord defined as $\frac{S_{wing}}{b_{wing}}$

Wing Root Sweep is the quarter chord sweep in degrees for the first wing element.

Wing Tip Sweep is the quarter chord sweep in degrees for the last (tip) wing element. Note: Since only the root element sweep is actually modified, while the tip is not modified, these two sweep values are the only ones needed to define the wing. (see section 4.3.2)

Range Was calculated using a modified form of the Breguet range equation which includes the expanded equation for TSFC:

$$R = \left(\frac{\eta_t \eta_p h_r}{g}\right) \frac{C_L}{C_D} ln \left(\frac{W_{initial}}{W_{final}}\right) \tag{4.3}$$

Where h_r is the chemical heating value of the fuel in $\frac{joule}{kg}$, g is the standard gravitational acceleration. $W_{initial}$ is the maximum take off weight less the extra fuel which is burned as a function of needing to climb to altitude. W_{final} is the aircraft weight at the end of cruise where all weight loss is assumed to be fuel. η_p is the propulsive efficiency of the engine and η_t is the thermal efficiency and defined as :

$$\eta_t = 1 - \frac{1}{\pi^{\frac{\gamma-1}{\gamma}} \left(1 + \frac{\gamma-1}{2} M_\infty^2\right)} \tag{4.4}$$

Where π is the pressure ratio across the compressor. For a complete explanation and derivation of this range equation and the compensation for climb fuel, see appendix A

Efficiency Is the $\frac{Range}{kg_{fuel}}$ $\frac{km}{kg}$

Wing MF stands for Wing Mass Fraction, that is the weight of the wing spar box compared to the total aircraft weight

4.3 Baseline Aerodynamic Optimization Discussion

As discussed in section 3.4.3, the initial aero optimization will focus on finding wing span, area, twist distribution, and to some extent, sweep. The second optimization adds wing thickness distribution and chord ratios (taper ratio) to the optimization.

Figure 4-2 shows the geometry for the initial guess, for one aerodynamic optimization and for the final planform. Figures 4-3 to 4-6 show the aerodynamic parameters for these runs. Table 4.2 gives the full data for the first and last aerodynamic optimization cases with the initial guess for comparison. (There was very little change between the second and third aerodynamic optimization, so this step has been left out.)

4.3.1 First Optimization Changes

There are significant changes between the initial planform and the first aerodynamic optimization. The initial aerodynamic case comes close to finding overall planform size and performance parameters. This includes the wing span, wing loading, aspect ratio and, to a lesser extent, lift distribution. The wing span increased by about 20% which increased the wing box weight and wing area for a lower wing loading overall. Perhaps the most surprising result is from comparing the $\frac{C_L}{C_D}$ for each case and noting that after the aerodynamic optimization the $\frac{C_L}{C_D}$ was actually *lower*. The reason for this apparent failure of the optimizer lies in the application of numerous aerodynamic constraints, the most significant

of which is the Static Margin. This is a constraint on the longitudinal pitch stability of the aircraft which forces positive static stability and hence negative tail loading. Without this constraint, the optimizer is happy to find a parabolic, positive loading on the wing and the tail. The initial structural case did not have a negatively loaded tail and but otherwise had reasonable lift distribution as seen in figure 4-3 and also in the tail incidence distribution in figure 4-4

Data for:	Initial	First Aero	Final
Convergence Error	5.02637e-03	5.42186e-02	0.64771
Structural and Geometry Data			
Wing Semi-Span (m)	14.97945	17.75835	18.81145
Wing Area (m^2)	56.25	73.887	75.8075
Wing Aspect Ratio	7.97809	8.53629	9.33604
Tail Volume	0.709333	0.474256	0.495170
Spar Box Mass (kg)	970.073	1382.72	1410.78
Tail Spar Box Mass (kg)	86.7567	92.4398	96.9838
Wing Root Sweep (deg)	24.6236	26.6516	35.0633
Wing Tip Sweep (deg)	24.6236	24.6236	24.6236
Performance Data			
Wing Loading (Pa)	4347.20	3312.16	3228.12
Cruise C_L	0.40862	0.31133	0.30343
Cruise C_D	1.61261e-02	1.26475e-02	1.17905e-02
Inviscid Cruise C_D	0.00000	0.00000	0.00000
Viscous Cruise C_D	8.82066e-03	8.30894e-03	8.20581e-03
Cruise Wave Drag C_D			
Cruise L/D	25.3389	24.6158	25.7350
Range (km)	7.9804e+03	7.7526e+03	8.1051e+03
Takeoff speed (m/sec)	70.0000	75.6418	75.6418
Landing speed (m/sec)	54.8138	54.8138	54.8138
Performance Metrics			
Efficiency range/fuel Km/Kg	0.723639	0.702909	0.734968
Wing M.F. (spar box/total)	0.024966	0.035586	0.036308
(Fuel mass)/(wing mass)	11.368423	7.976525	7.816811

Table 4.2: Baseline Case data for Initial guess, after first aerodynamic optimization and the final optimized design

The increase in area was in response to enforcement of a no-stall condition during all flight conditions. The initial case needed C_l values in excess of the maximum available for the take off and landing high lift conditions. With wing area as a variable the optimizer satisfied the (internal) constraint that no wing panel exceed a user-specified maximum C_l value. This was responsible for the 42% increase in wing area and corresponding decrease in wing loading, and also had a negative impact on $\frac{C_L}{C_D}$ and reduced the cruise C_L to 0.303, well below the optimum value of $C_l = 0.7$ for $\frac{C_l}{C_d\, maximum}$.

This increase in wing area then requires an increase in span in order to keep the aspect ratio relatively constant. At the same time, the sweep is not going to increase much because

of the relatively high wing loading at the wing tip which provides a negative pitching moment and makes the static margin constraint more difficult to satisfy.

4.3.2 Final Planform Changes and Performance

The second aerodynamic optimization is able to adjust chord ratios (taper ratios), hence a finer adjustment of area distribution. The wing span and loading change a little, while the sweep changes a significant amount and the overall lift distribution is tweaked for better $\frac{C_L}{C_D}$. The final aerodynamic case makes very fine adjustments to this case. There are a number of aspects to the optimized planform which seem to be not "quite right". Some of these are functions of using too simple a physical model, some are functions of constraints.

The $\frac{t}{c}$ profile of the finished aircraft is quite thick, as shown in the lower plot of figure 4-2. Most of the wing has a $\frac{t}{c} \geq 0.20$. This is a problem with using a set of actual drag polars which include compressible drag instead of a separate compressible drag model. While the polars provide more accurate drag information for a final design, they don't properly penalize the optimizer for increasing $\frac{t}{c}$ to lighten the wing. Attempts to constrain the $\frac{t}{c}$ to a more reasonable value resulted in poorly converged optimizations.

The final planform exhibits a short section of forward swept trailing edge. This is a direct result of applying the landing gear constraint which forces the compiler to leave enough space in the wing root to retract landing gear. Normally, this section of the trailing edge would simply run perpendicular to the body long enough to accommodate landing gear, flap track motors etc. However, the optimizer doesn't care how easy the wing would be to build so it finds more interesting shapes. Note: this rapid increase in chord near the root is what causes a dip in the lift distribution at the root. The $\overline{C_L}$ which accounts for this in the normalization shows a "nicer" looking lift distribution.

There is a significant increase in sweep in the final planform. The relevant design variables were the sweep of the root element and the variables governing the sweep transition. All element break points were continuous except the break between the third and fourth wing elements (from the root). The root sweep increased from a starting value of 26.6° to 35° while the tip sweep remains relatively constant at 25°. A number of different combinations of element sweep design variables and continuity settings were tried. Too many elements with variable sweep and or discontinuous sweep resulted in a wing with numerous bends (like the B2 trailing edge, but worse). Constraining all sweep to be continuous again resulted in convergence problems so the current arrangement is a non-ideal compromise. The sweep increase resulted in a larger negative pitching moment from the wing and the tail was moved aft 2m to compensate. The value of using tail volume as a metric can be clearly seen in this instance, since despite the changes in planform, the tail volume is almost constant at the value needed to satisfy the pitching moment constraint.

The final configuration meets all the necessary flight conditions, satisfies the constraints and performs slightly better than the initial guess. The final range is about 8100 km with a fuel burn efficiency of 0.735 km/kg compared to the starting planform which was 0.724 km/kg.

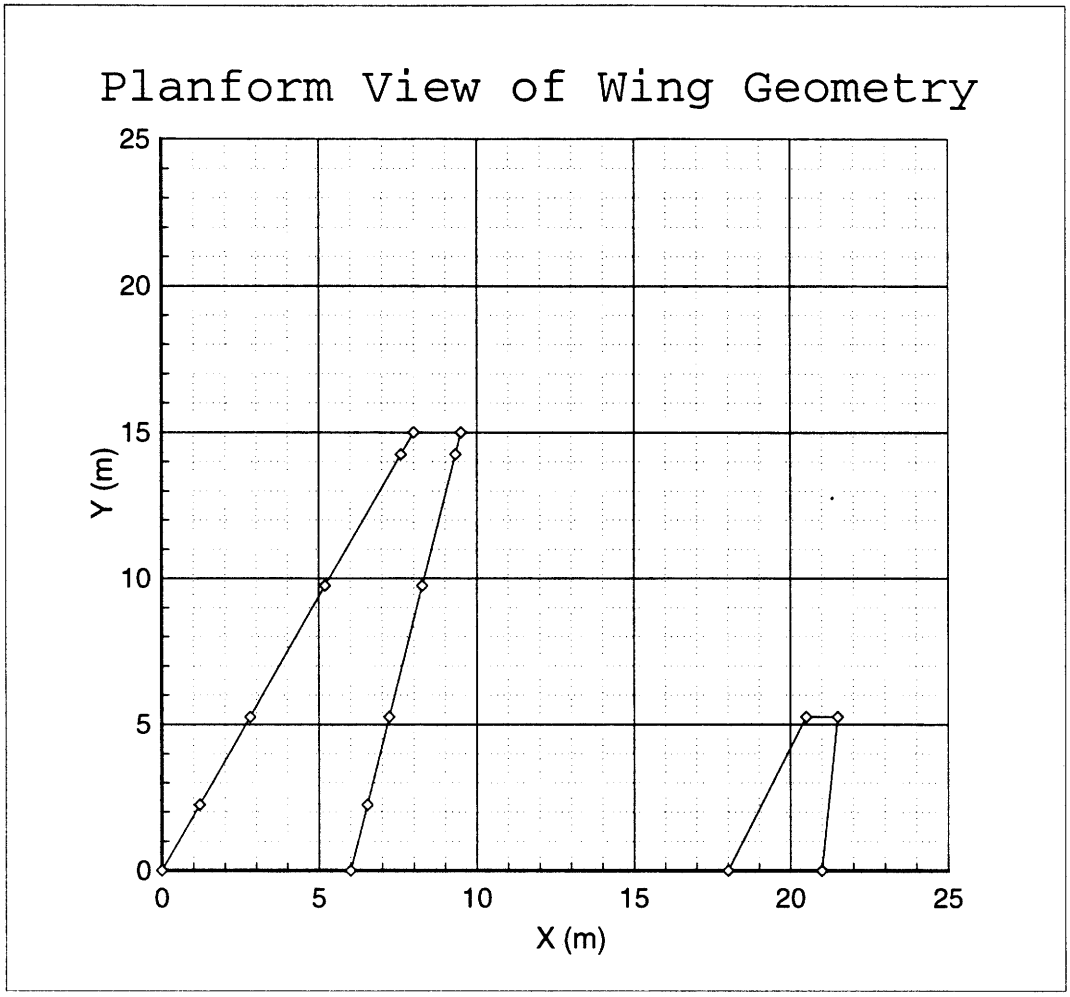

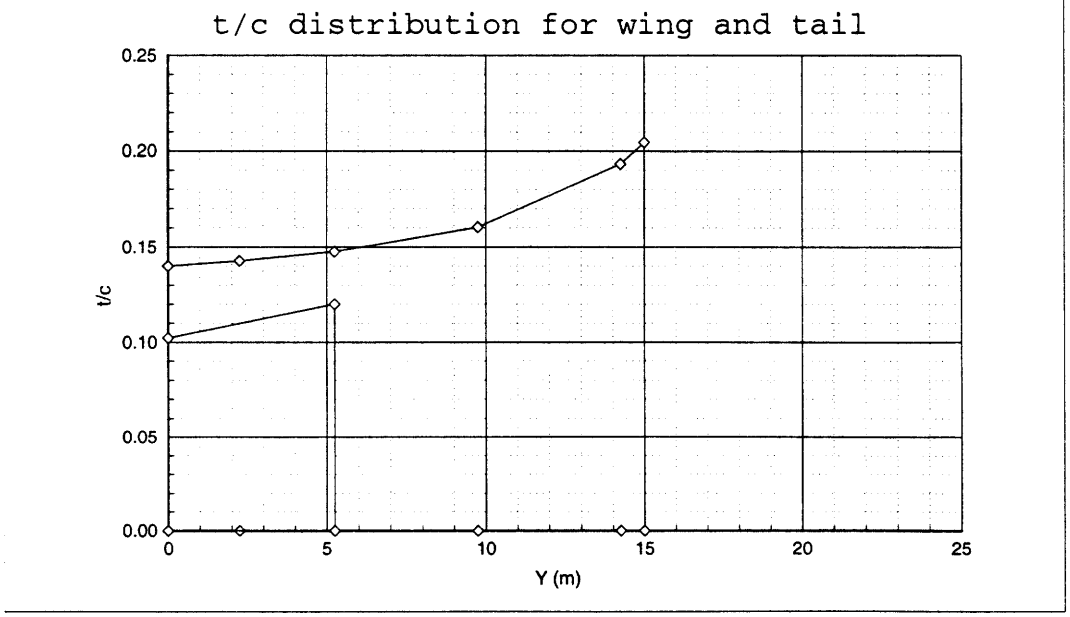

Figure 4-1: Baseline Starting Geometry

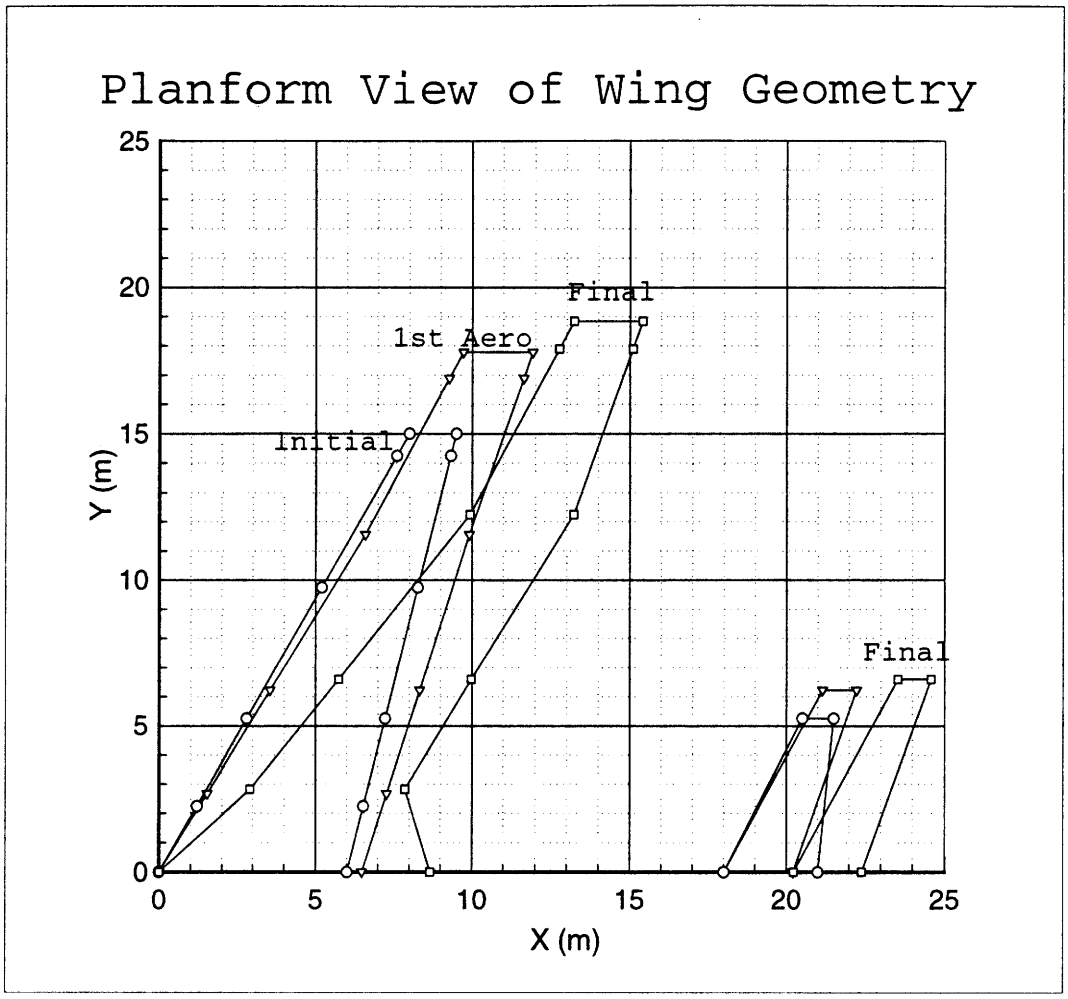

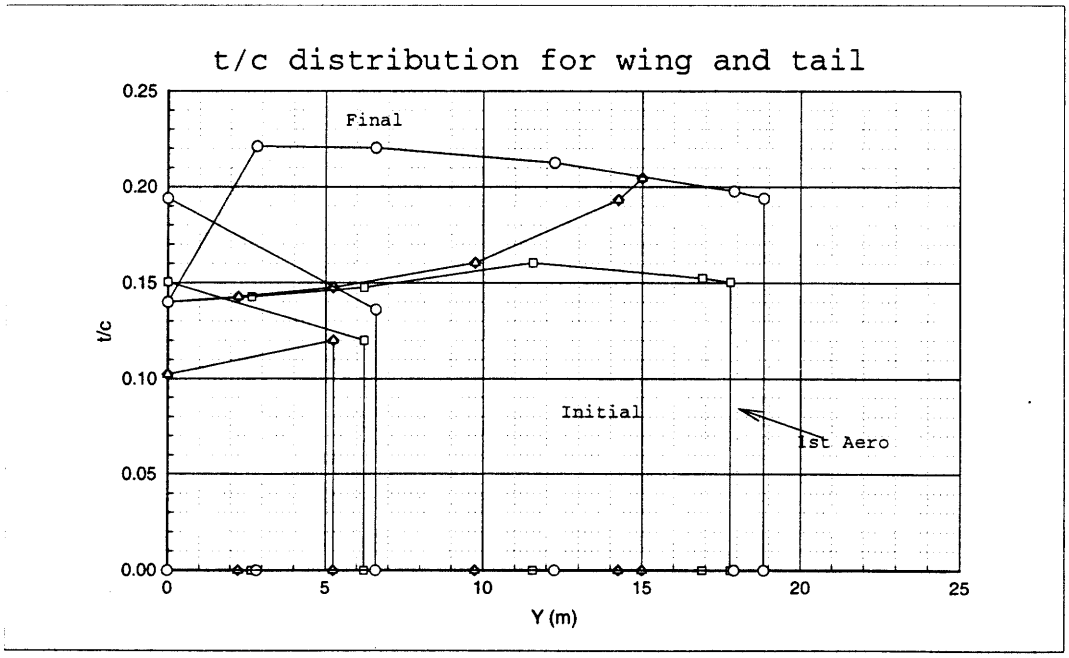

Figure 4-2: Baseline Optimization case; starting guess, one aerodynamic optimization and final planform

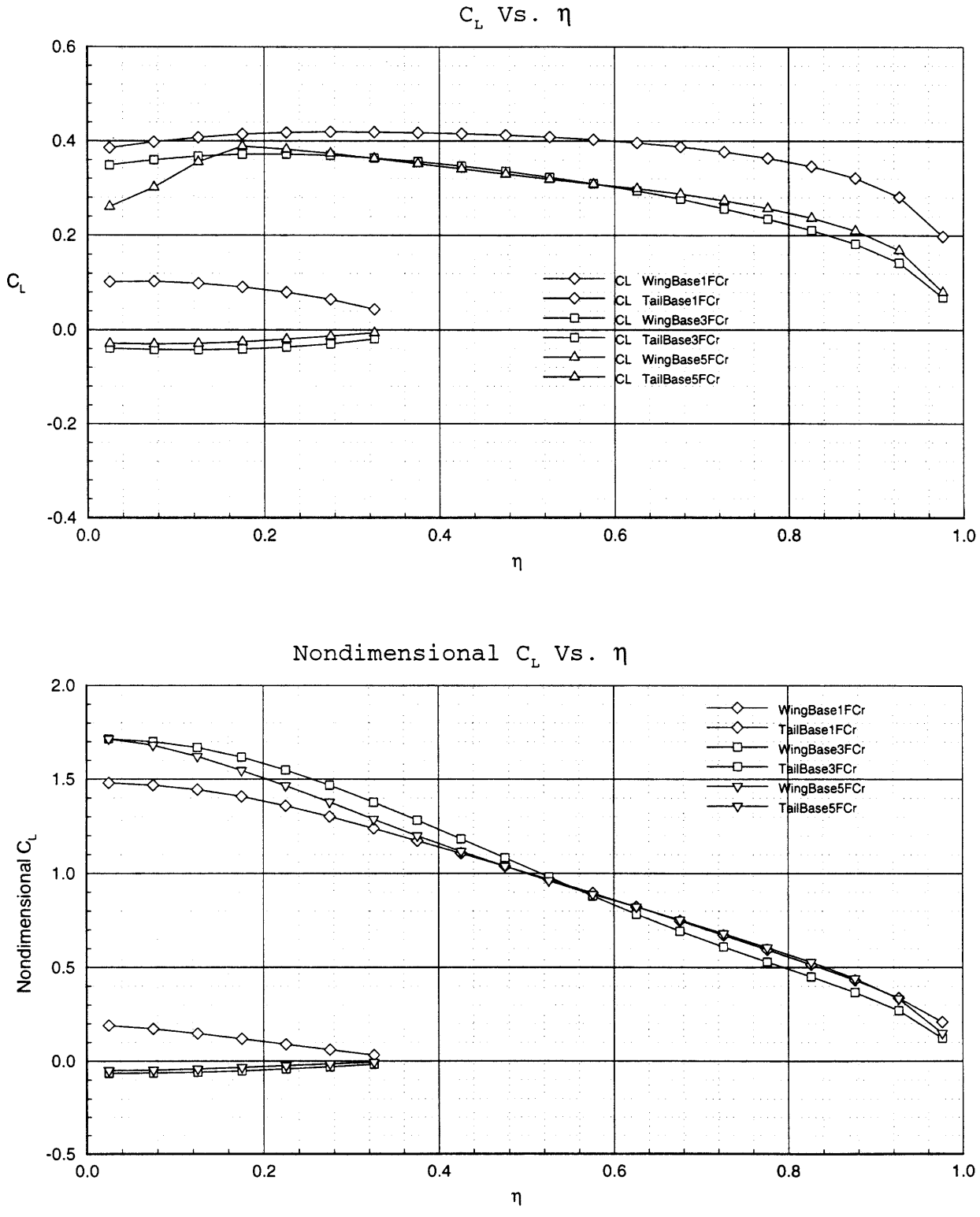

Figure 4-3: Baseline Optimization case; aero data for initial guess, one aero optimization and final design

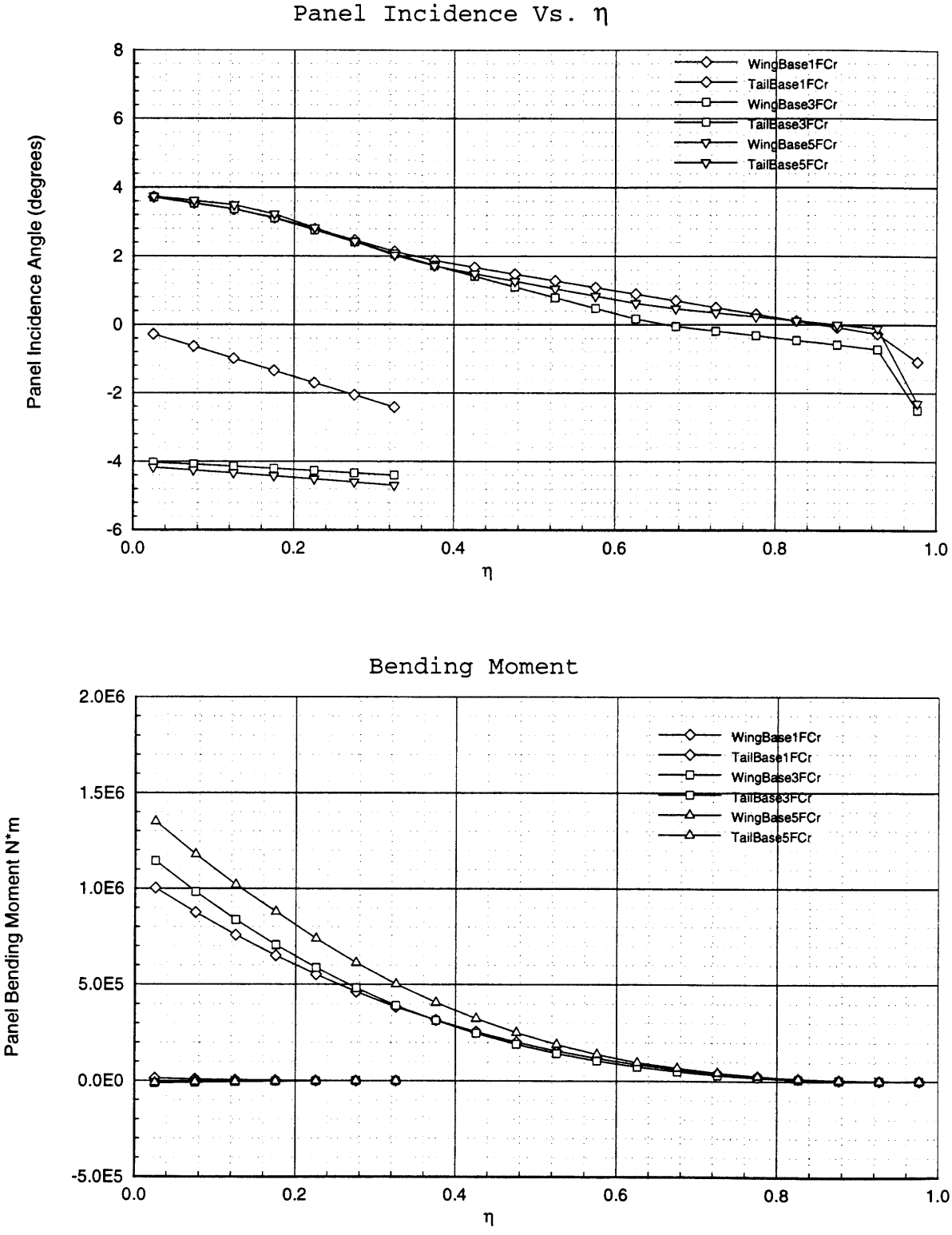

Figure 4-4: Baseline Optimization case; aero data for initial guess, one aero optimization and final design

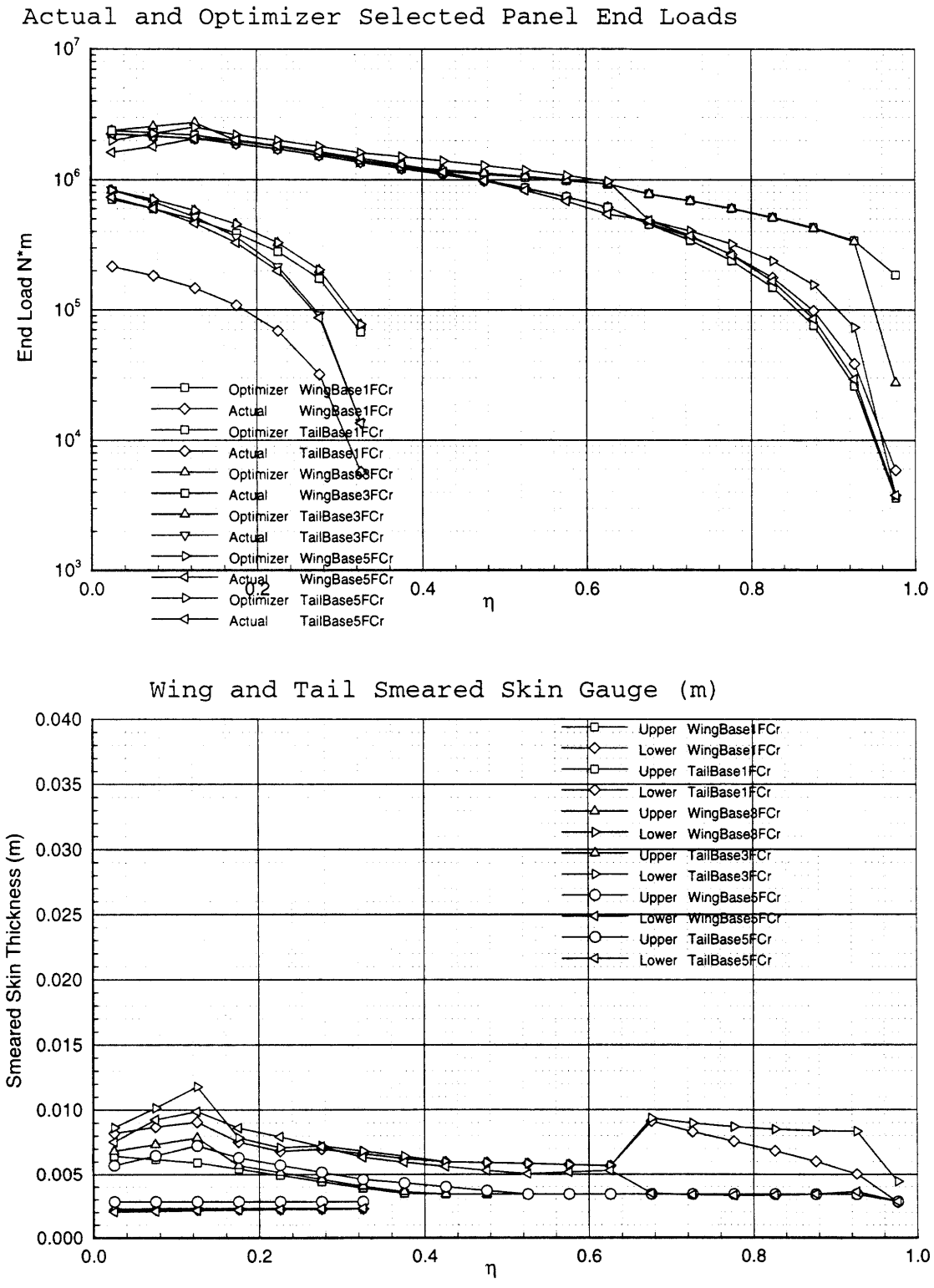

Figure 4-5: Baseline Optimization case; aero data for initial guess, one aero optimization and final design

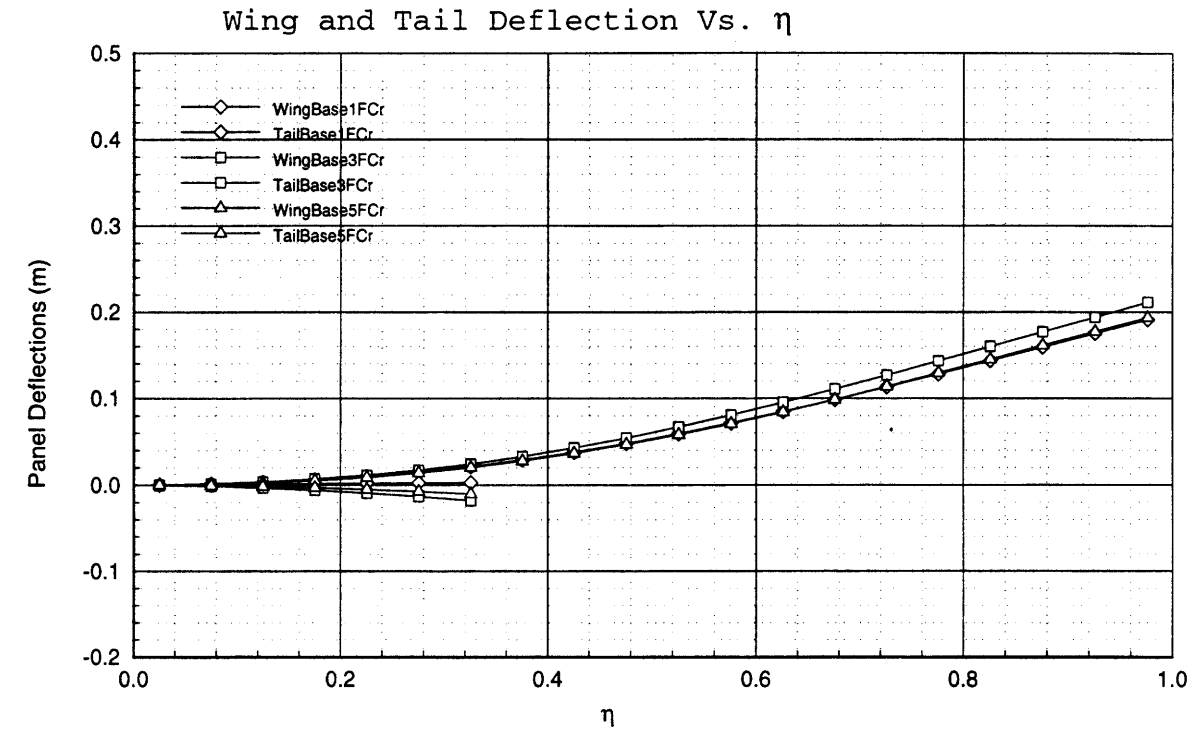

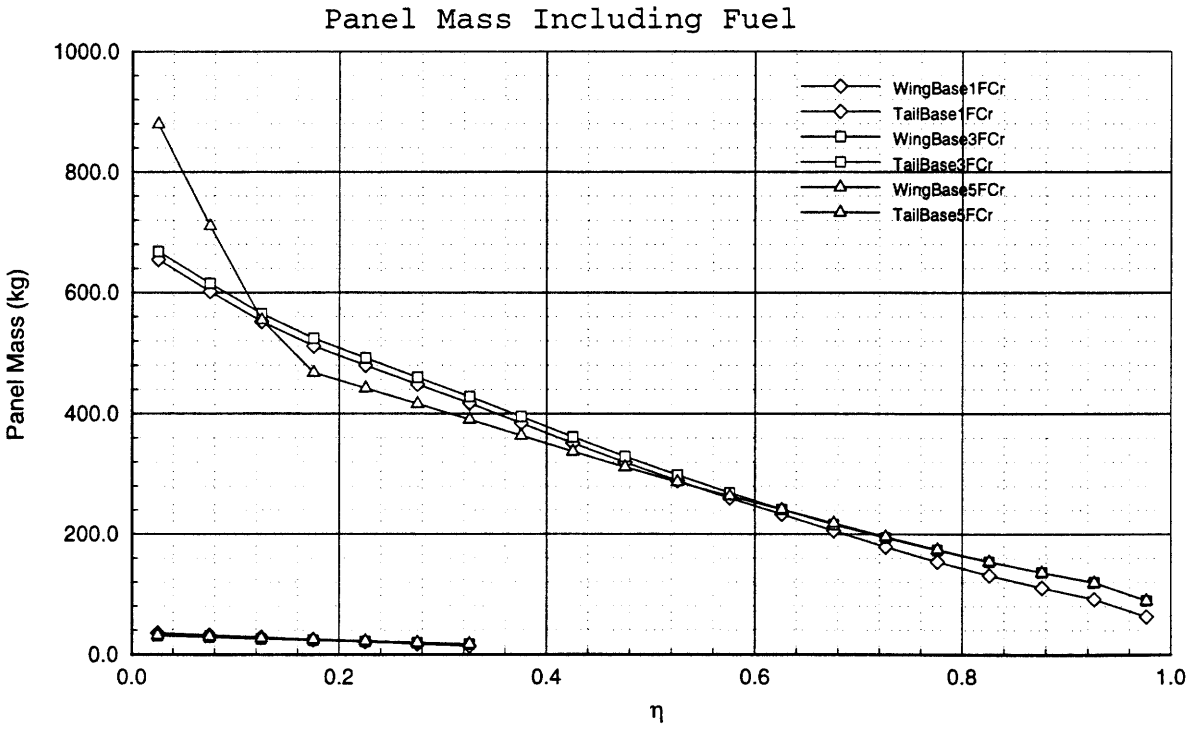

Figure 4-6: Baseline Optimization case; aero data for initial guess, one aero optimization and final design

4.4 Default Drag Models

For all data presented thus far in this chapter the drag information was determined by using a set of user input drag polars. While this is more accurate for total drag prediction with a well defined airfoil, it has several disadvantages. Because the polars are independent of geometry, there is no strong link between increasing thickness and wave drag, so the wing will tend to end up too thick. Another problem is that the viscous and compressible drag effects are now combined into a single number so that it is impossible to examine the effects of each drag type independently.

The original code used two separate functions to generate each type of drag. The C_{D_v} was calculated from a simple flat plate drag analysis according to local R_e. The C_{D_c} was found using the crest critical Mach number method by Shevell and described in section 1.4.6.1. Since two of the trade studies described in chapter 5 needed to adjust these drag parameters independently, the default drag models were used for those studies. To validate these drag models, the baseline case was run again without the polars. Table 4.3 has the data comparing the output from the two final planforms, and figure 4-7 shows the resulting planforms.

The first attempt to use the compressible drag model resulted in an unreasonable design with a very high C_{D_c}. To alleviate this problem the "critical Mach number" which signals the onset of wave drag can be increased by some offset. For this case, the offset was set to an increase of 0.08 Mach. This produced reasonable results, but is not in any way a magic number. Chapter 5 describes some of the trade studies done using the code, one of which used this offset parameter as the test variable to study the effects of small changes in compressible drag on the final planform.

There are a number of differences between the two cases including wing span, sweep, AR, loading and thickness distribution. As mentioned in section 4.3.2, using polars places too little emphasis on keeping the wing thin to minimize wave drag. Figure 4-7 clearly shows that with a wave drag model the optimizer will find a thinner wing, even though the result is substantially heavier.

There is no way of separating viscous and compressible effects in the polars, however the total drag (not including C_{D_i}) for the polars case is 0.0082 while the viscous drag alone with the models is 0.00946 and there is the additional 0.00112 C_{D_c}. To compensate for these factors, the optimizer drove the design towards a higher AR design so that C_{D_i} decreased from 0.00358 to 0.00278. Also, wing sweep increased by several degrees to minimize the C_{D_c}. The final wing comes out 3.5 m longer and nearly three times heavier than the original baseline. However, due to the combined changes in C_L and C_D, the over $\frac{C_L}{C_D}$ increased slightly resulting in a small range increase.

These changes also applied to the tail which uses the same airfoil geometry. The final tail using drag models also had a much higher aspect ratio (same shape, it goes off the page slightly), lower $\frac{t}{c}$ distribution and increased sweep. To pay for these changes, the new tail weighed nearly ten times more than the baseline! The tail is moved aft a little to compensate for the lower area and the increased pitch requirements of the more highly swept wing.

Data for:	Drag Polars	Drag Models
Convergence Error	7.14863e-02	0.21822
Structural and Geometry Data		
Wing Span (m)	18.81145	22.23985
Wing Area (m^2)	75.8075	64.8455
Wing Aspect Ratio	9.33608	15.2550
Tail Volume	0.495173	0.584886
Spar Box Mass (kg)	1410.77	4154.77
Tail Spar Box Mass (kg)	96.9843	958.344
Wing Root Sweep (deg)	35.0633	37.0883
Wing Tip Sweep (deg)	24.6236	24.6236
Performance Data		
Wing Loading (Pa)	3228.12	3773.83
Cruise C_L	0.30343	0.35472
Cruise C_D	1.17906e-02	1.33607e-02
Inviscid Cruise C_D	3.58472e-03	2.78027e-03
Viscous Cruise C_D	8.20583e-03	9.45829e-03
Cruise Wave Drag C_D	0.00000	1.12211e-03
Cruise L/D	25.7350	26.5499
Range (km)	8.1051e+03	8.3617e+03
Takeoff speed (m/sec)	75.6418	75.4643
Landing speed (m/sec)	54.8138	54.8138
Performance Metrics		
Efficiency range/fuel Km/Kg	0.734955	0.758213
Wing M.F. (spar box/total)	0.036308	0.106927
(Fuel mass)/(wing mass)	7.817008	2.654347

Table 4.3: Baseline Case with drag polars and Similar case with code drag models, M_{cc}offset 0.08

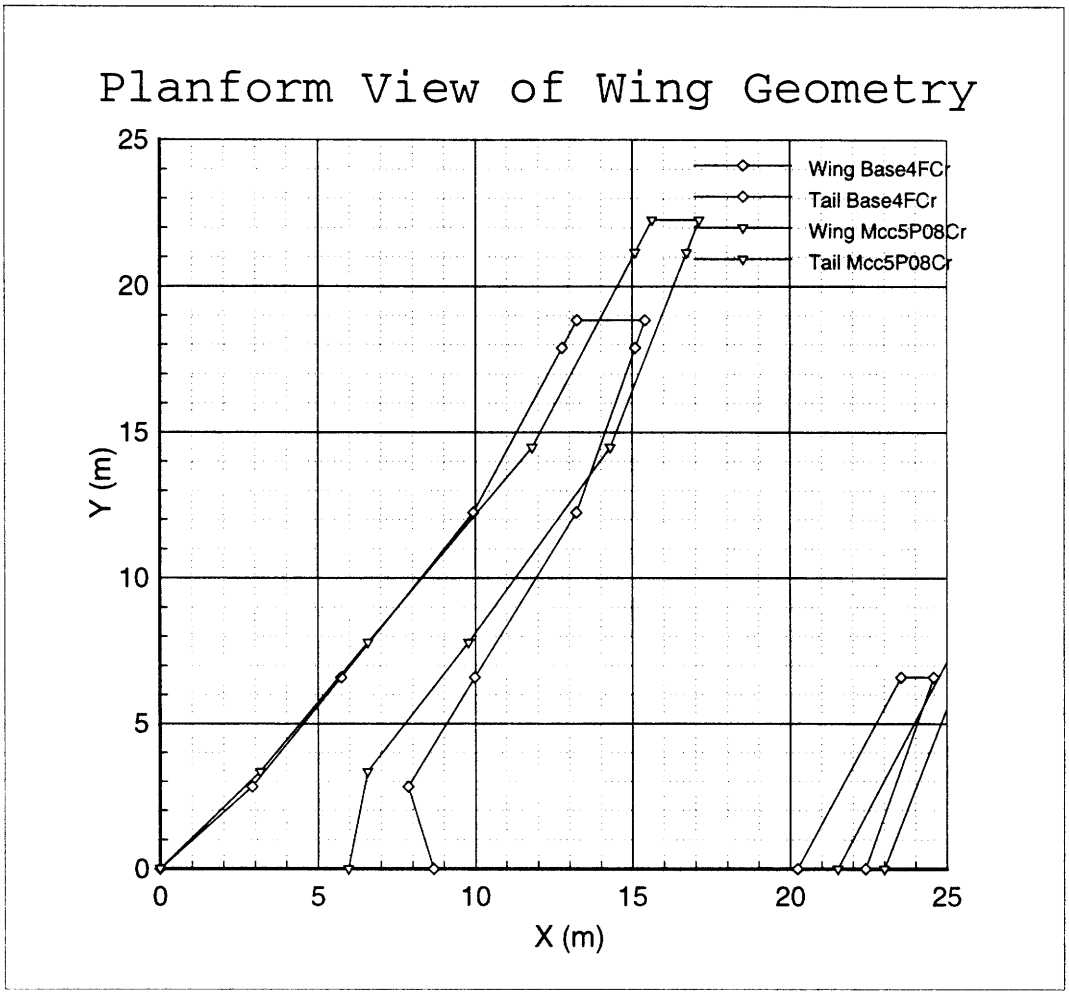

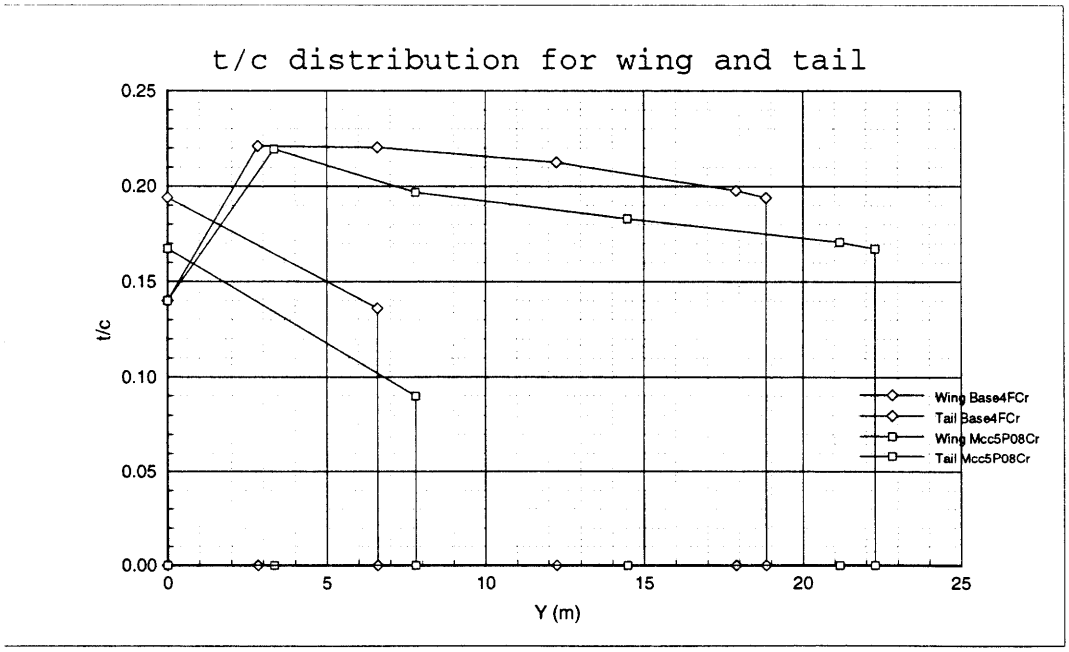

Figure 4-7: Baseline Optimization second aero iteration with Drag polars and Drag models

Chapter 5

Trade Studies Performed with the Code

Once the baseline case had been established, the code was used to run a series of "trade studies" to examine the impact of key design parameters on the final optimized planform. The term "trade study" means to examine the trade-offs necessary to change a performance characteristic. Consider the following question: If a proposed airfoil could reduce wave drag by 3%, but would also induce a higher negative pitching moment, is the airfoil worth investing in? To answer this question, a set of runs are executed using the code to find curves of performance increase for an incremental drag decrease, and corresponding performance decrease for an incremental pitching moment increase. These "trades" can then be used in evaluating the benefit or cost of proposed airfoils for that particular aircraft design.

The nonlinear optimization code offers a unique ability to do trade studies not just for a particular localized portion of the aircraft design, but for the wing and tail as a single unit. One might expect, for example, that if the viscous drag could be reduced to near zero, the wing would grow substantially larger as a higher aspect ratio and lower wing loading were exploited for performance gains until structural weight and wave drag caught up. This example is somewhat exaggerated since such massive changes in planform would tend to invalidate some of the assumptions made by the physical models in the code. For this thesis, a total of six trade studies were done on various aerodynamic and structural parameters such as the airfoil pitching moment, the upper surface Mach number at which wave drag becomes significant, and others described in the next section. The parameters were incrementally varied around the baseline parameter, usually by no more than $\pm$ 20%. The results and analysis are presented in the next chapter.

5.1 Airfoil pitching moment C_{m_0}

Supercritical airfoils, while pushing the shock back and decreasing wave drag, also tend to cause a pitching moment penalty from the lower surface cusp used to get the necessary pressure recovery. The C_{m_0} for these airfoils can be strongly negative where a negative pitching moment is defined as a nose down. This trade study looks at the impact of strong negative pitching moment on the planform design with the expected problems meeting static stability margins.

Baseline Value: 0.0

Trade Range min/max: -0.01 to -0.10

Importance of Parameter: An airfoil with a highly negative pitching moment[1] will require extra down-load on the tail. This translates directly into drag, especially at cruise. At best, the the extra pitching moment cancels some of the drag reduction benefit of the aft loaded foil. At worst, the increase in tail volume needed to supply this down load may be more than is feasible resulting in a poor overall design.

Expected Behavior: As the C_{m_0} is increased, the tail moment arm should increase in an attempt to meet necessary down load constraints without increasing the tail area too much. With a strong nose down pitching moment, the wing will most likely un-sweep a little and the loading distribution will shift towards the center of the wing. Tail volume will also increase.

The next several parameters are related to the structure. See section 2.2 for details on the structural model.

5.2 Upper to Lower skin maximum stress ratio

The upper skin is sized according to maximum compressive stress, while the lower skin is under tensile stress. In addition, the alloys for the two skins are often different. The ratio of these stresses is usually of order 1.

Baseline Value: 1.36

Trade Range min/max: 1.10 to 1.43

Importance of Parameter: The skin is responsible for the majority of the weight of the wing. One of the major reasons for the baseline value of 1.36 is that the upper skin alloy, while stronger, is not as durable in low cycle fatigue. If a lower skin alloy of similar strength could be found, would there be the weight saving benefits?

Expected Behavior: To summarize the weight model, since only one end load is known along the wing, and this is assumed to apply to the upper skin. The stress relations are known, and the resulting skin ratios can be found through an iterative process. Figures 2-1 and 6-3 show plots of stress ratio vs. skin thickness ratio. While a 1:1 correspondence does not exist, a reduction in stress ratio generally indicates a reduction in skin ratio. Since the maximum stress for the upper skin is fixed, this translates to effectively increasing the maximum stress of the lower skin. Thus, as stress ratio decreases, the lower skin should be stronger and thinner and the spar box weights should be lighter. Presumably the optimizer should take advantage of this to find a thinner, higher aspect ratio of about the same weight but higher performance.

5.3 Material density

Baseline Value: $\rho = 2800 \frac{kg}{m^3}$

Trade Range min/max: 2600 to 3000

[1] This tends to be a problem with multi-element airfoils and highly cusped supercritical designs

Importance of Parameter: Adjusting the weight of the material is a quick and easy way to examine what impacts a new, lightweight material with equivalent strength would have on planform.

Expected Behavior: With a lighter, stronger material, the bending loads from structural weight could be reduced resulting in a (slightly) longer wing. Naturally, the entire wing box structure will be lighter for an equivalent structure. However, the optimizer may find that it is even more feasible to build a longer, thinner, heavier, but considerably more efficient wing.

The next two parameters adjust the viscous and the wave drag of the wing independently. This required using the built in drag models instead of the drag polars as were used in all previous test cases. Sections 1.4.6 and 1.4.6.1 contain a summary of the default drag models. Section 4.4 discusses the differences in drag using the polars or the drag model, and figure 4-7 shows the baseline case for each type of drag model.

5.4 Skin Roughness (% skin friction drag)

The viscous drag is calculated from [1, p44]

$$C_f = K_{cf} \frac{0.455}{(log_{10} R_e)^{2.584}} \tag{5.1}$$

Where the K_{cf} is a multiplicative factor to account for "surface roughness". (An empirical correlation for the DC-9 was used to set this value to 1.14 for the original code [1, p46]).

Baseline Value: $K_{cf} = 1.0$

Trade Range min/max: $K_{cf} = 0.98 \rightarrow 1.04$

Importance of Parameter: When using the default drag model, the inviscid drag, which is the drag due to lift and other axial vorticity, is calculated in the Treffetz plane while the viscous drag and wave drag are calculated separately. By varying this multiplicative factor, the percentage of overall drag related to skin friction can be varied. This type of trade would be useful in gauging the importance of increasing the amount of airfoil experiencing laminar flow through surface quality improvement. High surface quality comes at high cost, so an marginal gain in performance would indicate that attempting to improve this area of the design would not be worthwhile. On the other hand, if the wing could be made significantly smaller and lighter by reducing viscous skin friction, this could be quite beneficial.

Expected Behavior: Decreasing viscous drag should allow the wing chord to stretch for the same overall drag. Of course, this would then decrease aspect ratio and increase induced drag so a new balance would need to be found. A larger wing overall would reduce landing speeds and the need for heavy, complex high lift devices (however, since these weights are not evaluated by the code, this will not be taken into account). The optimizer might still see the total reduction in drag and find a slightly larger wing because of the low speed flight conditions. However, because the actual optimization goal is maximum range, It would seem more logical that the planform would remain relatively unchanged, or if anything the extra area would be used to extend the wing span and thus boost aspect ratio which would also improve $\frac{C_L}{C_D}$.

5.5 Effect of Wave Drag

The code compressibility drag model which was described in section 1.4.6.1 first calculates the Mach number at which compressibility drag should occur (M_{cc}) based on C_L and $\frac{t}{c}$. The code then checks along the wing for local $M_\perp > M_{cc}$ and calculates wave drag from $\frac{M_\perp}{M_{cc}}$ empirical relations. The user modification to this technique is to be able to specify an offset to M_{cc} which is the equivalent of reducing upper surface shock strength or moving the upper surface shock aft on the foil as given in equation 1.4. A positive offset, which is a fraction of Mach, effectively delays the onset of mach drag, by a fractional value which will depend on the cruise Mach (always 0.82 for this study) and the original M_{cc} value.

Baseline Value: Not applicable because the Baseline was run with drag polars.

Trade Range: 0.05 to 0.16

Importance of Parameter: The maximum cruise speed of an airliner is related to the Mach drag rise speed of the wing. This is the point at which the flow on the upper wing surface briefly goes supersonic and then returns to subsonic with a shock. Delaying the onset of wave drag until as high a Mach number as possible is the focus of high speed airfoil technology, However, improving the M_{cc} is also very expensive in wind tunnel and computer simulation time.

Expected Behavior: As the M_{cc} is increased the wave drag will decrease. Since Wave drag is the only factor which drives an increase in sweep angle, this should reduce sweep for the full wing and result in a lighter wing. Reduced sweep also allows a better loading distribution at the wing tips without paying a high penalty in negative pitching moment, so the horizontal tail should not have to move as far aft to supply the required down load

5.6 Desired Cruise Mach Number

Baseline Value: 0.82

Trade Range min/max: 0.675 to 0.85

Importance of Parameter: While not a performance parameter in the same fashion as airfoil performance parameters, varying the cruise Mach does have some purpose. The need for increased sweep with increased Mach is obvious and so this type of trade study should serve as a check on process of running trade studies with a planform optimization program. The most interesting parameter will be how much weight penalty will need to be paid for the increased sweep. The straighter and shorter the wing, they cheaper it is to build so the importance of sweep is more than just aerodynamic.

Expected Behavior: The expected behavior is well known; as the Mach increases, the sweep must increase to prevent the wave drag from becoming excessive. This moves the center of lift aft increasing the negative pitching moment. The tail will start to move aft to maintain adequate tail volume.

Chapter 6

Trade Studies Results

This section contains results for the trades described in the last section. The data presentation includes data tables of the same format described in section 4.2.1. There are plots of the geometric and some aerodynamic parameters with the same format as described in 4.2. There is also a set of "trade plots" which are plots of geometry and aerodynamic parameters and also a set of trade plots. The trade plots are a set of 12 performance and geometry parameters which have been plotted with the active trade parameter as the independent variable. These plots show directly the trends of these parameters with respect to the independent trade variable. All figures referred to in the discussion are in the last section of this chapter.

6.1 General Comments on Trends in the Results

Figures 6-5 and 6-6 are typical sets of important parameters plotted against the independent variable for a trade study (in this case, C_{m_0}). Each trade study will have a thorough discussion of the trends in these plots as they relate to the geometry and the optimization process. However, some relationships occur consistently between data sets and can be explained just once in this section.

The wing spar box weight is usually driven most strongly by sweep, not span. The wing span is the straight, y-axis distance, not the distance along the quarter chord of the wing. Thus, a wing of the same span and higher sweep will be effectively longer and heavier. However, in cases where the sweep values are all within a few degrees, the weight is once again mostly a function of span.

The tail span and area tend to be very noisy parameters. In many cases, these values tend to have the opposite trend from the related wing parameters. Like the wing, the tail weight is a function of span, which often maps to being a function of sweep.

As a possible explanation for the wide variance in the tail spans and areas, consider the sizing routines. The function of the tail is to balance the wing with a down-load and provide for positive pitch stability. The tail must be large enough to rotate the aircraft for take off, control the aircraft during a flaps-down go-around and of course provide positive pitch stability at cruise and maximum load conditions. Since the center of lift moves aft as the wing sweep increases, an expected consequence would be for the tail area and weight to increase correspondingly. However, *the optimizer also has the choice of increasing the length of the tail moment arm* (see the note in the next paragraph), a move which comes without any weight penalty since the structure of the fuselage is not being considered. In

most cases, as the sweep increases the tail moment arm is quickly increased to preserve pitch properties, the tail sweep changes very little and the actual areas and weights later fall out of the tail sizing conditions (take off and go-around).

The coordinate system used by the code places (0,0,0) at aircraft center of gravity. One of the design variables used in all aerodynamic optimizations is the location of the wing root quarter chord with respect to the center of gravity. The rest of the wing is extrapolated from this location based on the sweep, panel width, dihedral and taper ratio. The distance from root quarter chord of tail to the center of gravity is fixed, however the movement of the root quarter chord makes it appear that the tail moment arm is increasing. The geometry plots also encourage this perception because the coordinate system for the plots has (0,0) at the leading edge of the wing and the center of gravity location is not shown.

6.1.0.1 Effects of the Static Margin Constraint on Tail Loading Profiles

Another feature to look for in the results is the tail loading profile. This is determined by the static stability constraint, which was discussed in section 3.3.2. When there is sufficient static stability the tail will have an approximation to the standard, inverse parabolic loading. As this constraint becomes marginal the tail loading seems to shift so that the tips are very highly loaded, although the total load on the tail is small and slightly negative. Total failure of the static margin constraint comes as the net tail load becomes positive, still with most of the tail load occurring at the tips. Changing this constraint could have major effects on total planform as will be seen in the results of several trade studies and demonstrated in figure 6-4. The maximum loading on the tail usually occurs at the take off rotation at maximum weight with maximum forward CG location. Figure 6-1 shows a comparison between the $\overline{C_l}$ profiles between two data runs. The K_{cf}=0.99 case was well behaved with sufficient static margin to provide tail down load during cruise. The K_{cf}=1.06 case came very close to zero tail load at cruise. The tail loading profiles at take-off are also shown, and the interesting item to note here is that the increment between take off and cruise loads are quite similar between the cases. In this case, the tail moment arm for the low K_{cf}case is about 3 m shorter than for the high K_{cf}case. This necessitates the higher tail loading at at take off for the low K_{cf}, lower sweep angle cases.

6.1.1 Key to the Trade Studies Plots

There are twelve plots, 6 to a page. The layout is intended to concentrate the geometric parameters on one page and the aerodynamic parameters on the second page. Figure 6-5 is a typical example of a set of geometric parameter plots with C_{m_0} as the independent variable. Proceeding from upper left, upper right, middle left, middle right etc. the plots are:

1. Wing Spar Box weight (kg) This is the weight of the spar box only including skin smeared gauge but no other weights such as ribs etc.

2. Tail Spar Box Weight (kg)

3. Wing Area. This is the total area of the wing planform in m^2 for both halves of the wing (and there is no area taken out for a fuselage). This is the area used to compute the C_L, C_D and other coefficients. This parameter is usually abbreviated S_{ref}

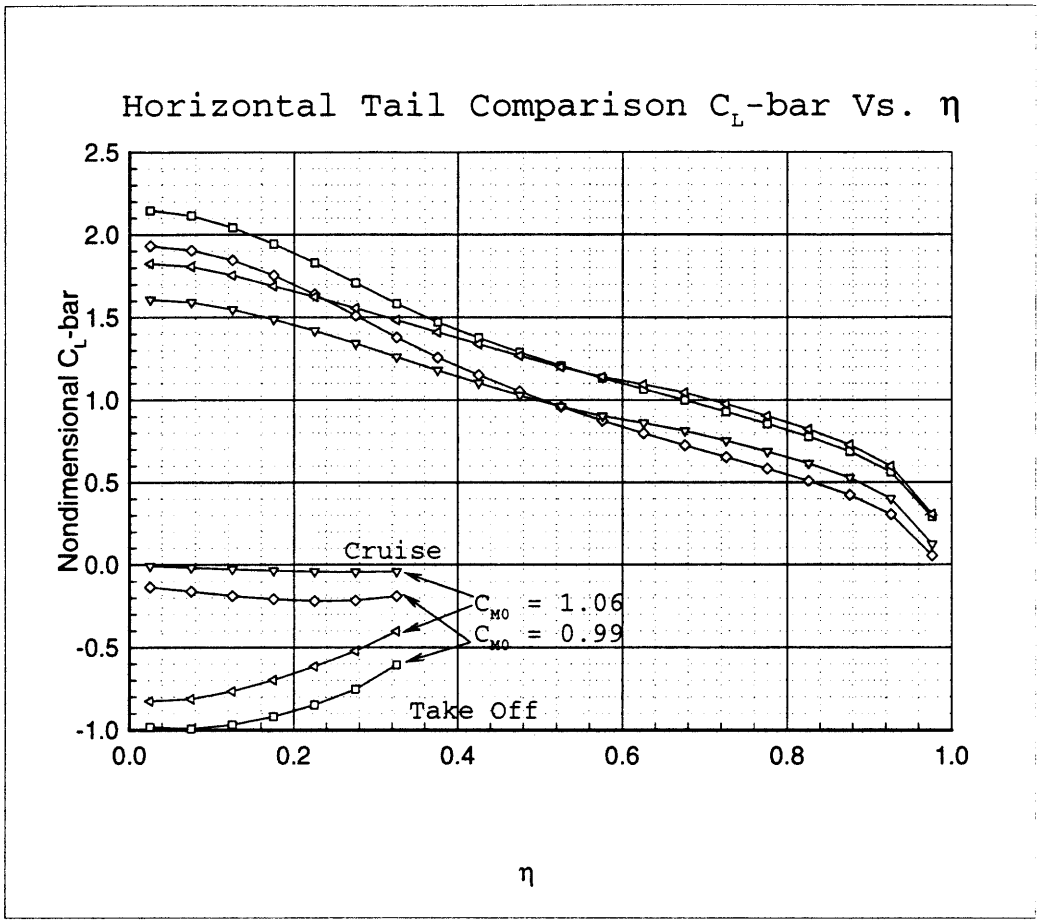

Figure 6-1: Comparison of $\overline{C_l}$ profiles for take off and cruise at small and large K_{cf} values

4. Root element quarter chord sweep in degrees. This is a straight geometric value measuring the sweep of a line drawn from the quarter chord of the root of the wing to the quarter chord of the tip of the same element. This value will be affected by the relative taper. The first three elements have the *same* quarter chord sweep but can have very different taper ratios and so may appear to have different sweep angles.

5. Wing Reference Span in meters is the full wingspan of the final planform in standard (x,y) coordinates (this is the projected span, not the distance along the wing). This parameter is usually abbreviated b_{ref}

6. Reference Aspect Ratio is, as per definition, $\frac{b_{ref}^2}{S_{ref}}$

The second six plots are aerodynamic parameters, see figure 6-6 for a typical example. Proceeding in the same order the plots are:

1. Cruise C_L for the full configuration and calculated at the maximum take off weight (488,000 N)

2. Cruise C_D for same conditions as above.

3. Cruise C_{D_i} which is the inviscid drag calculated in the treffetz plane by the lifting line model.

4. Cruise C_{D_v} for the cases run with drag polars this is actually all other non-inviscid drag including compressibility.

5. $\frac{C_L}{C_D}$ simple combination of the above C_L and C_D curves

6. For cases using the drag polars this plot is Range in km (see appendix A for the equations used to calculate range). For cases which use the built in drag models, this plot is C_{D_c}, the compressible drag at cruise.

6.2 Error Bars

An important consideration when analyzing trends in data is the probable error of the data points. Calculating error bars (data point $\pm$ 1 standard deviation) is not an easy process, especially since there are so many potential sources of error.

As has already been mentioned, none of the final optimization cases actually managed to fully converge. For non-converged cases the optimizer always tags one or two variables which were the most problematic when trying to find a search path. Starting from the baseline case for the Mach Crest Critical offset trade study, a number of "final" cases were re-run. Each case adjusted the the scaling and or step size of the problem variables from the previous case to try to improve the solution. Additionally, a limit was imposed on the number of iterations in the final case stopping the optimization 1 iteration and 2 iterations short of the original optimization. This approach should have the effect of testing the amount of change which is still present in the design variables as the optimizer approaches the final planform. Variables which are still changing significantly between iterations will be subject to much higher error from exactly when the optimizer determines that there is not further search path and quits. The final results were analyzed for the standard parameters of mean, standard deviation and percent standard deviation[10]. This procedure was done twice, once for optimizations using the drag *models* and once for a case using drag *polars*, The results are summarized in table 6.1. The first three columns or data are for the drag models, the last column is the percent deviation only for the polars. Note that in this case, the numbers are for the full wing span and area. Note: for the drag polar case, $C_{D_v} = C_{D_c} + C_{D_v}$ where C_{D_v} is the *viscous* drag (not vortex drag) and C_{D_c} is compressible (wave) drag.

A quick look at the % error figures shows that most of the aerodynamic parameters are quite stable in the final stages of optimization. The planform geometry span and area are very stable. However, the planform sweep is not very stable and shows a deviation of up to $\pm$ 2 degrees. The C_{D_i} is quite stable, but the C_{D_v} shows some error. The only really large error bars go on the spar box weights for the wing and tail. There are two reasons for this. The first is simply that the box weight is sensitive to small changes in sweep and span. The second is that the primary optimization is for maximum $\frac{C_L}{C_D}$, not minimum weight so that in the final phases of the optimization, the wing weight is still fluctuating by as much as 100 kg each iteration while the goal variables, C_L and C_D are changing very little.

Also important from the table is the comparison of the drag polar vs. drag model errors. While some of these were at least same order, there are major differences. The drag polars seem to produce a much more stable wing sweep angle which results in a much lower deviation for wing and tail weights. However, the errors for the actual span and area for the drag polars were quite a bit higher than for the models. In this latter case, the drag model results seem rather optimistic and are most likely particular to this data set which

	Drag Models			Polars
Parameter	Mean	Standard Dev.	% Deviation	% Deviation
Wing Box Weight	2886.11	440.42	15.0	5.3
Tail Box Weight	102.62	16.40	16.0	3.1
Wing Area	148.08	1.54	1.0	1.7
Tail Area	16.67	1.022	6.1	0.51
Wing Span	41.57	0.011	0.03	1.3
Wing AR	11.67	0.12	1.0	1.6
Root Wing Sweep	36.9	3.63	9.9	2.5
Cruise C_L	0.311	0.0033	1.0	0.6
Cruise C_D	0.0127	0.00057	4.5	0.99
Cruise C_{D_i}	0.003163	0.000146	4.6	3.1
Cruise C_{D_v}	0.008660	0.000293	3.4	0.6
$\frac{C_L}{C_D}$	24.56	0.96	3.9	0.79
Range	7736.13	303.05	3.9	0.79

Table 6.1: Statistical error information

had a very stable wingspan.

In consideration of the rest of this chapter, the actual percentage errors are less important than simply remembering which parameters displayed the least stability when analyzing trends, especially with noisy data.

6.3 Optimizer Bifurcation

On a number of the trade studies and interesting pattern occurred involving the wing span. There would be a split between two possible wing spans, the shorter of which would be on the order of 21m $\pm 0.5m$ and the longer of which would be about 3 m longer with the same variance. These changes in span have not been traced to any particular variable or constraint. They are in no way periodic with the design trade variable. The shorter span is the dominant planform the optimizer finds, but out of about 10 trade runs, two or three will come out with the longer wing span.

Attempting to analyze both sets of wings together is a relatively meaningless exercise. The longer wings have vastly different aspect ratios, C_{D_i} values, spar box weights and etc. Although, looking at the overall performance metrics such as $\frac{C_L}{C_D}$ and Range, the planforms come out fairly close. Interestingly enough, the longer wings are usually slightly worse on maximizing $\frac{C_L}{C_D}$ presumably from the penalty paid for the extra weight and drag area which is not fully made up for by the increase in $\frac{C_L}{C_D}$. Therefore, the approach for these results has been to throw out the long wings if there were two or fewer occurrences in the trade study. If there were enough long span wings to make up a family, the two families of planforms were analyzed separately.

Reasons for the bifurcation remain unclear. For most cases, the initial aero optimization finds a wing span which is within a meter of the final planform design value. However, the cases which diverge from this planform do so during the second aero optimization, usually adding about 3m to the span over the course of several iterations.

This bifurcation problem also showed up in the root quarter chord sweep values. For example, all of the C_{m_0} planforms have about the same sweep except for the C_{m_0}=-0.015 which is swept nearly 5°higher than the rest. In this case, there is a possible link to certain constraints which may affect this behavior. The constraint is the "static margin" which, when set to a large enough positive number, will force the optimizer to find a statically stable planform with the center of gravity ahead of the center of lift and the horizontal tail providing a down load. The value of the static margin must be determined by the user, and it can vary anywhere from 1.5 up to about 4. If the margin is too small, the tail will shift into a lifting surface. If the margin is too large the tail will carry a huge inverse load and become very heavy. There are also some significant changes in sweep which go with the changeoveaccommodateA slightly low static margin displays an odd, linear tail loading distribution with the maximum load at the tips. This is usually accompanied by an increase in wing sweep which has two effects. The center of pressure should move back, which should make the wing more stable, but, on wings with a negative C_{m_0}, the integrated sum of the pitching moment moves back as sweep increases. Since this is a negative C_{m_0} applied behind the center of mass, the result is a nose positive wing pitching moment. A design which is only borderline stable will be caught in a region where any one of several small changes in planform can lead to a significant changes in final sweep value.

Unfortunately, this problem was not easily solved by simply increasing the static margin. In some cases this approach worked (most notably the Cruise Mach Number trade study). However, in other cases, an increased static margin simply led to a poorly converged case and a very heavy tail which was being forced into down loading but still with the adverse, linear tail loading profiles.

The skin stress ratio trade study has a good example of this behavior. In the skin stress ratio trade study a stress ratio of 1.30 produced a long wing, while 1.27, 1.31 and most of the other cases produced the regular shorter wing. The run time outputs for cases 1.30 and 1.31 were examined with the intent of finding any design variable or constraint which seemed to be significantly different. The very first iteration of the 1.30 case increased the span by over 1 m, while the wing span for the 1.31 case hardly changes over the full optimization run. From that point, the wing span, sweep and weight are, of course different, but all other design variables and constraints behave consistently. The longer wing is not any more over-constrained than the short wing so that this bifurcation should not be the result of the optimizer running along a set of constraints looking for a way out.

6.4 Coefficient of Pitching Moment

The results from the C_{m_0} trade study begin with figures 6-5 and 6-6 show the trends in a specific variable across the runs. The independent variable has a range of $C_{m_0} = -0.10 \rightarrow -0.01$. All C_{m_0} values are negative, so for this section, the expression "increasing C_{m_0}" is meant to mean "increasingly negative C_{m_0}".

Wing and Tail Box Weights and Root Sweep Weight of the wing spar box decreases steadily with increasing C_{m_0}. The reason for this is clear in the plots of wing geometry (figure 6-7 for the various C_{m_0} values. The wing span tends to decrease as C_{m_0} increases, and there was also a minor decrease in sweep with increasing C_{m_0}. Reasons for the decrease in sweep will be discussed in the Wing Area and C_D sections. Note: as mentioned in section 1.4.1.1, the structural model sizes the wing for bending loads

only. Were the effects of torsion included, parts of a wing with a high C_{m_0} airfoil might be sized instead by torsion thus increasing weight again.

The tail mass has the opposite trend of the wing mass. In this case, the reason can be found by Looking at the tail loading profiles in figure 6-8. As C_{m_0} increases, the tail is carrying an increased load to compensate for the wing pitching moment.

Wing and Tail Reference Areas The Wing area peaks at C_{m_0}= -0.04 and then falls off again. This behavior requires looking at several parameters for the pattern of optimizer behavior. The AR, which on average increases as C_{m_0} increases, the wing span, which peaks and falls off, and the wing sweep, which is more easily visualized from the geometry plots, 6-7. Looking at all three of these we can trace the following path: As the C_{m_0} first starts to increase, the optimizer responds by un-sweeping the wing. This is a natural response since a swept wing provides greater pitching moment which must be then supported by the tail, which increases tail weight and induced drag. However, un-sweeping the wing will increase the compressible drag, so the optimizer looks to make up for this by extending the wing to increase AR and reduce the C_{D_i}. This also increases the wing area. As the C_{m_0} continues to increase however, additional increases in span are not feasible from a weight standpoint, so the wing area must decrease to get the same aspect ratio, and it becomes more desirable to reduce drag by reducing the amount of wing, which eventually results in a shorter, straighter and smaller (area) wing than the low C_{m_0} starting point. The Tail Area (not shown) increases steadily with increasing C_{m_0} as the tail needs to provide more pitch authority.

It will be noted that there is one case which sticks out as contradicting at least some of these trends. This is the C_{m_0}=-0.015 case which has several more degrees of sweep at the root than all of the other wing planforms. From figure 6-8, this run clearly exhibits the only slightly negative tail loading and poor tail lift distribution which is characteristic of a design bordering on insufficient static stability. However, since all designs of higher or lower C_{m_0} had plenty of static stability, it would appear that the optimizer has found a negatively stable *optimization* point where attempts to improve performance actually drive the planform away from a reasonable design. Such is the hazards of the nonlinear optimizer with such a large number of design variables and constraints. It is up to the user to spot and throw out this type of behavior even though all standard indications, such as the convergence errors, point to the case being perfectly reasonable.

Reference Span and AR The wing span Peaks at $C_{m_0} = -0.03$, then falls off gradually. This trend was explained in the explanation of Wing Reference Area. The AR increases steadily with increasing C_{m_0}. This behavior is anticipated as a method to counter-act the performance loss that should accompany the increasing C_{m_0} due to increased tail load.

Cruise C_L and C_D parameters These parameters display an interesting bucket shape, with a minimum at C_{m_0} = -0.04 which is also the value for maximum wing area. Since the weight is constant the lift and drag scale quite closely with area.

$\frac{C_L}{C_D}$ **(LonD)** Is the combination of the already discussed C_L and C_D curves. The interesting part here is that there is still a bucket shaped curve with a minimum at

cmz=-0.04 and a maximum $\frac{C_L}{C_D}$ occurring at C_{m_0}=-0.10. The planform at C_{m_0}=-0.10 is the smallest (area), heaviest and has the highest AR among the planforms. It is also the only design with increased the tail volume.

This surprising result goes directly against the predictions of steadily decreasing performance with increasing C_{m_0}. Is it possible then, that some finite value of C_{m_0} is actually more efficient for a trimmed planform than none at all? A more plausible explanation for this performance curve lies in the optimization path. In this case it is less likely that having a wing with a specific C_{m_0} is preferable, and more likely that in the inevitable string of compromises to reach an optimum design, the choices made for the C_{m_0}=-0.10 design reached a better conclusion than for no C_{m_0}. To test this idea the finished planform from the C_{m_0}=-0.10 design was run again with C_{m_0}=0 and the planform rigid. Table 6.4 shows a few numbers from the results of that test. An airfoil with no pitching moment can clearly be made lighter and more efficient for a given planform (The $\frac{C_L}{C_D}$ here does not reflect that because both aircraft use the same gross weight to find $\frac{C_L}{C_D}$, and of course planform is fixed).

Data for:	C_{m_0}=-0.1	C_{m_0}= 0.0
Spar Box Mass (kg)	2330	1820
Tail Spar Box Mass (kg)	171	106
Cruise C_L	0.35	0.35
Cruise C_D	1.20e-02	1.18e-02
Inviscid Cruise C_D	3.10e-03	2.90e-03
Viscous Cruise C_D	8.91e-03	8.86e-03
Cruise L/D	28.73	29.32
Range (km)	9050	9240
Efficiency range/fuel Km/Kg	0.82	0.84

Table 6.2: Comparison between the final planform for C_{m_0}=-0.1 and the same planform run with C_{m_0}=0.0

Range The range in this case was on the order of 8500 km, at which point the effects of take off fuel burn etc. are negligible and the Range is approximately proportional to the $\frac{C_L}{C_D}$.

The C_{m_0} trade revealed some surprises in the $\frac{C_L}{C_D}$ curve which contained a pronounced minimum at C_{m_0}=-0.04. However, on inspecting the mechanism by which this optimum point was reached it seems that this performance optimum is more a function of the C_{m_0} parameter supplying a kick to the optimization path than an actual performance gain.

6.5 Skin Stress Ratio

Figures 6-9 and 6-10 show the results of the trade studies with the skin stress ratio as the independent variable. This ratio governs the wing spar box weight by changing the skin thickness ratio between upper and lower surfaces as was discussed in section 2.2. For this trade study the values of the Skin Stress Ratio (abbreviated Sr) ranged from 1.27 to 1.46

This trade study turned out to be quite noisy and in fact was taken twice. The initial data set contained both a high amount of noise and two instances of the wingspan bifurcation described in section 6.3. More data points were taken around the two bifurcated points to see if there was any pattern to the anomaly, but none appeared. However, this second attempt at data was over a month after the original data set. The code had been re-compiled following very slight modifications and used for a number of runs before re-running a test case to verify the output of the new compilation. Unfortunately the test case run did not fully agree with the data from the previous executable.[1] Therefore the entire skin stress ratio data set was taken over again for the sake of maintaining within-data-set consistency. This second data set did not display the wing span bifurcation problems exhibited by the original data, but it was just as noisy. Curve fits were attempted, however, since most of the data fluctuations were well outside of 1 or even 2 standard deviations from the calculated error bars in table 6.1, a curve fit seemed to be the incorrect approach to the data.

There are many possible reasons for the instability dealing with the optimizer oscillating between constraints, forking on a certain value of a design variable etc. With over fifty design variables and several hundred constraints this is very difficult to track down. Also to be considered: from examining table 6.1, in normal optimization the spar box mass has by far the most error for relatively similar looking planforms. In this case, this weight is being directly affected by the independent variable so that one of two outcomes could be expected. The first is that adding small perturbations into an already noisy system would have little or no impact since the changes would also be in the noise. The second outcome would be that the optimizer could be perturbed far enough off the usual path to find a completely different planform. As will be seen in section 6.6, another case which exhibited significant bifurcation was the trade done with the density of the structural material as the independent variables. This case (6.6) also directly modifies the weight of the wing and and would be expected to have the same noise problems as the stress ratio.

Expected behavior is also a tricky matter and it helps to break the problem down into two phases. The first phase is the fixed planform optimization for minimum weight. As discussed in section 5.2, by maintaining a fixed maximum stress on the upper surface and then adjusting the stress ratio, the effect is the same as adjusting the maximum stress in the lower surface. One would naturally expect that the lower the stress ratio, the stronger the lower skin material and the lighter the spar box. Figure 6-2 shows the spar box weights after the final fixed planform, minimum weight optimization and the spar box weights follow exactly this pattern. This is a good confirmation that the model and code are working properly.

A much more difficult problem is predicting what effect this will have on the final planform. The initial planform is clearly lighter with reduced stress ratio, but as to whether the optimizer will take advantage of this for increased span, sweep or just plain reduced weight is unclear. Since the MTOW is a fixed number, as is the amount of fuel on board, it would seem that the weight of the spar box is not a very strong driver in the aerodynamic

[1] The code displayed several warning signs of internal instabilities. The most telling of these is that answers differed depending on optimization flags set at compile time. The answers from a code compiled with the debugging flag were almost complete garbage, and there was considerably difference between optimized and non-optimized code. This is without question a sign that somewhere in the code something is very wrong, most likely having to do with memory management. However, the code is long and complex and time was short and this type of problem is very difficult to track down. Therefore, as long as a specific compiled version of the code continued to produce self consistent answers, the deeper problems were ignored. If the code ever gets used on a regular basis this problem will be quite serious and need to be fixed.

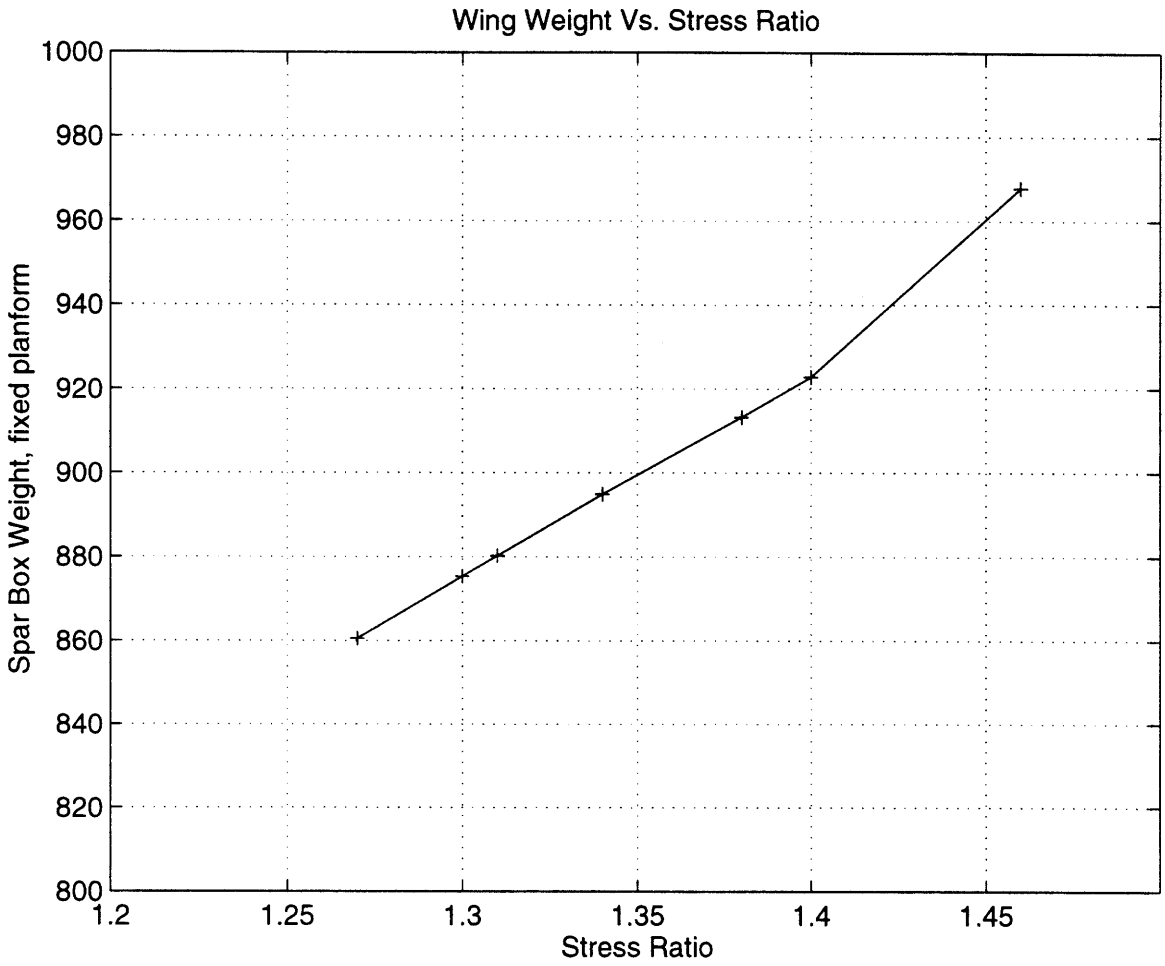

Figure 6-2: Spar Box Weight Vs. Stress Ratio for fixed planform structural optimization

optimization process, so some aerodynamic improvement such as decreased $\frac{t}{c}$ or increased AR at a relatively constant weight could be expected. However, there is the added complication introduced by the fact that the stress ratio *does not* scale directly with the skin thickness ratio. To recall why, here is a brief summary of the iterative process used to to find the skin thickness ratio given a desired stress ratio.

1. The optimizer picks a panel end load
2. This load is assumed to be for the upper skin, and is directly related to the upper skin thickness by definition: (End Load) = $\sigma_{max} t_s$. The maximum allowable skin stress (σ_{max}) was set by the user in the input deck, and this sets the skin thickness (t_s) required.
3. From the t_s for the upper wing, an iterative solver can be used to find the actual skin *thickness* ratio.
4. These skin thicknesses determine the spar box weight.

Figure 6-3 shows plots of Stress Ratio Vs. skin thickness ratio for several different locations (η) along the wing. These figures were for the baseline case, fully optimized wing.

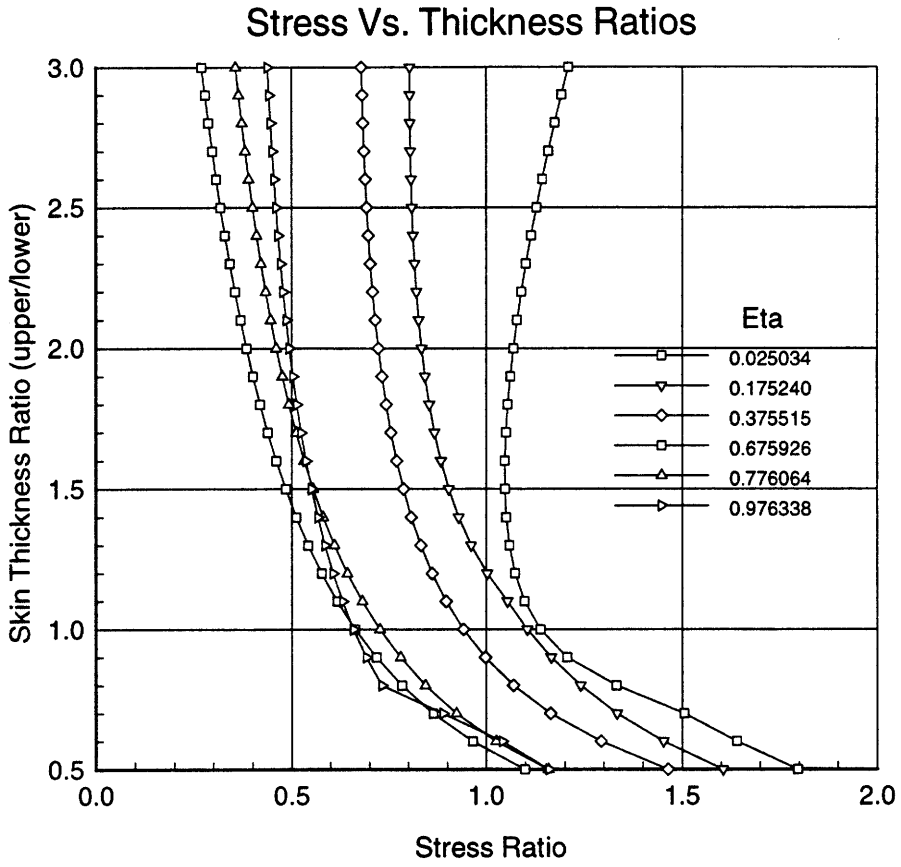

Figure 6-3: Skin stress ratio and thickness ratio relationship

There is no simple relation on this graph since the ratios depend on the quadratic terms of the geometry (moment of inertia). The geometry consists of parabolic skins which are not symmetric in any axis so the relationships change when the geometry is scaled to local chord. The stress ratios set for the trade study were mostly in the vicinity of 1.36, that is, the upper skin was significantly stronger than the lower skin[4]. The graph shows skin thickness ratios on the order of .5 to .75 for these stress ratios, so that the lower skin is up to twice as thick as the upper. As the stress ratio decreases, the number of locations where the thickness ratio is also one increases. Since the σ_{max} was fixed, for a given end load the upper skin thickness would be the same and the lower skin gauge would decrease. So again the simple answer is that a decreased stress ratio should make for a lighter wing. However, as the figure shows, the weight ratios promptly change as the geometry scaling changes, so that less weight savings benefit is seen as the airfoil scales down towards the wing tip. This would strongly inhibit the optimizer from trying to reduce $\frac{t}{c}$. In the end, it is very difficult to predict just what effect this parameter should have. Because of the noise in the data, the "trends" which might exist are hardly convincing.

6.5.1 Stress Ratio Structural Parameters

Wing and Tail Spar Box Weights The Wing spar box shows a trend of maximum weight

right in the vicinity of the baseline Stress Ratio (1.36). From the geometry plot, 6-11, the wing at 1.27 is lighter and longer than most of the other wings which would be as predicted. The tail box weight is quite noisy with no particular trend.

The rest of the trade parameter plots will be discussed as a group since most of the information is closely related.

The wing area and span both decrease gradually as the stress ratio increases. This results in an almost constant aspect ratio distribution with the exception of the 1.4 case. However, in looking at the various components, it is not clear if the 1.4 case is an exception or a logical trend. From the sweep plots, 1.4 is fine and 1.38 is the noisy point. From the Wing span plots, 1.4 is the noisy point with all other falling inline. From the area plots, both of these points are just fine.

6.5.2 Aerodynamic Parameters

The aerodynamic plots are considerably smoother indicating that despite the rather abrupt changes in geometry, the optimizer was still focusing on the same optimum performance range. C_{D_i} and to a lesser extent C_D increase steadily with increasing stress ratio. This indicates that the optimizer is indeed taking advantage of the lighter wing structure to improve aerodynamic performance and the spar box weight is following as a secondary, and not very smooth result. The C_{D_v} is almost completely flat, with perhaps a very small negative slope (decreasing C_{D_v}) over the optimization range. This leads to a full C_D trend of gradual increase with increasing stress ratio. Again, this is to be expected since the higher stress ratio is not as efficient and this will have to show somewhere even if the planform optimization process is good at masking where exactly the inefficiency lies. It should be a straight matter of the spar box getting heavier, but as the optimizer changes all the other planform variables to compensate, the net result apparent to the user is that there is an optimum $\frac{C_L}{C_D}$ at a stress ratio of about 1.34. Just to make sure this is completely obtuse, this is the heaviest wing with one of the smallest areas. Both of these drive up the C_L with the end result that the $\frac{C_L}{C_D}$ turns out the highest

6.6 Wing Material Density

Changing the density of the wing structural material has the same effect as changing the strength/weight of the material in use. The changes in ρ made here were not drastic enough to indicate the effects of a totally new material such as a composite wing. The real-life explanation would be an improved alloy of aluminum which slightly improves the strength to weight properties.

The discussion of the stress ratio parameter noted that the structural variables were the most prone to error which ended up having two consequences. The first was that the data was noisy, the second was that for two cases the optimization diverged with the result of substantially increased wing spans. For this parameter, the noise of the overall data set was lower, but there was a much more obvious bifurcation. Of the seven final planforms which converged to a usable tolerance, 3 had wing spans of almost 24m, the other 4 has spans around 21 m. (Additional cases which finished but did not converge well enough to be counted in the final data set also exhibited this bifurcation). Figure 6-16 shows the final planforms for the shorter spans, and figure 6-17 shows the longer spans. Note that there is **no** logical split in the actual ρ values. The short spans include ρ=2600,2825,2850 and

3000 $\frac{kg}{m^3}$ while the long spans include ρ = 2700, 2750 and 2900 $\frac{kg}{m^3}$. (Baseline value for aluminum was 2800 $\frac{kg}{m^3}$). Figures 6-14 and 6-15 have plots for both families with the data points for the short wing indicated with an "o" and the long wings with a "+". There were only 3 long wings and with the usual scatter, there is very little trend information. The data is included for comparison but will not be analyzed for relevance to the independent parameter.

Spar Box Weight The wing weight is most closely tied to the sweep of the wing. The net trend in box weight was remarkably flat considering that the material density was changing and box mass is simply ρA where A is the cross sectional area. However, from the geometry plots in figure 6-16, the optimizer has taken advantage of the changes in rho not to reduce the box weight but to increase sweep and decrease wing thickness. As the performance plots will show, this approach didn't actually work. The tail spar box weight continues the trend of mirroring the wing weight.

Area The wing area decreases with increasing ρ This at first sounds counter-intuitive, but since the optimizer has tended to keep the wing mass constant, so the area drives with the sweep. The highest ρ is also the minimum sweep and hence the minimum area for the same projected wing span. The tail area, as always, is noisy and mirrors the wing area to some extent but is too noisy to draw any conclusions of trend.

Span and AR The wing spans were remarkably constant, with ever so slight an increase as ρ increased and the sweep decreased. The corresponding change in area also meant a slight increase in Aspect Ratio as the ρ increased which leads into the rather backwards looking performance figures.

C_L and C_D Both of these parameters were steady enough to count as almost flat. However, there was a slight increase in C_L as ρ increased and the wing area shrank. There was a corresponding decrease in C_D especially C_{D_i} as the aspect ratio increased so that when the $\frac{C_L}{C_D}$ is computed, there is an obvious trend (or really more of a jump) to a higher performance as ρ *increases.*

The results from this trade study were quite unexpected. Instead of a healthy performance gain with a decrease in ρ, the opposite occurred. This appears to make no sense. Why would an inferior material of lesser strength to weight produce a better wing? The answer lies in the weighting of the driving factors. From the output geometry, it is obvious that the optimizer finds drag to be a considerably stronger driving factor than weight. While all final wings are about the same weight, the optimizer takes advantage of the lighter material to increase wing sweep and decrease wing thickness in an attempt to reduce the C_{D_v} and C_{D_c}. This ultimately backfires since the heaviest material now produces the wing with the highest aspect ratio, least pitching moment, smallest area and, as a result, better performance.

This shows that the optimizer does not follow the expected path in configuration space.

6.7 Effects of varying the Skin Roughness Parameter

By varying the K_{cf} factor from equation 1.3, the amount of C_{D_i} compared to C_{D_v} for a fixed planform should change. The parameter was varied from 0.98 to 1.10 to see what

K_{cf}	C_D	C_{D_i}	C_{D_v}
0.98	1.380e-02	3.285e-03	9.205e-03
0.99	1.308e-02	3.127e-03	8.893e-03
1.01	1.366e-02	3.289e-03	9.263e-03
1.03	1.384e-02	3.383e-03	9.255e-03
1.04	1.338e-02	3.475e-03	8.966e-03
1.06	1.217e-02	2.749e-03	9.416e-03
1.10	1.477e-02	3.389e-03	1.020e-02

Table 6.3: Component Drag Data for Skin Roughness coefficient trade study

effect this would have on the final planform sweep, span etc. Table 6.3 shows the Cruise C_D, C_{D_i} and C_{D_v} for each condition.

From the table, the C_{D_i} was very stable and accounted for about 25% of total drag. The C_{D_v} was about 67%, although this varied by about ±3%. Thus the optimizer seems to find a relatively constant balance between the three drag components despite artificial offsets. To do this will require planform modification as can be seen in figure 6-23. Since C_{D_v} accounts for about 2/3 of the total planform drag, it would seem that modifying this parameter even a small amount should have a strong effect on the final planform.

The predicted trends from 5.4 were that a decreased C_{D_v} value would mean that the wing area could be increased without paying any drag penalty. The optimizer was expected to take advantage of this phenomenon especially in the low speed regime and design a slightly larger wing. However, it was also anticipated that there would be an overall decrease in cruise C_D, which figure 6-22 shows is clearly not happening.

Given that the optimizer will most likely balance component drags to quite steady percentage contributions and further that the drag of the complete planform is expected to stay almost fixed, the original predictions need to be reconsidered. There is also the problem of losing the changes in the noise as the following discussion will show.

Overall this data set was quite noisy. A lot of data was taken, most of which had to be discarded as the optimizer took off on wild tangents. The final data plotted here was actually from the second aerodynamic iteration since most of the runs were not able to complete the third. Often there would appear to be some bifurcation problems, but this was never consistent enough to define two distinct families of sweep or wing span.

There is a total spread of 6% change in wing area, which would mean that the C_{D_v} should theoretically decline 6% for the same area, or the area should decrease by about 6% to keep the C_{D_v} constant. The fluctuations in C_D over the trade studies is up to 4.5%, although usually within ± 1%. The actual C_{D_v} values (with the exception of K_{cf}=0.99) actually *decrease gradually* as K_{cf} *increases.* At the same time, the C_{D_i} is showing a steady increase with increasing K_{cf}. It should be noted that all of these variables are changing on the order of 6%, although it is not clear as to whether this actually means anything.

Spar Box Weights The wing spar box weight is remarkably well behaved, although this is to be expected from figure 6-23. The spans of the wings are quite constant and for the first four cases the sweep does not vary much. In fact, the wings fall into two families, the 0.99 and 0.98 cases are very similar and are a bit more swept than the 1.02 and 1.03 cases. (Note: the 0.98 case is not shown, but is nearly identical

to 0.99) The 1.04 case is just completely off the wall. This was not expected, the change in K_{cf} was certainly not extreme. On the other hand, the 1.04 case converged quite nicely - better than most of the other cases, and it isn't different enough in planform to consider it to be part of a bifurcation family. In any case, there is a steady decline in box weight over the full range of K_{cf} with the initial decline being related to decreasing sweep. For the 1.04 case, the sweep increased significantly, but at the same time, the span decreased by over 1m for a net decrease in box weight

The tail box weights actually don't mirror anything anymore. The weights fluctuate a huge amount, $\pm$ 100% and as usual show no specific trend.

Wing and Tail Areas With the exception of case 1.04, the wing areas are also nicely behaved, although there is not obvious trend towards decreasing wing area as K_{cf} increases. Without the 1.04 run, there would be a slight negative slope to a linear curve fit, but the last point is many standard deviations off course and foils any attempts at curve fitting. However, it is important to note that the trend, if any can be inferred from the noise, is to *reduce* wing area as K_{cf} increases. At least this parameter is more or less behaving as originally predicted.

Span and AR Again, 1.04 is the anomaly, otherwise there is a mostly consistent and quite gradual decrease in span with increasing K_{cf}. This trend is matched almost exactly with the AR, which means that as the area is decreasing to compensate for higher C_{D_v}, the wing span is also decreasing, and in fact decreasing faster than the decrease in area so that the C_{D_i} is not being maintained. Again, the 1.04 case drops almost off the chart with a large area and short span.

C_L and C_D The C_L is directly related to wing area, but due to the smaller values, the fluctuations are not as apparent. This graph shows the typical variation which is on the order of 6% or less. The variations in C_D are even less, but there is not clear trend in these plots, that will have to wait for $\frac{C_L}{C_D}$.

Drag components The C_{D_i} graph shows a remarkably smooth curve with a steady positive slope for increasing C_{D_i} with increasing K_{cf}. This relates mostly to the associated decrease in AR. The C_{D_v} is not as well behaved, but overall shows (ignoring case 0.99 out of sheer desperation), a clear *decrease* in the C_{D_v} values with *increasing* K_{cf}. Why would this be? The area is certainly not shrinking as fast (percentagewise). Perhaps the answer is in the calculation of areas. The reference area as graphed here is the straight geometric planform area, defined simply as the straight geometric area of the trapezoid formed by two element breaks and the associated leading and trailing edges. The area for drag is actually corrected for wetted area, sweep and appears to be compensated for C_L From the code, the correction for wetted area is:

$$S_w = 2.04(1 + S_2\frac{t}{c}) + \left(\frac{t}{c}\right)^4 \tag{6.1}$$

Where the S_2 is another sweep correction factor:

$$S_2 = 2 - 0.25\frac{cos(\lambda)}{\sqrt{1 - .25cos^2(\lambda)}} \tag{6.2}$$

The $\frac{t}{c}$ is on the order of 0.2, but raised to the fourth power this is negligible. However,

the S_2 term is quite large, and introduces a dependence on sweep. The combined effect of a first order $\frac{t}{c}$ and S_2 is on the order of 0.35, which means that both sweep and $\frac{t}{c}$ are linked to changing the viscous drag (this was not known until after the data had been taken). This may explain the moderately large range of $\frac{t}{c}$ values shown in figure 6-23 and also the sudden sweep shown in case 1.04.

$\frac{C_L}{C_D}$ and Range The values for the $\frac{C_L}{C_D}$ are also a little noisy, as is to be expected from the components. However, there is a fairly obvious trend towards decreasing $\frac{C_L}{C_D}$ with increasing K_{cf}. This is perhaps the most interesting result from the case. We have seen that the optimizer has tried hard to keep the C_D fractional components roughly equivalent, and indeed keep the total planform C_D mostly constant. However, in the end the price paid for this was a decrease in performance with the increasing drag. The range of course shows this same trend amplified.

As has been described above, the data from this trade run was disappointing. This should have been a clear cut case where the drag was being deliberately modified in a way which the optimizer should have tried to compensate for by manipulating the planform. As seen from the noise, it turned out to be not that simple. Complicating the matter is the fact that the skin friction was not calculated off the simple geometric area, but rather a complicated formula which modified the area for sweep and $\frac{t}{c}$. This has the effect of coupling the K_{cf} modifications with the C_{D_c} since these are the two parameters which would usually be the driver of C_{D_c}.

The result of this was to produce some startling changes in wing sweep over a rather small range K_{cf}, and a rather drastic change in sweep as K_{cf} was further increased. However, while the optimizer managed to keep total drag constant, it was not able to compensate fully for the increase in C_{D_v} with a corresponding decrease in C_{D_c} and C_{D_i} with the net result being simply that if C_{D_v} is increased, there will be a performance loss.

6.8 Crest Critical Mach Number Offset

As discussed in section 5.5, adjusting the crest critical mach number offset effectively adjusts the mach number at which the drag model starts applying a wave drag to the wing. From equation 1.4, the value of the offset does not have a direct correlation to what local Mach number governs the onset of wave drag.

Naturally this trade study was done using the built in drag models. The only other trade study to do so was the skin roughness coefficient (K_{cf}) trade study, and for those cases the Mach Crest Critical (Mcc) offset was set to 0.25 This is essentially the same as setting it high enough that the influence of wave drag on the final planform is minimal. This means that there was no "baseline value" of Mcc offset to bracket with the trade study, so a range of values from 0.0 up to 0.14 was used. Several values higher than 0.14 were tried, however there was minimal change after that point. Table 6.4 shows the component breakdown for cruise drag for each of the trade cases. The last column is the $\frac{C_{D_c}}{C_D}$ and shows a steady decline from a maximum of 40% down to about 9%.

Note: The changes in planform and performance implied by these large changes in drag distribution meant that the range of final planforms was considerably larger than in the previous studies. The axis limits on a number of the graphs in figures 6-25 and 6-26 had to be enlarged to show all values. In addition, the geometry plots in figure 6-27 have axis values from $0 \rightarrow 30$ which is slightly larger than the usual $0 \rightarrow 25$

Mcc Offset	Cruise C_D	C_{D_i}	C_{D_v}	C_{D_c}	% of total C_D
0.0	1.91e-02	3.86e-03	7.66e-03	7.57e-03	0.40
0.03	1.51e-02	3.58e-03	8.09e-03	3.39e-03	0.23
0.06	1.16e-02	3.44e-03	7.49e-03	6.99e-04	0.060
0.12	1.26e-02	2.11e-03	9.42e-03	1.10e-03	0.087
0.14	1.28e-02	2.12e-03	9.57e-03	1.12e-03	0.088

Table 6.4: Component Drag Data for Mcc Offset coefficient trade study

6.8.1 Geometry

Overall the data trends from this trade study were refreshingly logical. The expected results of modifying the contribution of wave drag of course is that higher wave drag will increase the wing sweep and decrease $\frac{t}{c}$. Note: *higher* wave drag is *lower* Mcc offset so that looking at the plots, the wave drag proceeds from left to right, highest to lowest. The sweep plot in figure 6-25 shows the desired trend in Sweep (with a little glitch at Mcc=0.03). The $\frac{t}{c}$ plot in figure 6-27 shows two families of $\frac{t}{c}$, with a significantly thinner wing for the low Mcc, high wave drag cases. The same figure shows the usual planform plots. There is a significant difference in wing spans and sweeps (not shown is the Mcc=0.12 case, which falls nicely between Mcc=.14 and Mcc=0.06). With these figures in mind, the usual analysis of parameters is:

Wing and Tail Spar Box Weights Unlike the previous cases where the wing spans were relatively constant and sweep was the strong driving factor for spar box weight, wing span and thickness are now the major drivers for box weights. While the $\frac{t}{c}$ decreased for the low Mcc cases, the actual chord increased significantly so the real thickness of the wing is higher, and the span is short resulting in a light spar box despite the high sweep. The Tails showed the *same* trend (again, opposite from normal), which is quite logical from the figures since the tails also tended to grow long and thin (and heavy) with increasing Mcc. It is also worth noting again that the structural model sizes the spar box based *only on the bending load* while a highly swept wing would have significant amounts of torsional wing sizing.

Wing and Tail Areas The wing area drops steadily with rising Mcc, The primary driver for this was to reduce the $\frac{t}{c}$ of the wing without making the wing too thin (heavy). With very high wave drag, the wave drag is a stronger driver than C_{D_i} and C_{D_v}, although total performance suffered substantially, as will be seen in the next section. The tail areas (not shown) followed roughly the same trend decreasing from $18m^2$ down to $16m^2$

Quarter Chord Sweep Also behaves nicely with steadily decreasing sweep as Mcc increases. The slight glitch in the plot is for Mcc=0.03, and this can be explained by looking at the actual planform in figure 6-27. The Mcc=0 and Mcc=0.06 cases which both have higher quarter chord sweep do *not* need a trailing edge yehudi in the inboard element (since the wing chord is already large enough to accomedate the landing gear), while the Mcc=0.03 case has as trailing edge nearly perpendicular to the flow. Since the quarter chord sweep is a very simple geometry value, this change in taper

registers as a change in sweep. A more accurate comparison is simply looking at the wing tips where indeed the Mcc=0.03 case is slightly less swept than the Mcc=0.06 case. However, these differences are also within the error bands on wing sweep seen in table 6.1

Wing Span and Aspect Ratio As is obvious from the geometry plot by now, the high Mcc values were accompanied by very much higher sweeps, with corresponding changes in aspect ratio. The effects of the aspect ratio changes will be very obvious in the performance section. Note: Both of these graphs needed to have the axis changed to fit all the data.

6.8.2 Performance Parameters

This section refers to figures 6-26 and 6-28. Note: the usual plot for Range has been replaced with a plot of C_{D_c}. The range plot is very similar to the the $\frac{C_L}{C_D}$ plot in trend with a minimum range of about 4200 km and a maximum of 8200 km.

As with all other cases, the maximum weight is fixed so the C_L simply depends on area. At the high wave drag, large area conditions, the C_L was driven down to almost 0.25 which is substantially below optimum for the foil.

Unlike the K_{cf} case where the optimizer consistently found a planform that would keep the total C_D about constant, this trade study was quite the opposite. The very high wave drags at low Mcc seem to have thrown the optimizer well off of the usual path to a decent planform resulting in very high C_D at Mcc=0, a minimum drag at Mcc=0.06 and a very slight increase in C_D for higher values of Mcc.

Looking at the component drag values, the very high sweep cases pay a large penalty in C_{D_i}, although the C_{D_v} actually shows a mostly steady *increase* with increasing Mcc. This seems contrary to what would be expected given the area distribution. However, the C_{D_v} is calculated from the simple flat-plate turbulent reynolds number equation (1.3), and since the R_e is based on MAC which is much higher for the high area wings, this reverses the expected trend. The C_{D_c} graph is similar in form to the C_D graph making it obvious which of these components is the driving factor.

The existance of a minimum at Mcc=0.06 is another interesting point. There seems no particular reason why some amount of wave drag should produce a lower total C_D. More likely what this indicates is that the optimizer has an easier time of finding an optimum if all the component drags are at least somewhat balanced.

Figure 6-28 shows the plots of C_L and $\overline{C_l}$. For most cases thus far, these have had a nice tight distribution, which is clearly not true here. Looking at the C_L distribution; the Mcc=0 case actually shows a nice flat C_L "roof" which is typical of the loading on a modern transport wing. This effect is picked up again somewhat by Mcc=0.14, although by this time the AR is much higher and the loading is moving towards parabolic. In the middle, an interesting combination of loading and chord distribution results in the tips and center section being most highly loaded. The $\overline{C_l}$ plot normalizes by the chord which makes these plots look slightly more normal but the loading is still rather strangely distributed.

Much more disturbing are the tail loadings. The output data indicates that the optimizer did in fact satisfy the static margin constraint for each case, which *should* indicate that the configuration displays positive pitch stability. However, for all planforms except Mcc=0.14, the tail loading is clearly positive and the Cruise pitching moment is also positive for the three highly swept cases. The formula for the Static Margin, originally given in 3.2 and

repeated here:

$$SM = \frac{-\left(\frac{dC_m}{d\alpha}\right)}{\left(\frac{dC_L}{d\alpha}\right)} C_{ref} \tag{6.3}$$

So that the static margin is satisfied when the ratio of the C_m slope to the C_L is small. However, the reference chord is the MAC, which varies up to 1m in this trade study. With the highly swept wings in particular, the MAC is higher than usual which exacerbates the stability situation even further. Forcing the SM higher at this point resulted in unrealistically high sweep. Thus it appears that there are some conditions in which the SM constraint is not a reasonable way to constrain the planform to a positive static stability.

6.9 Cruise Mach Number

Theoretically, testing a range of cruise mach numbers is one of the simpler trade studies to do with the code. Fundamental to high speed subsonic wing design is the need to add sweep to the wing to reduce Mach rise drag. The same size transport designed to cruise at Mach 0.65, 0.75 and 0.85 should have very different looking wing and tail planforms with wing sweep and weight increasing steadily with Mach number. Once again the optimizer found unanticipated paths through configuration space. This trade study also experienced problems with the Static Margin being insufficient and then experiencing major planform modifications once the SM was increased enough to force a stable design. The importance of the static margin was not fully realized until very near the end of the studies and section 7.2 in the conclusions chapter will discuss what was learned about the importance of this constraint.

Figures 6-29 and 6-30 show the usual assortment of parameters plotted against the cruise Mach number. Figure 6-31 shows a sample of the wing planforms and figure 6-32 shows the aerodynamic parameters.

6.9.1 Planform Analysis

Following the standard planform analysis routine referring to figures 6-29, 6-30, and 6-31:

The first feature of notice in figure 6-29 is the glaring peak in the data for the root sweep at Mach number 0.75 and 0.775. Both of these cases have a root sweep value almost 10°higher than the rest of the planforms which were more or less consistent. Again, this seems to be a problem with the loading of the tail and loading of the wing. Referring to figure 6-32 and looking at the tail loading profiles, all cases display an inverse parabolic loading except the M 0.75 This case displays a linear loading which is maximum at the tip of the tail. This is extremely inefficient from the standpoint of inviscid drag on the tail, however the net tail load is also quite small so the drag penalty is not very large.

Earlier this study the two highest Mach number cases, Mach 0.825 and 0.85 had to be re-run with higher static margins to prevent the optimizer to find a lifting tail configuration. When this was done the wing planform changed drastically, as seen in figure 6-4. The Mach 0.75 and 0.775 cases did not have problems with a lifting tail, but to test the influence of the SM in this situation, a range of higher static margin constraint values were tried. The wing sweep did decrease several degrees, however the tail loads also increased significantly resulting in a much heavier than practical tail. Thus, almost in the way of the bifurcation with span earlier, there seems to be a small range of bifurcation in Sweep. Although, in

this case, these two wings are the *most* efficient of the study.

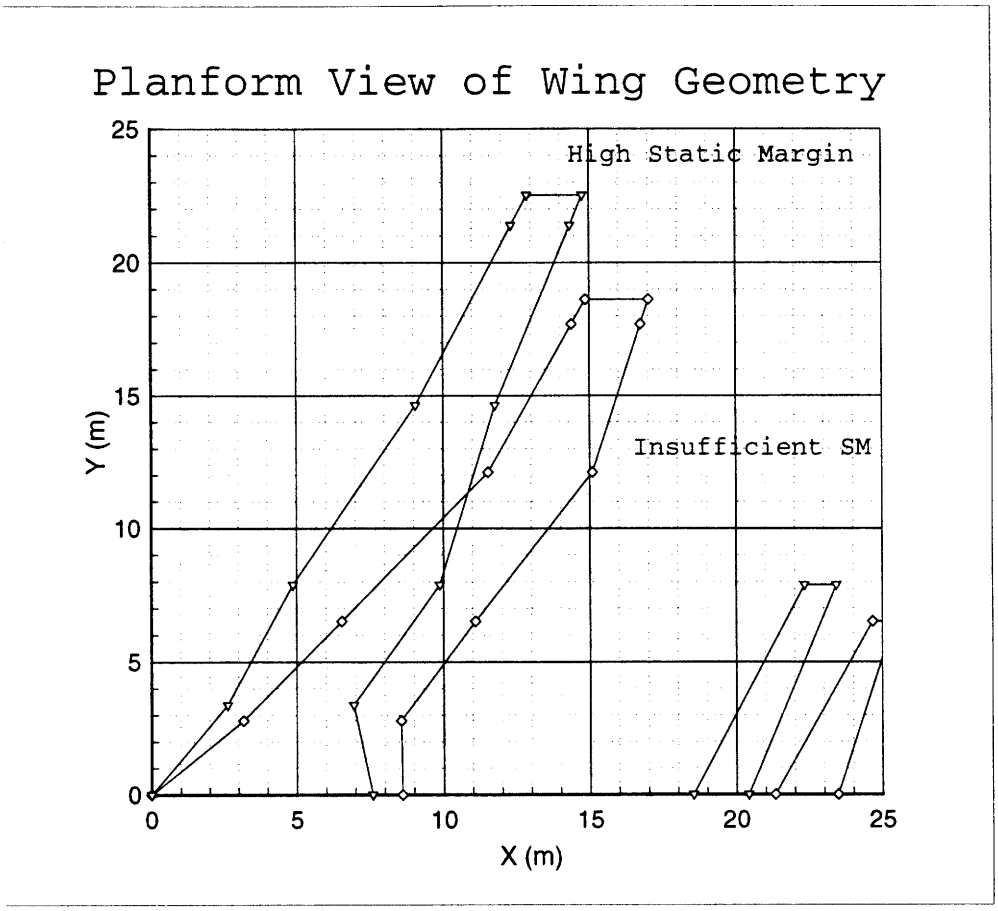

Figure 6-4: Effect of enforcing a down loaded tail with Static margin on the wing and tail planform

Keeping in mind that these two runs are not going to fit in with the rest of the data, the trade study analysis is as follows:

6.9.2 Wing and Tail Geometry analysis

With the exception of the two highly swept wings, there is an obvious trend towards *decreasing* spar box weight with increasing Mach. This is completely opposite of what would be expected. However, with the increased SM constraint value on the high Mach number runs, the optimizer found it better to keep the wing sweep nearly constant and shorten the wing span a little to compensate for the increased $C_{d_{corr}}$. This shows up clearly in the plots of wing span and wing sweep. The spans also decrease steadily with mach while the sweep values (again, with the obvious exceptions) are nearly flat. The wing area at first seems surprising since there was a slight increase in area with increasing Mach, but this is actually completely predictable as will be explained in the next section with C_L and C_D. The AR followed a more expected trends with a steady decrease with increasing mach, and a more rapid decrease for the last 2 runs. This is to be expected since as the wave drag starts rising rapidly the optimizer will try to pull the wing in as much as possible.

The tail weight is a bucket curve which related quite closely with the effective static margin of the tail. The swept wings with minimal tail loading had the lightest tails, and the

high mach cases with increased static margin had forced tail down loading and hence much higher tail weights. Figure 6-32 shows the C_L distributions for these cases and figure 6-33 shows the loads, the skin gauges and bending moments on the tails. As mentioned earlier, the swept wings had non-optimally loaded tails with load increasing steadily until the tip. However, the total load was still small enough for these tails to be lighter.

6.9.3 Aerodynamic Parameter Analysis

The behavior of the optimizer in configuration space was nearly completely opposite that witnessed in the previous trade studies. For the most part we have seen that the optimizer has a strong tendency to keep the aerodynamic parameters relatively constant and adjust the wing planform as necessary to do so. For this case, with the exception of the bifurcations, the geometry has stayed remarkably constant and now referring to figure 6-30 the results of this approach are very obvious. The changes in the aerodynamic parameters are pronounced and consistent. This change in approach, and the magnitude of the trends are both driven by the fact that the dynamic pressure and R_e changed in this case. Thus the C_L is no longer simply a function of area and the same applies to the C_{D_v}.

The C_L shows a marked decline with Mach number increase. As was mentioned previously, the optimum $\frac{C_L}{C_D}$ for this foil is in the range of 0.7, which is considerably higher than any of the C_L values seen in those cases or the baseline. This was attributed to the fact that wave drag increases significantly at higher C_L values so that the entire $\frac{C_L}{C_D}$ curve being shifted so that the optimum point now occurs at a considerably lower C_L. This trend shows up very clearly in these graphs and explains the wing area curve - the optimizer had to drive the area up to push the cruise C_L lower.

In complete agreement with the concept that the foil is being driven away from incompressible optimum point is the rapid decrease in the C_{D_i} values. The C_{D_v} does not decrease quite so quickly, although this is deceiving since the C_{D_c} is also included here so most of the C_{D_v} decrease with R_e increase is being lost to increased C_{D_c}. It should be noted that since this data was done with polars which were taken in the vicinity of mach 0.8, that extrapolating Mach drag rise much beyond this point will result in Mach drags which are lower than they should be. With a more accurate Mach drag rise, the the C_D would be expected to start increasing rapidly for the highest Mach numbers.

There was enough irregularity in the decline of both C_L and C_D for there to be a slight curve with a maximum for $\frac{C_L}{C_D}$. This actually occurs for the two bifurcated high sweep wings which have higher C_L and low enough C_{D_v} to offset their penalty in weight and C_{D_i}. Without these two planforms the $\frac{C_L}{C_D}$and Range would both show steadily declining performance as cruise Mach increases. This, of course is completely expected since one always pays a price for speed.

6.10 Data Tables and Figures

Are displayed on the following pages...

Table 6.5: Trade Data for variance of C_{m_0}

Data for:	Base5F.out	Cm5C015.out	Cm5C03.out	Cm5C04.out	Cm5C06.out	Cm5C10.out
Convergence Error	N/A	3.25880e-02	3.25588e-02	3.13718e-02	1.05487	0.89742
Structural and Geometry Data						
Wing Span (m)	18.81	21.52	23.59	23.10	22.88	22.53
Wing Area (m^2)	75.81	70.72	76.54	77.22	75.55	66.69
Wing Aspect Ratio	9.34	13.10	14.55	13.82	13.86	15.22
Tail Volume	0.50	0.52	0.52	0.50	0.52	0.73
Spar Box Mass (kg)	1410.78	2853.73	2691.74	2721.86	2642.84	2333.40
Tail Spar Box Mass (kg)	96.98	97.65	128.14	119.95	121.90	171.09
Wing Root Sweep (deg)	35.06	34.47	25.51	27.91	28.30	28.96
Wing Tip Sweep (deg)	24.62	24.62	24.62	24.62	24.62	24.62
Performance Data						
Wing Loading (Pa)	3228.12	3460.53	3197.22	3168.94	3225.68	3669.65
Cruise C_L	0.30	0.33	0.30	0.30	0.30	0.34
Cruise C_D	1.18e-02	1.13e-02	1.10e-02	1.09e-02	1.11e-02	1.20e-02
Inviscid Cruise C_D	3.58e-03	3.00e-03	2.45e-03	2.51e-03	2.63e-03	3.09e-03
Viscous Cruise C_D	8.21e-03	8.31e-03	8.55e-03	8.43e-03	8.48e-03	8.91e-03
Cruise Wave Drag C_D	0.00000	0.00000	0.00000	0.00000	0.00000	0.00000
Cruise L/D	25.73	28.75	27.34	27.22	27.30	28.73
Range (km)	8105.10	9053.20	8610.50	8571.30	8598.80	9048.50
Takeoff speed (m/sec)	75.64	75.69	75.74	75.77	75.84	80.67
Landing speed (m/sec)	54.81	54.81	54.81	54.81	54.81	54.81
Performance Metrics						
Efficiency range/fuel Km/Kg	0.73	0.82	0.78	0.78	0.79	0.82
Wing M.F. (spar box/total)	0.04	0.07	0.07	0.07	0.07	0.06
(Fuel mass)/(wing mass)	7.82	3.86	4.10	4.05	4.13	4.73

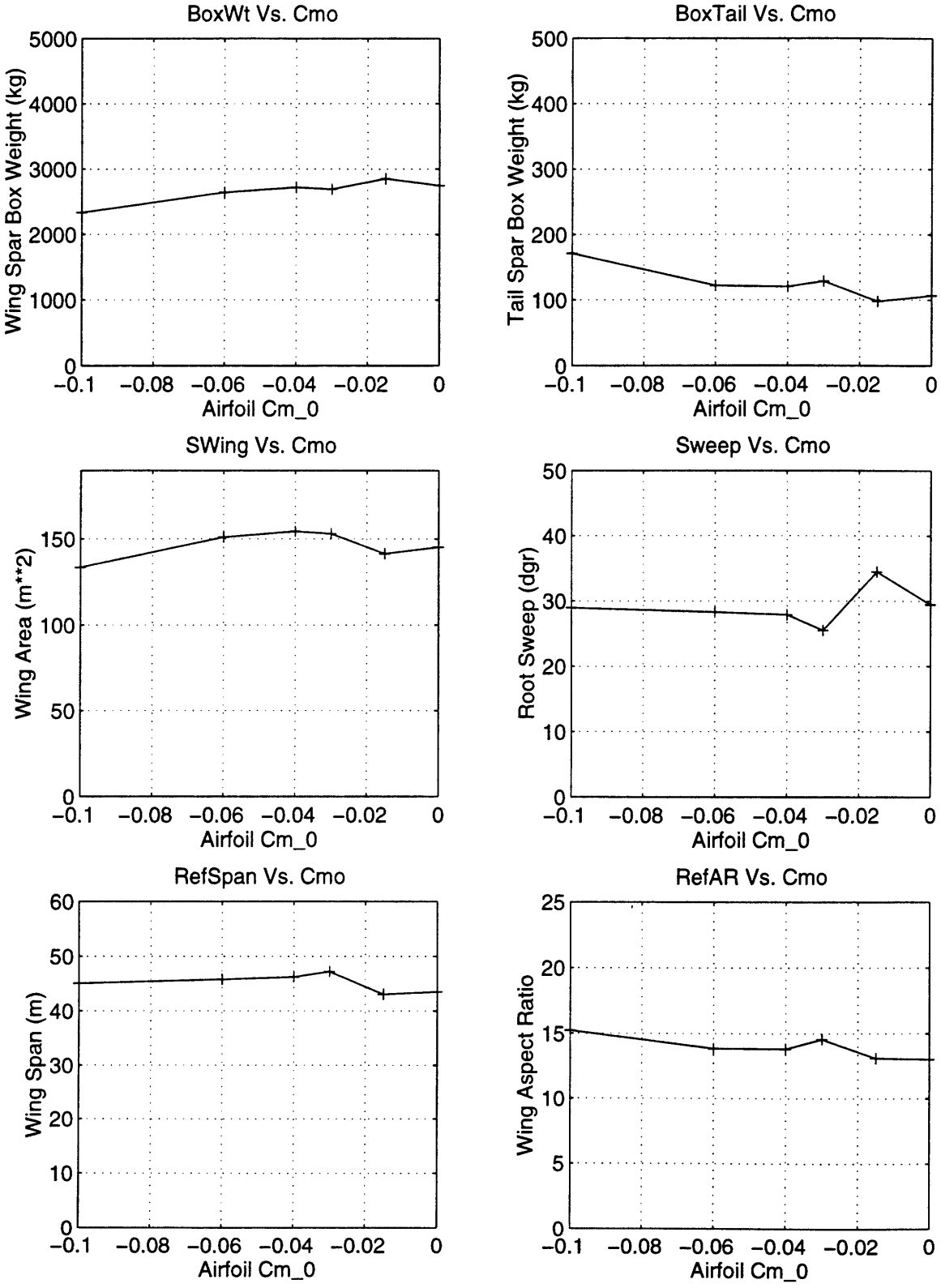

Figure 6-5: Trade Data for geometric parameters with variance of C_{m_0}

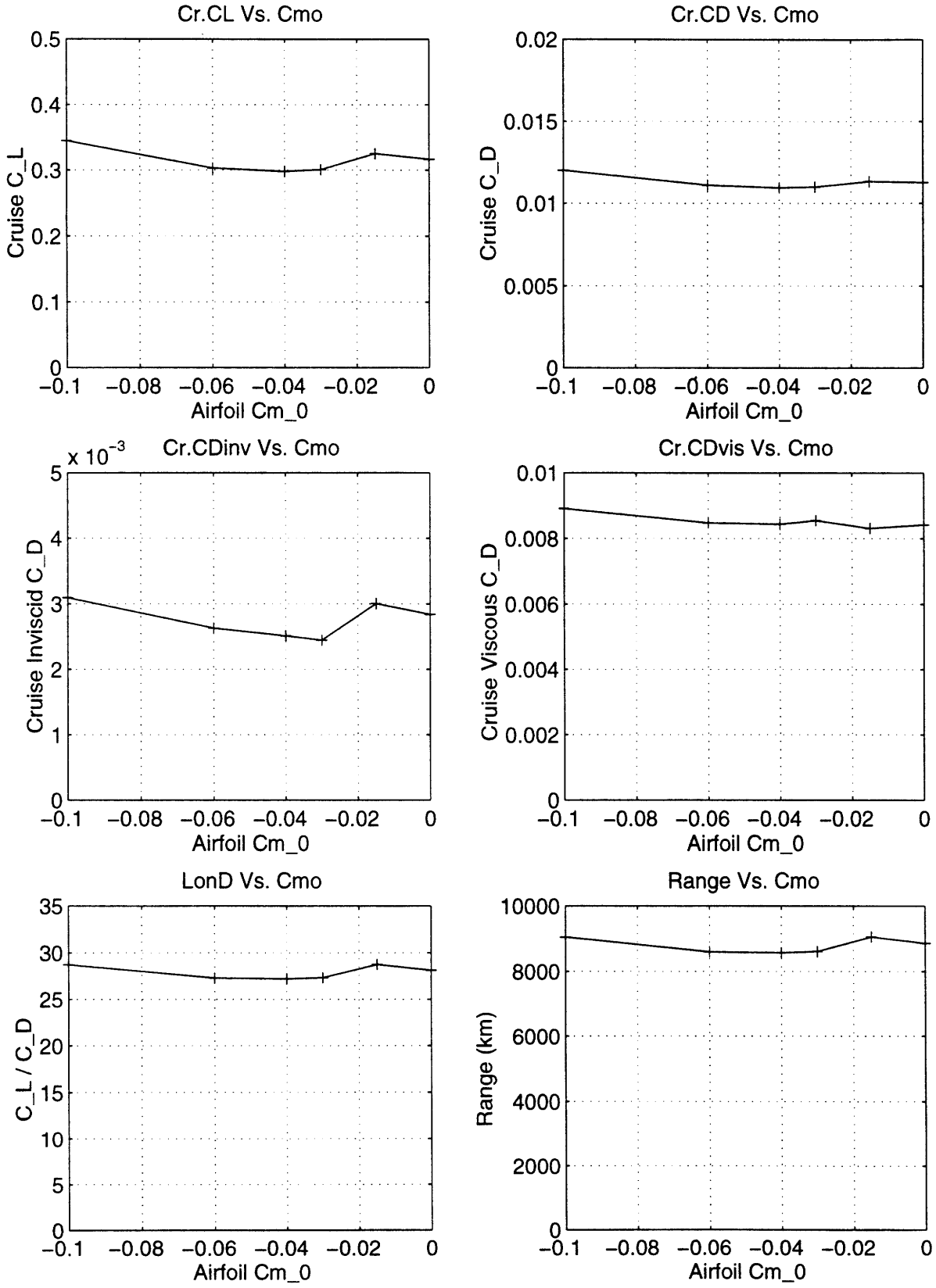

Figure 6-6: Trade Data for performance parameters with variance of C_{m_0}

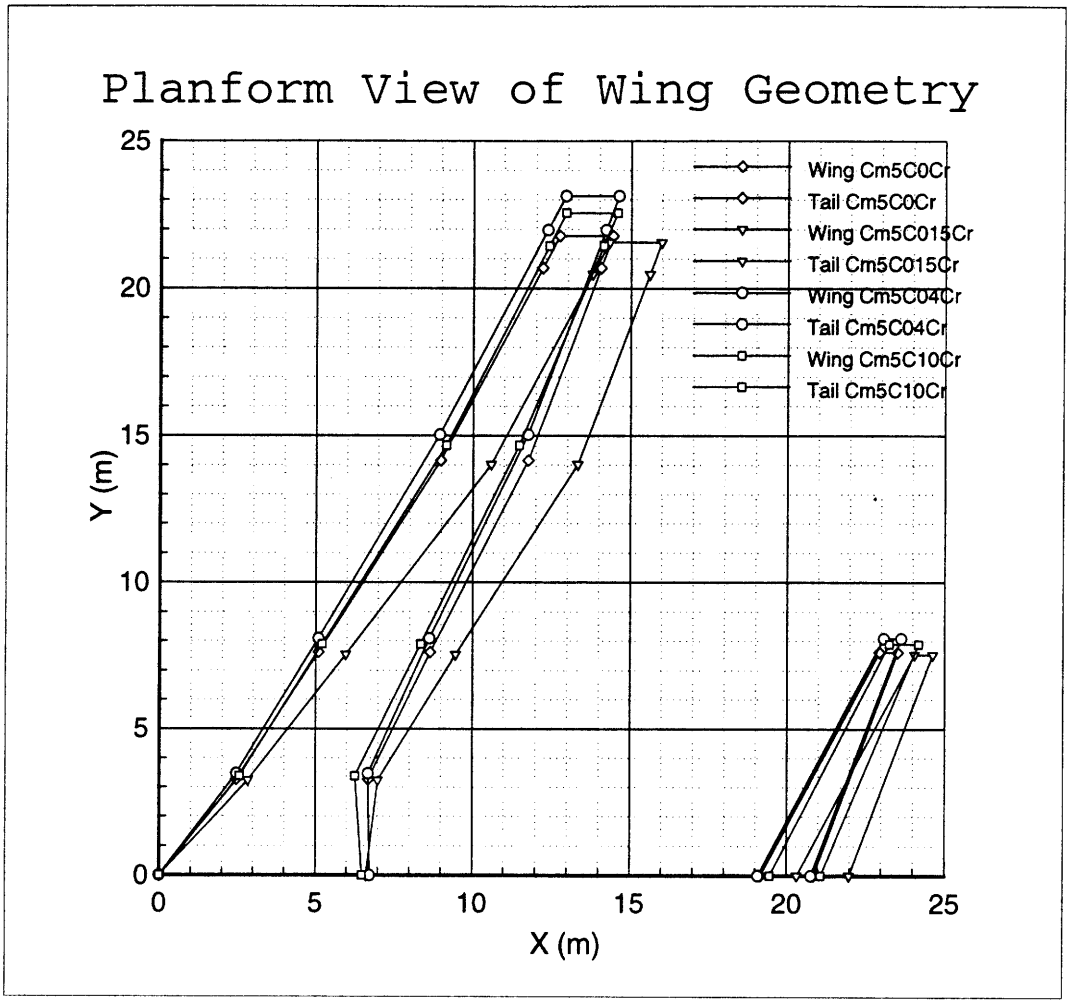

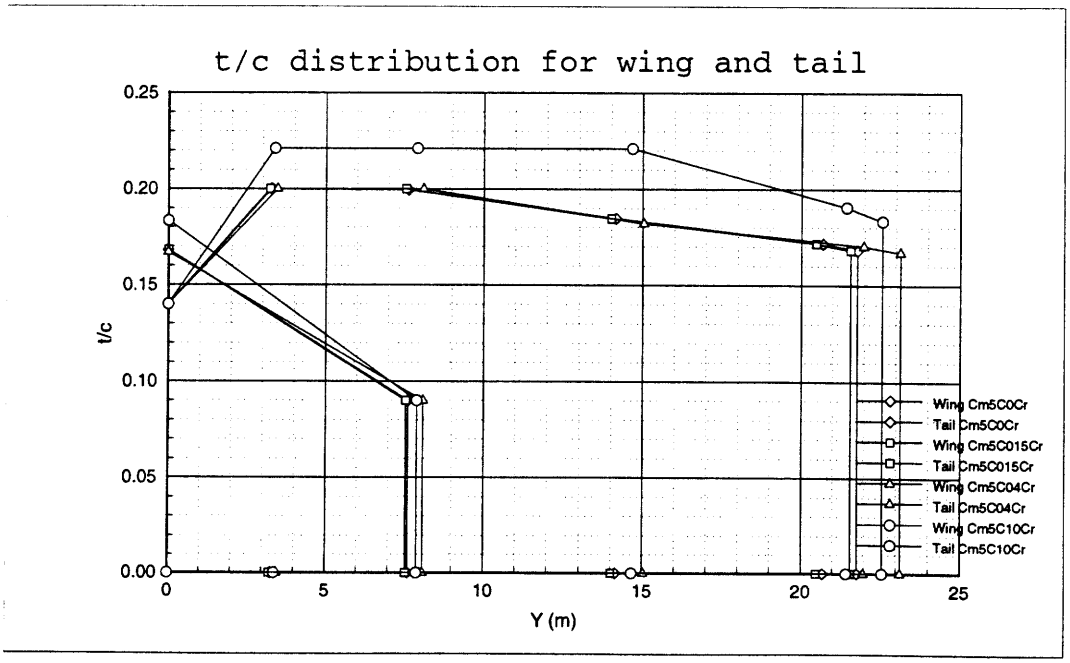

Figure 6-7: Planform data for C_{m_0} = 0 , -0.015, -0.04 and -0.10

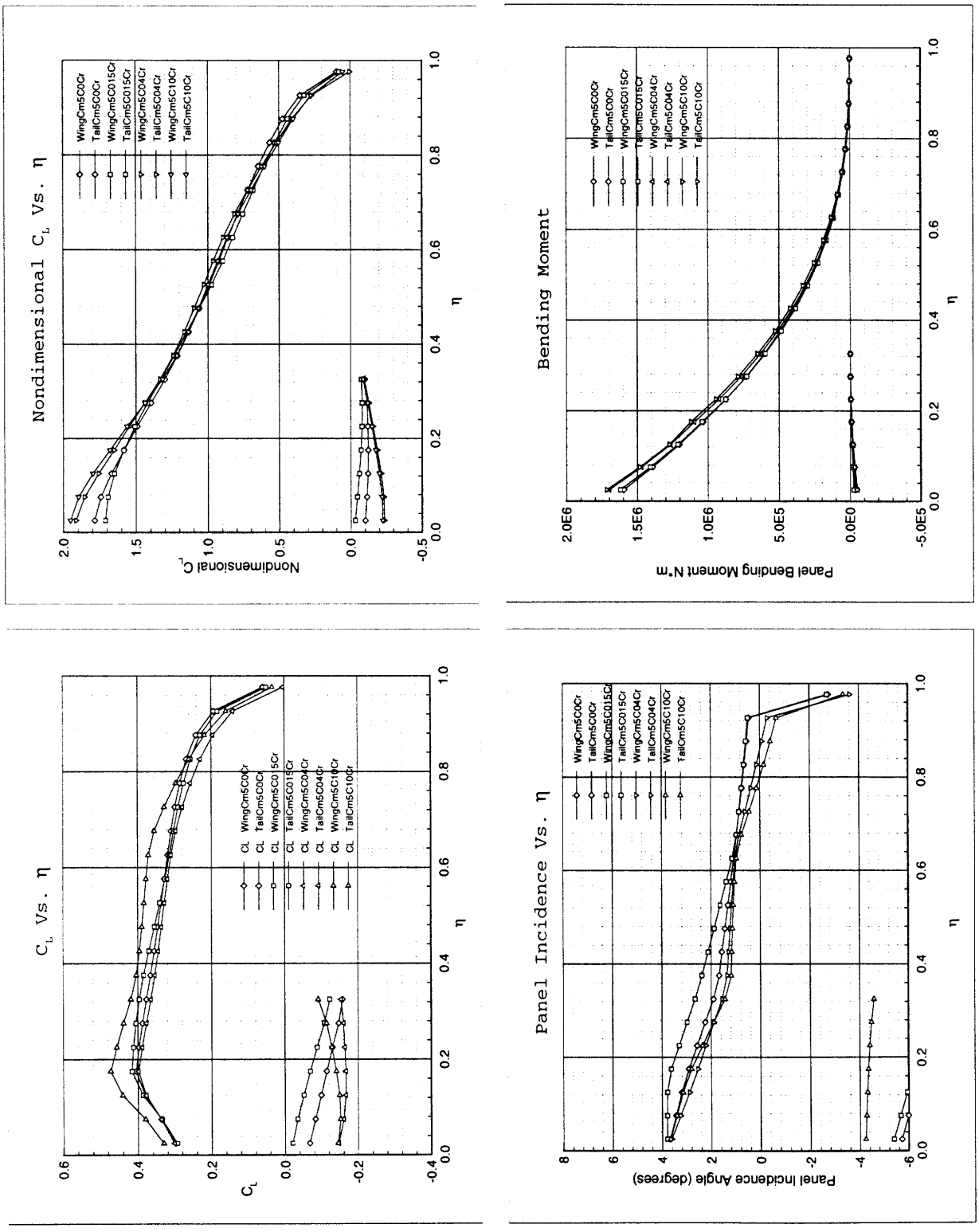

Figure 6-8: Aerodynamic data for C_{m_0} = 0 , -0.015, -0.04 and -0.10

Table 6.6: Trade Data for variance of skin stress ratio

Data for:	Sr5R27.out	Sr5R30.out	Sr5R31.out	Sr5R34.out	Sr5R38.out	Sr5R40.out	Sr5R46.out
Convergence Error	2.27241e-02	0.84651	0.70814	3.34029e-02	0.64665	0.62825	0.69143
Structural and Geometry Data							
Wing Span (m)	21.94	22.13	21.57	21.58	21.67	19.36	20.58
Wing Area (m^2)	81.52	75.07	72.95	72.03	71.76	75.32	75.20
Wing Aspect Ratio	11.81	13.05	12.76	12.93	13.09	9.95	11.26
Tail Volume	0.45	0.47	0.51	0.51	0.56	0.54	0.43
Spar Box Mass (kg)	2094.71	2425.18	2078.26	2724.17	2246.69	1464.72	2266.68
Tail Spar Box Mass (kg)	124.33	133.59	102.60	108.10	129.76	92.05	122.50
Wing Root Sweep (deg)	27.92	25.95	26.72	32.47	26.80	32.97	35.11
Wing Tip Sweep (deg)	24.62	24.62	24.62	24.62	24.62	24.62	24.62
Performance Data							
Wing Loading (Pa)	3001.90	3259.67	3340.67	3397.64	3410.08	3248.90	3240.07
Cruise C_L	0.28	0.31	0.31	0.32	0.32	0.31	0.30
Cruise C_D	1.08e-02	1.11e-02	1.14e-02	1.13e-02	1.15e-02	1.18e-02	1.15e-02
Inviscid Cruise C_D	2.54e-03	2.67e-03	2.89e-03	2.96e-03	2.91e-03	3.52e-03	3.46e-03
Viscous Cruise C_D	8.30e-03	8.46e-03	8.50e-03	8.33e-03	8.58e-03	8.28e-03	8.05e-03
Cruise Wave Drag C_D	0.00000	0.00000	0.00000	0.00000	0.00000	0.00000	0.00000
Cruise L/D	26.02	27.52	27.56	28.30	27.90	25.87	26.46
Range (km)	8195.70	8666.00	8678.60	8912.30	8787.10	8148.10	8333.20
Takeoff speed (m/sec)	75.64	75.64	75.64	75.64	75.64	75.64	75.64
Landing speed (m/sec)	54.81	54.81	54.81	54.81	54.81	54.81	54.81
Performance Metrics							
Efficiency range/fuel Km/Kg	0.74	0.79	0.79	0.81	0.80	0.74	0.76
Wing M.F. (spar box/total)	0.05	0.06	0.05	0.07	0.06	0.04	0.06
(Fuel mass)/(wing mass)	5.26	4.55	5.31	4.05	4.91	7.53	4.86

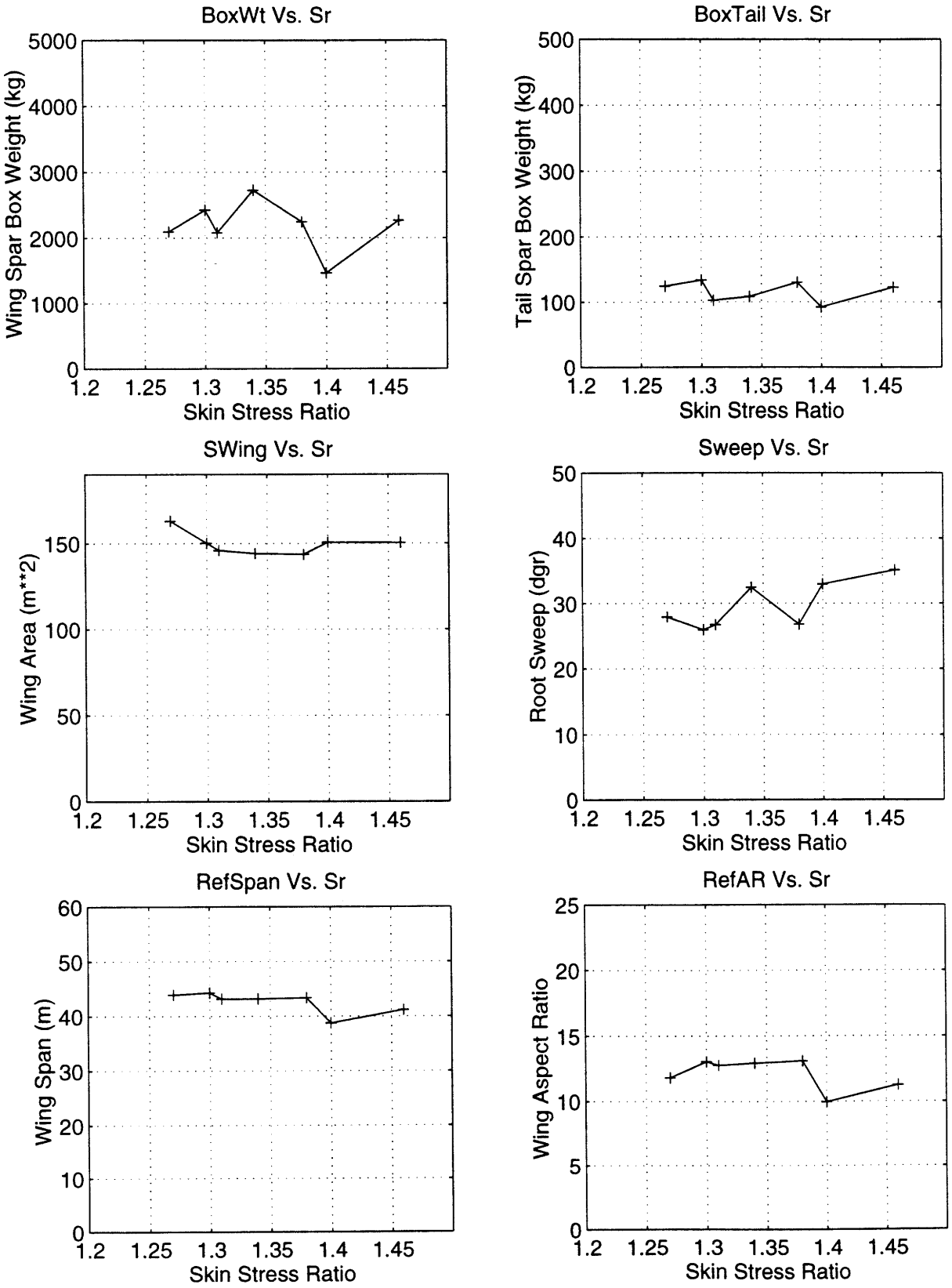

Figure 6-9: Trade Data for geometric parameters with variance of Stress Ratio

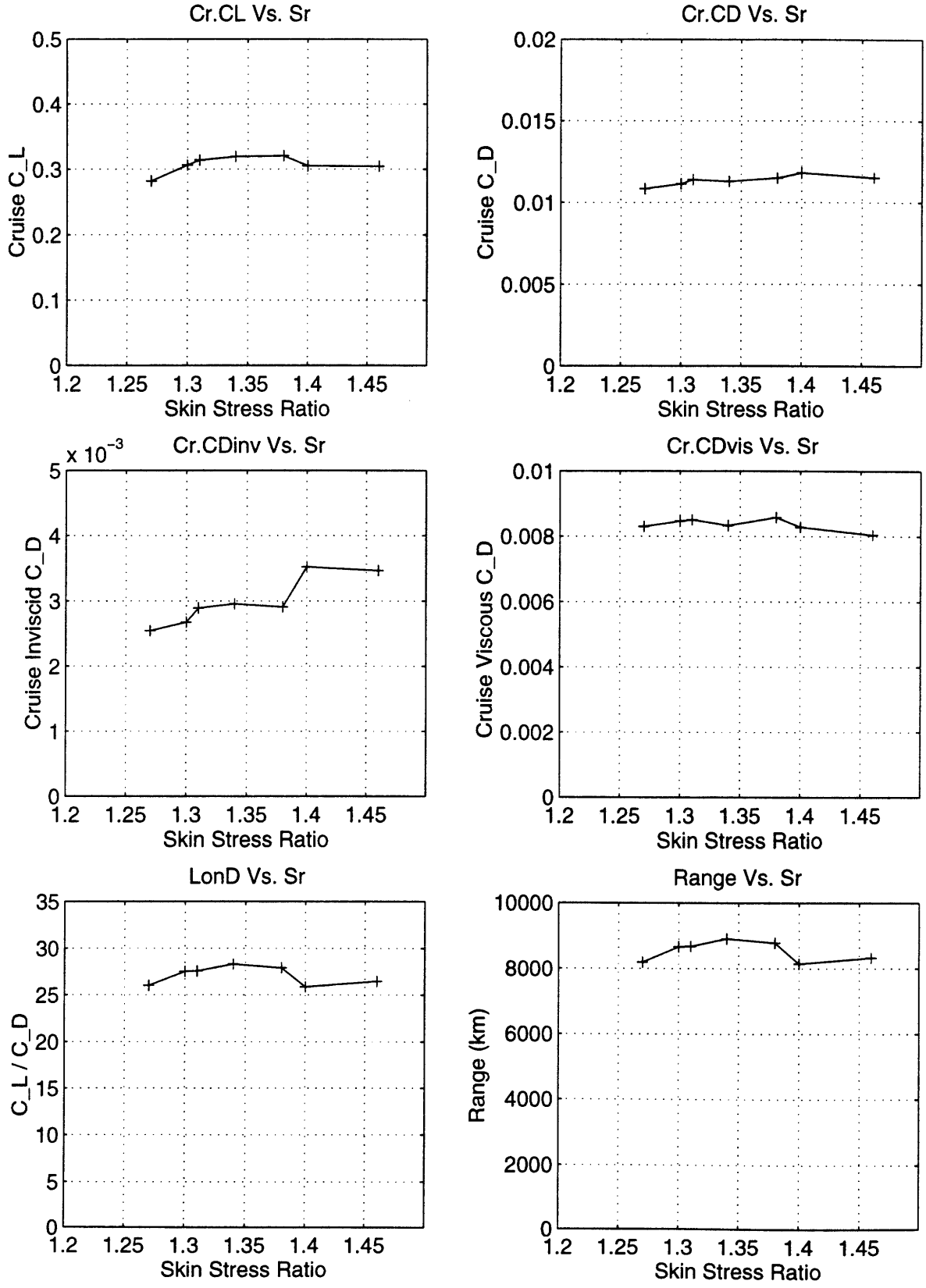

Figure 6-10: Trade Data for performance parameters with variance of Stress Ratio

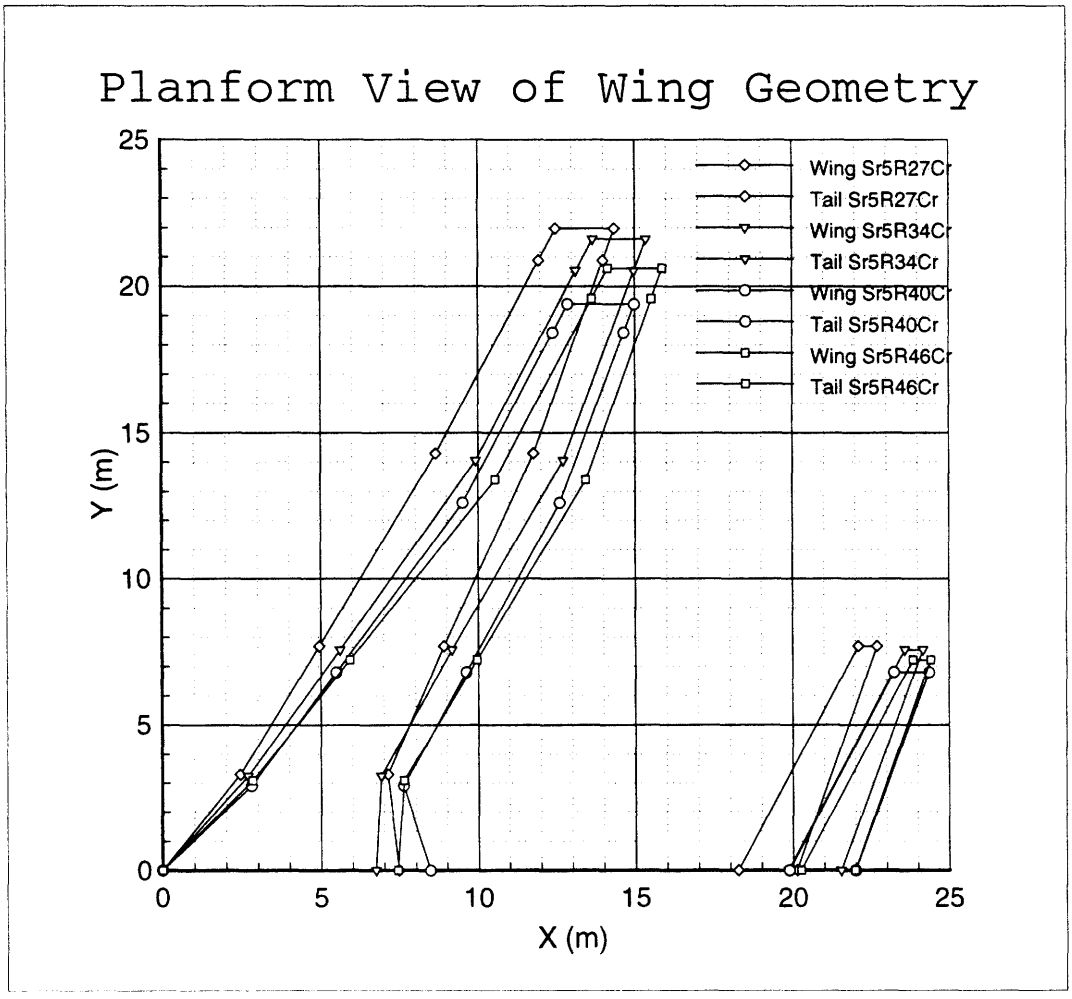

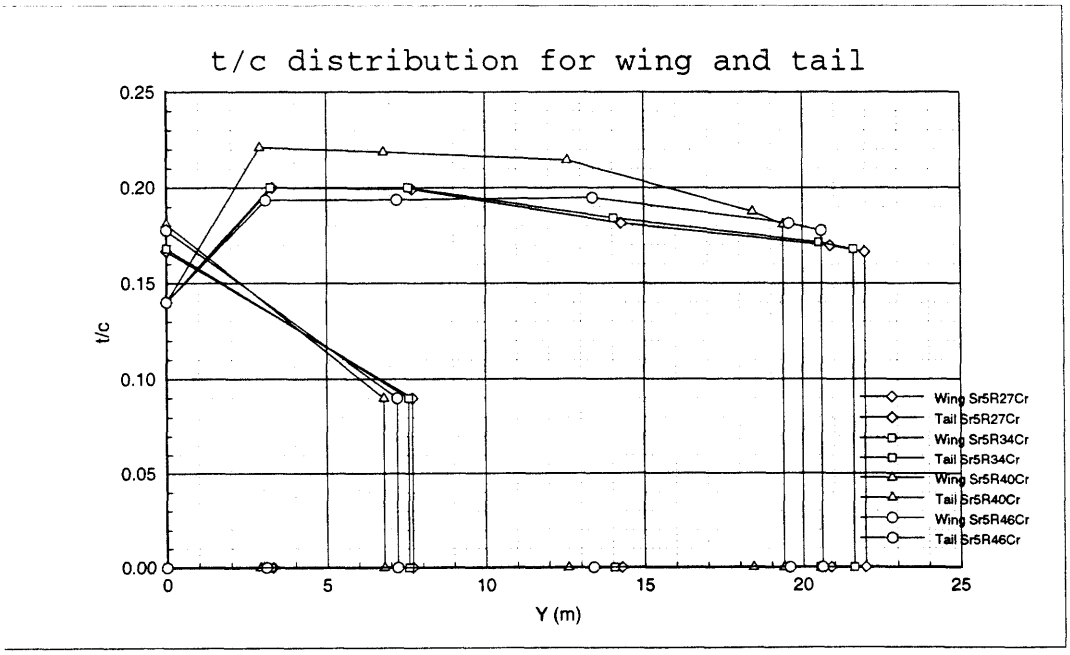

Figure 6-11: Planform data for Stress Ratio = 1.27 1.34 1.40 1.46

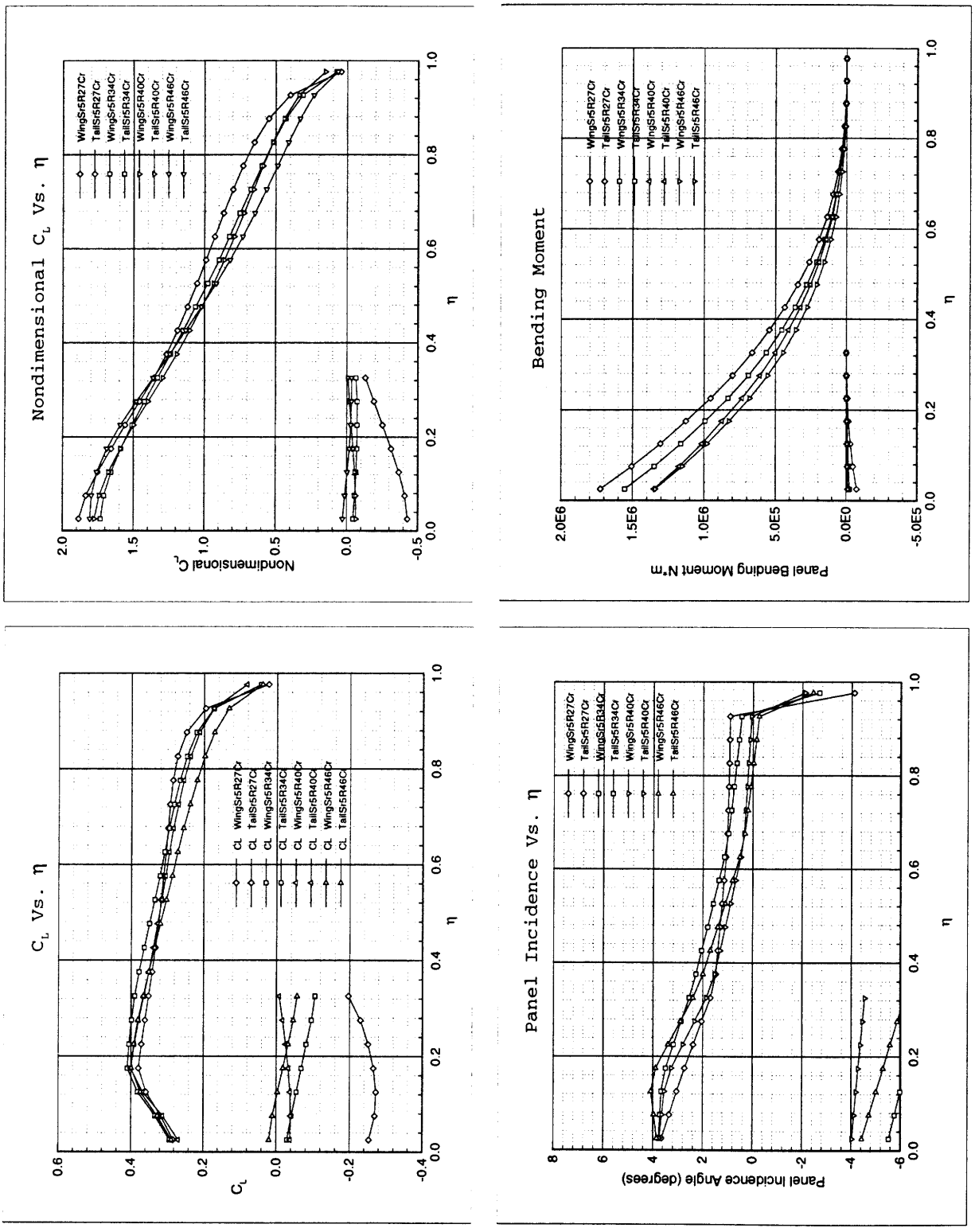

Figure 6-12: Planform data for Stress Ratio = 1.27 1.34 1.40 1.46

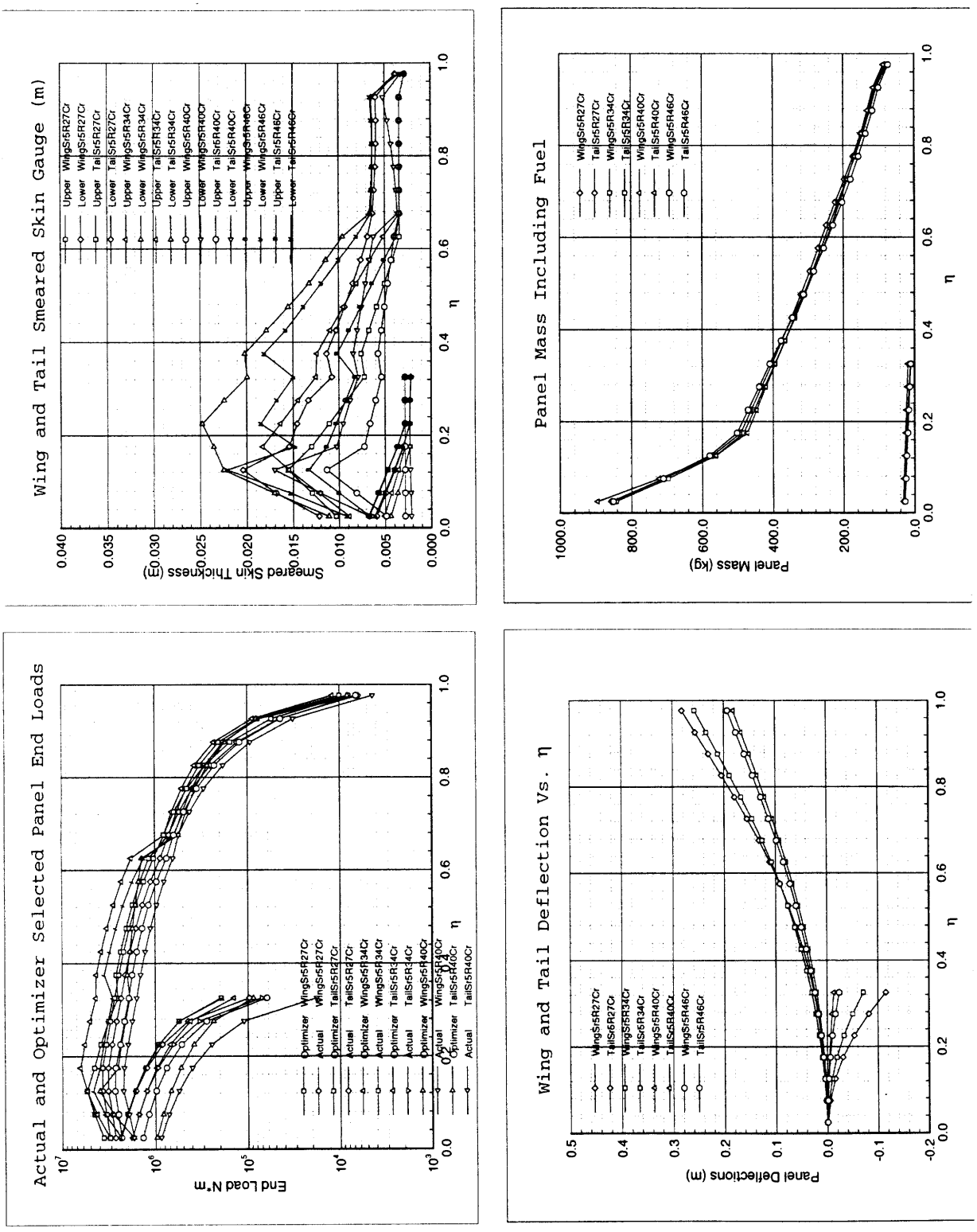

Figure 6-13: Skin data for Stress Ratio = 1.27 1.34 1.40 1.46

Data for:	ρ 2600	ρ 2825	ρ 2850	ρ 3000
Convergence Error	0.65018	3.58573e-02	3.48980e-02	0.63386
Structural and Geometry Data				
Wing Span (m)	20.92	21.05	21.30	21.44
Wing Area (m^2)	72.94	72.45	71.91	69.72
Wing Aspect Ratio	12.00	12.23	12.62	13.19
Tail Volume	0.52	0.49	0.50	0.62
Spar Box Mass (kg)	2350.80	2812.52	2804.72	2331.53
Tail Spar Box Mass (kg)	86.45	86.93	94.62	165.74
Wing Root Sweep (deg)	34.86	38.12	35.02	29.43
Wing Tip Sweep (deg)	24.62	24.62	24.62	24.62
Performance Data				
Wing Loading (Pa)	3338.65	3377.82	3402.96	3510.11
Cruise C_L	0.31	0.32	0.32	0.33
Cruise C_D	1.14e-02	1.12e-02	1.13e-02	1.16e-02
Inviscid Cruise C_D	3.14e-03	3.08e-03	3.04e-03	3.01e-03
Viscous Cruise C_D	8.24e-03	8.11e-03	8.24e-03	8.62e-03
Cruise Wave Drag C_D	0.00000	0.00000	0.00000	0.00000
Cruise L/D	27.59	28.37	28.36	28.36
Range (km)	8688.80	8935.80	8932.50	8932.60
Takeoff speed (m/sec)	75.64	75.64	75.64	75.64
Landing speed (m/sec)	54.81	54.81	54.81	54.81
Performance Metrics				
Efficiency range/fuel Km/Kg	0.79	0.81	0.81	0.81
Wing M.F. (spar box/total)	0.06	0.07	0.07	0.06
(Fuel mass)/(wing mass)	4.69	3.92	3.93	4.73

Table 6.7: summary data for ρ 2600, 2825, 2850, and 3000 $\frac{kg}{m^3}$

Data for: hline Convergence Error	ρ 2700 0.79753	ρ 2750 0.82698	ρ 2900 0.73485
Structural and Geometry Data			
Wing Span (m)	23.82	23.42	22.93
Wing Area (m^2)	70.36	74.35	68.03
Wing Aspect Ratio	16.12	14.75	15.45
Tail Volume	0.68	0.56	0.74
Spar Box Mass (kg)	2273.45	3121.06	2317.57
Tail Spar Box Mass (kg)	137.06	130.22	164.55
Wing Root Sweep (deg)	25.93	31.96	29.17
Wing Tip Sweep (deg)	24.62	24.62	24.62
Performance Data			
Wing Loading (Pa)	3477.75	3265.16	3562.86
Cruise C_L	0.33	0.31	0.33
Cruise C_D	1.15e-02	1.08e-02	1.17e-02
Inviscid Cruise C_D	2.66e-03	2.41e-03	2.89e-03
Viscous Cruise C_D	8.86e-03	8.41e-03	8.85e-03
Cruise Wave Drag C_D	0.00000	0.00000	0.00000
Cruise L/D	28.38	28.35	28.53
Range (km)	8937.10	8929.10	8983.90
Takeoff speed (m/sec)	75.64	75.64	75.64
Landing speed (m/sec)	54.81	54.81	54.81
Performance Metrics			
Efficiency range/fuel Km/Kg	0.81	0.82	0.81
Wing M.F. (spar box/total)	0.06	0.08	0.06
(Fuel mass)/(wing mass)	4.85	3.49	4.80

Table 6.8: summary data for ρ 2700 2750 and 2900 $\frac{kg}{m^3}$

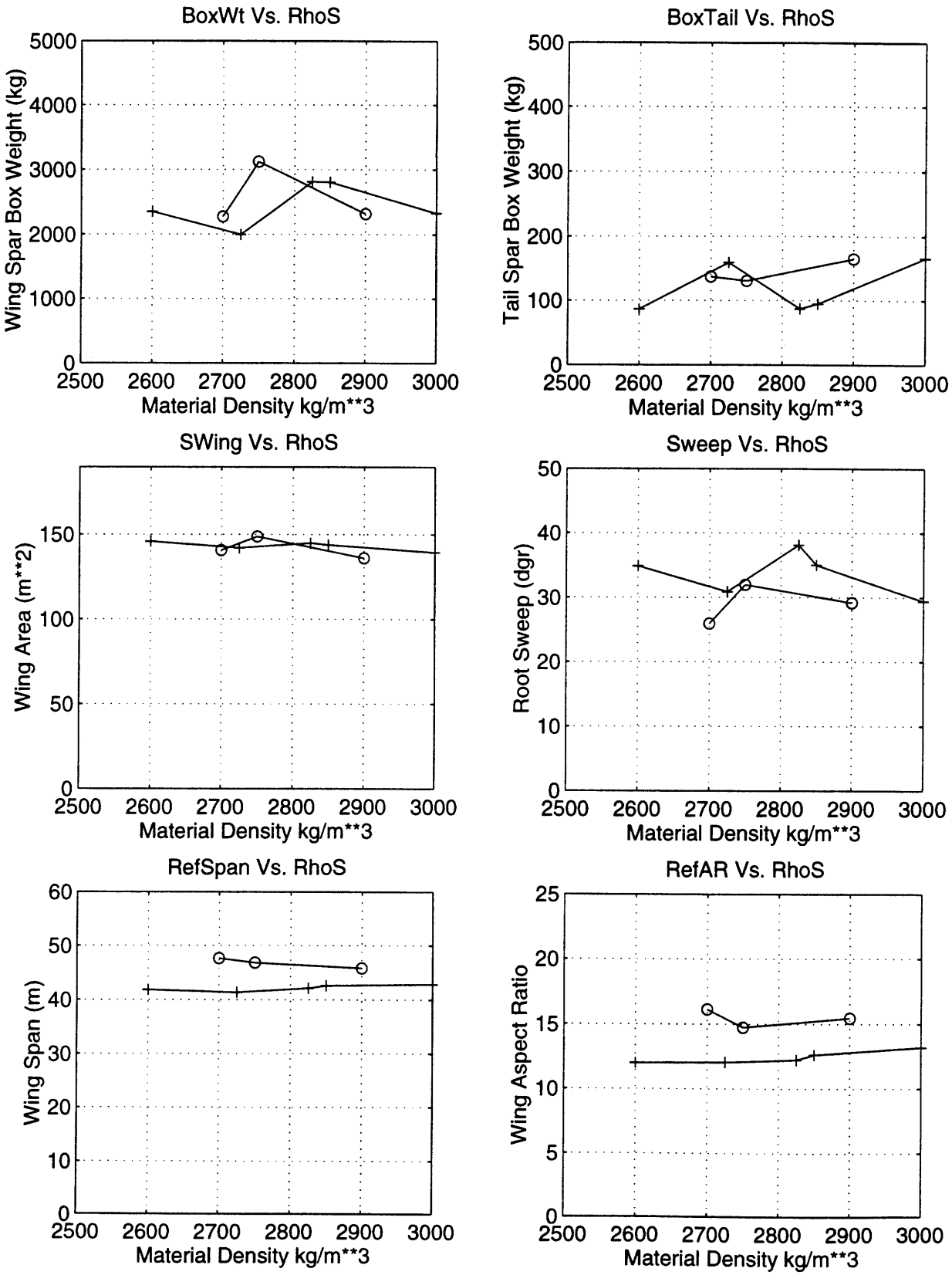

Figure 6-14: Trade Data for geometric parameters with variance of material density

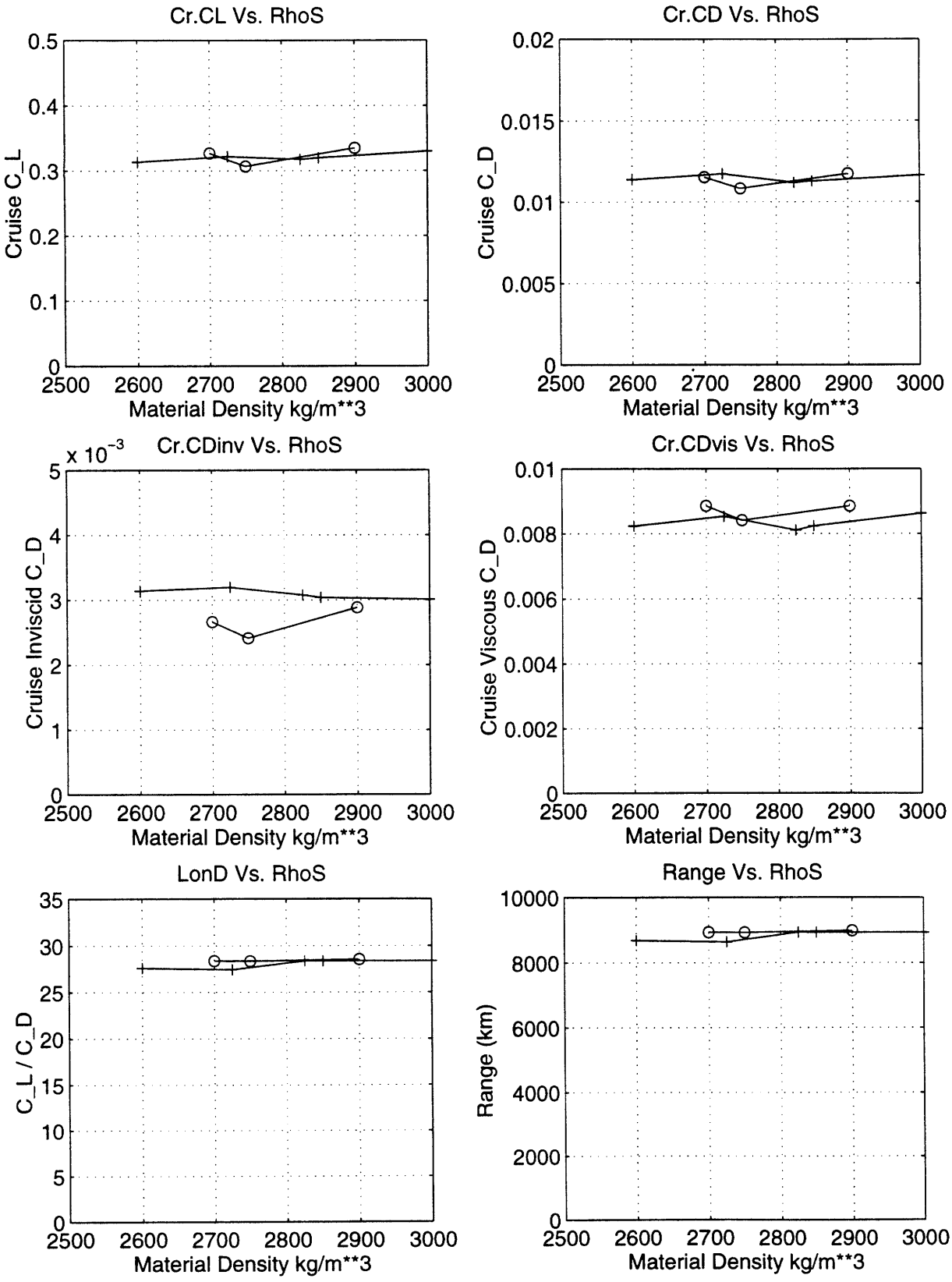

Figure 6-15: Trade Data for performance parameters with variance of material density

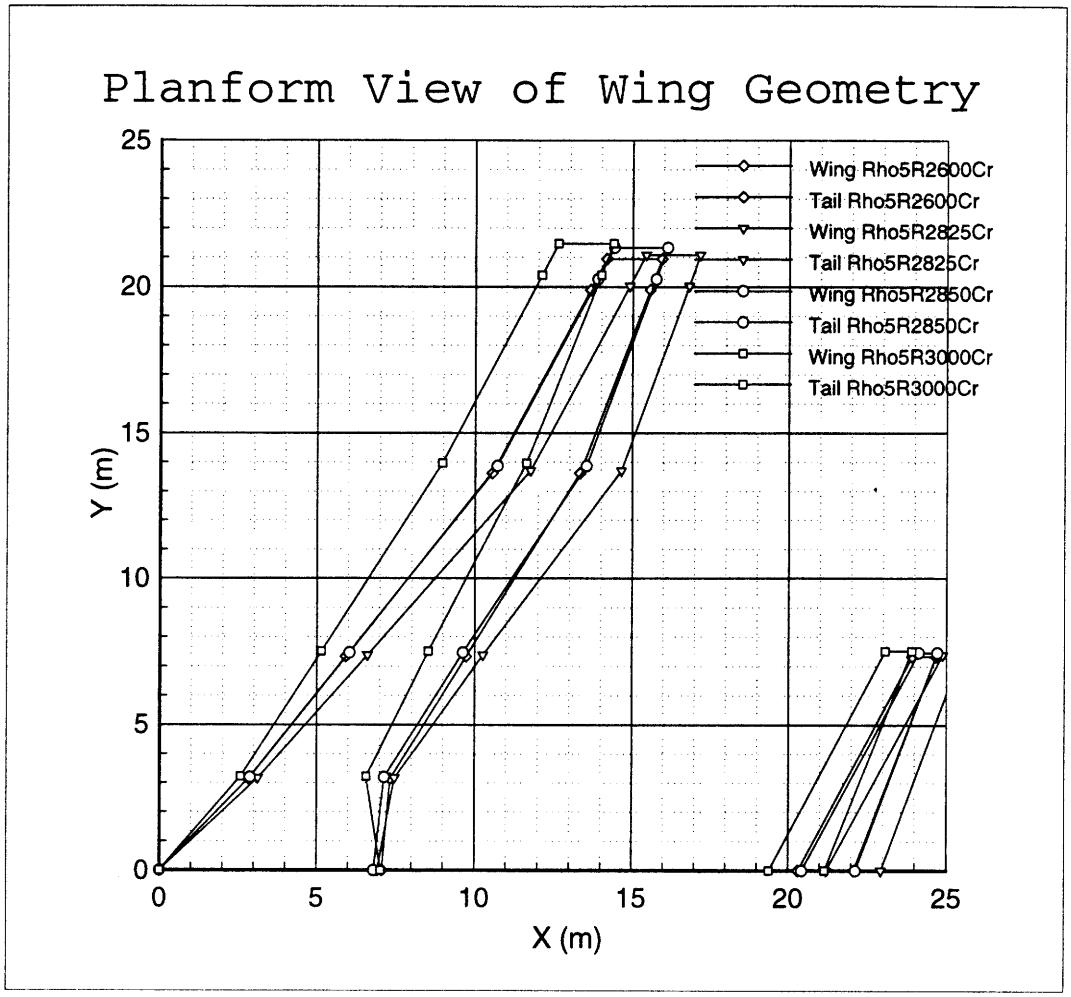

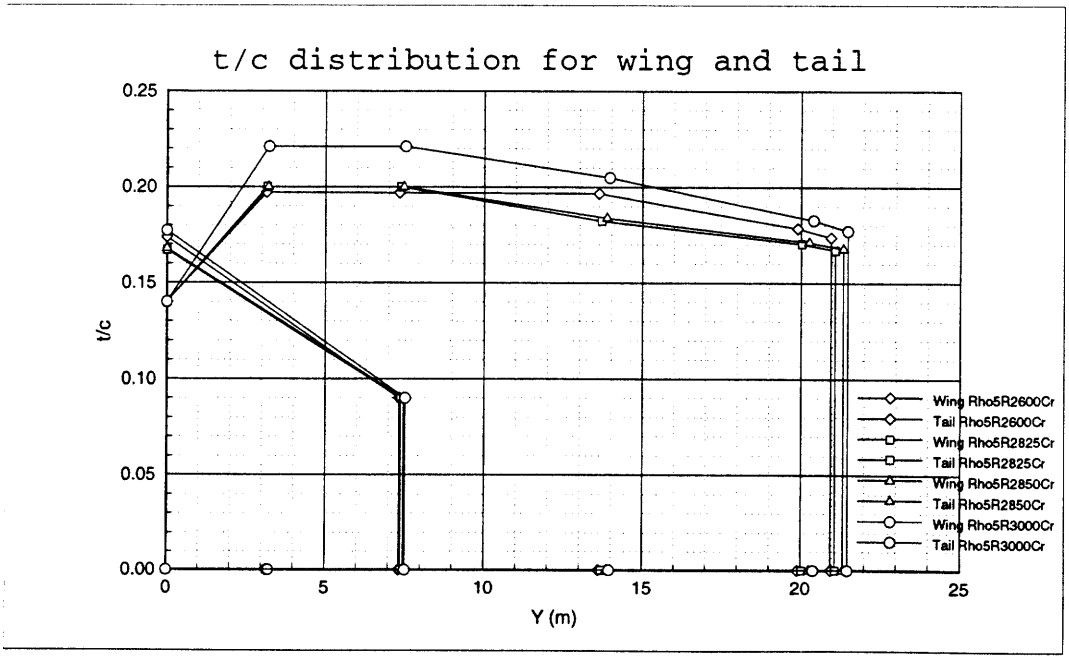

Figure 6-16: Planform data, short span, material density as independent variable

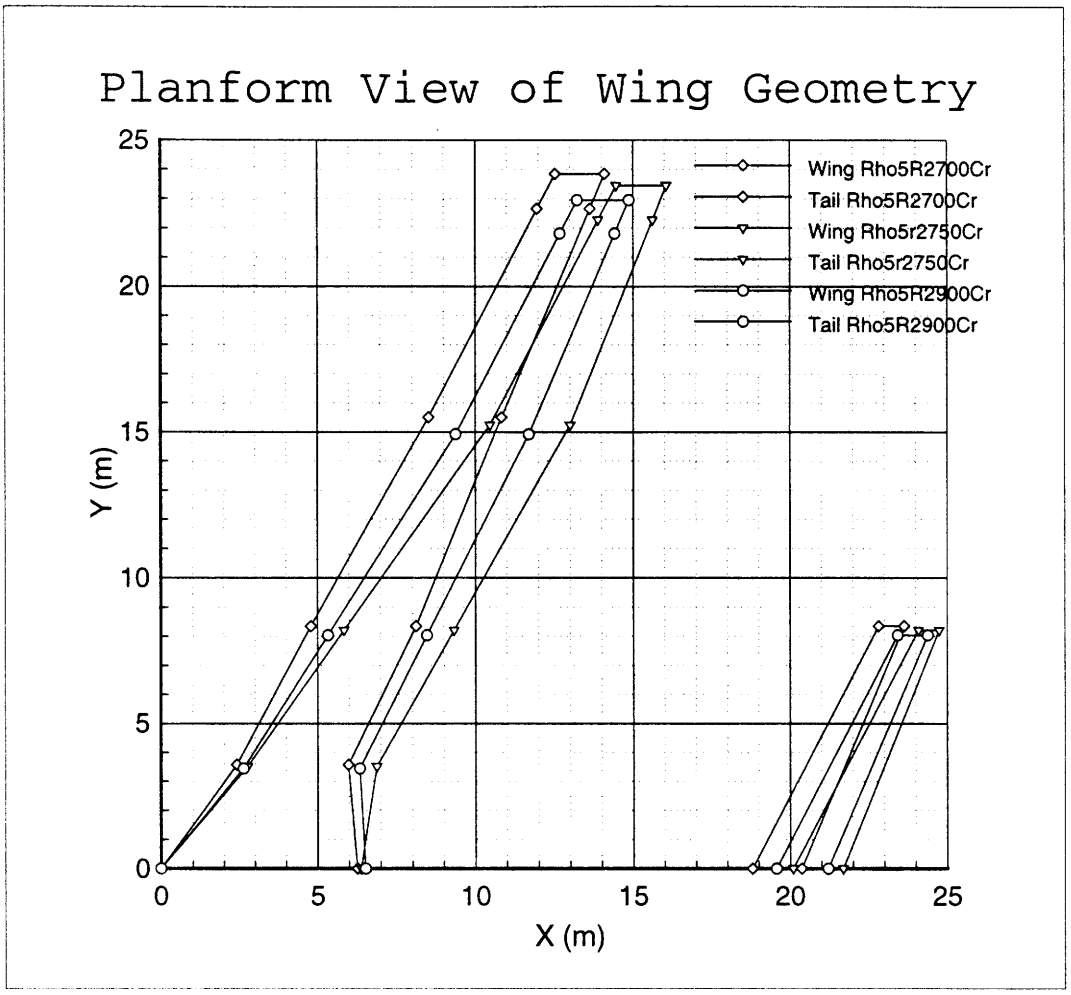

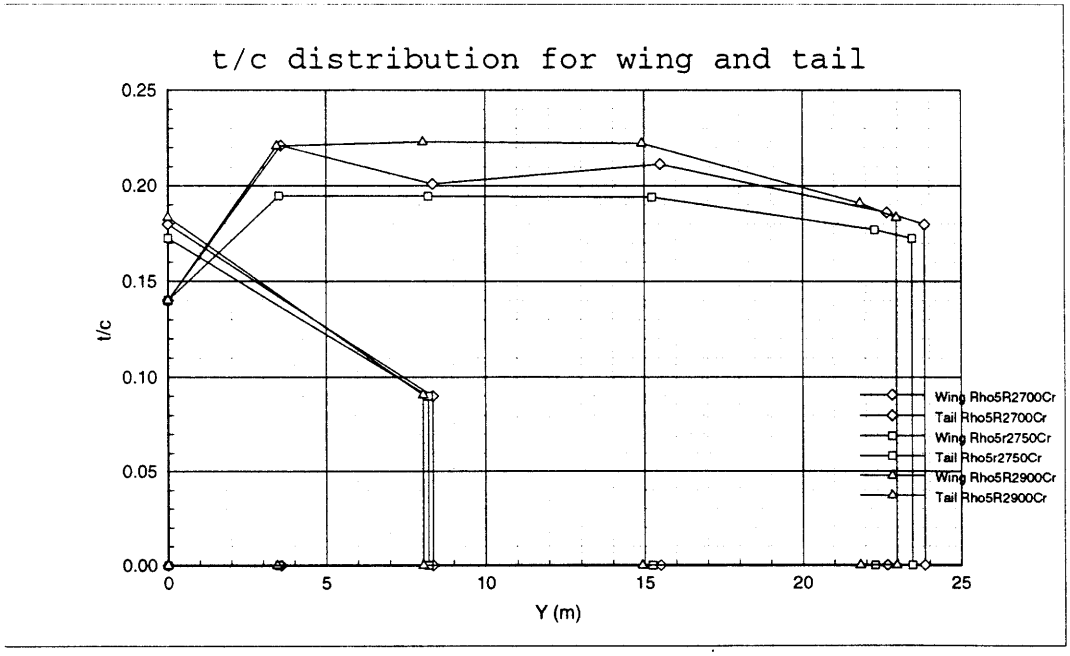

Figure 6-17: Planform data, long span, material density as independent variable

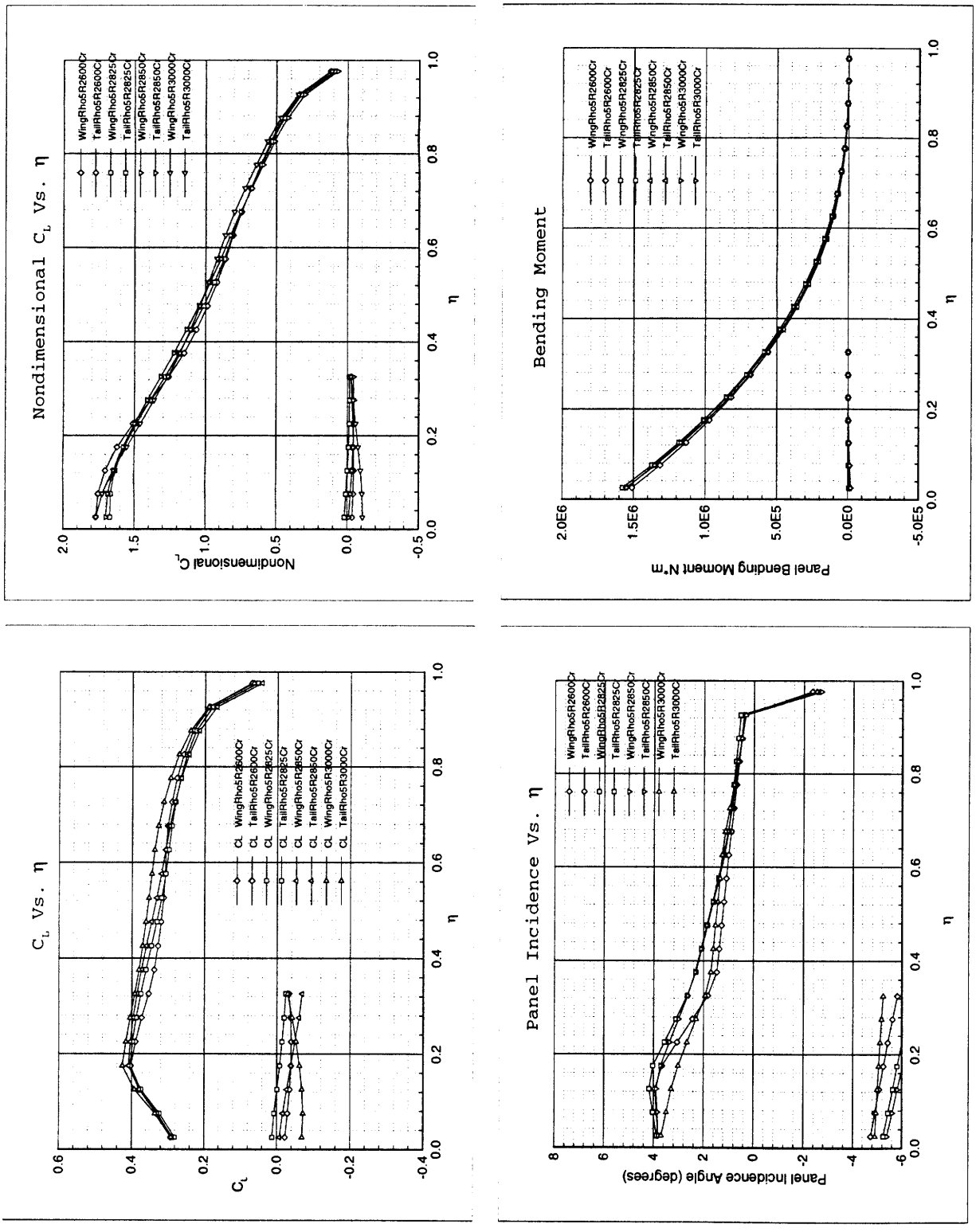

Figure 6-18: Aerodynamic data, short span, material density as independent variable

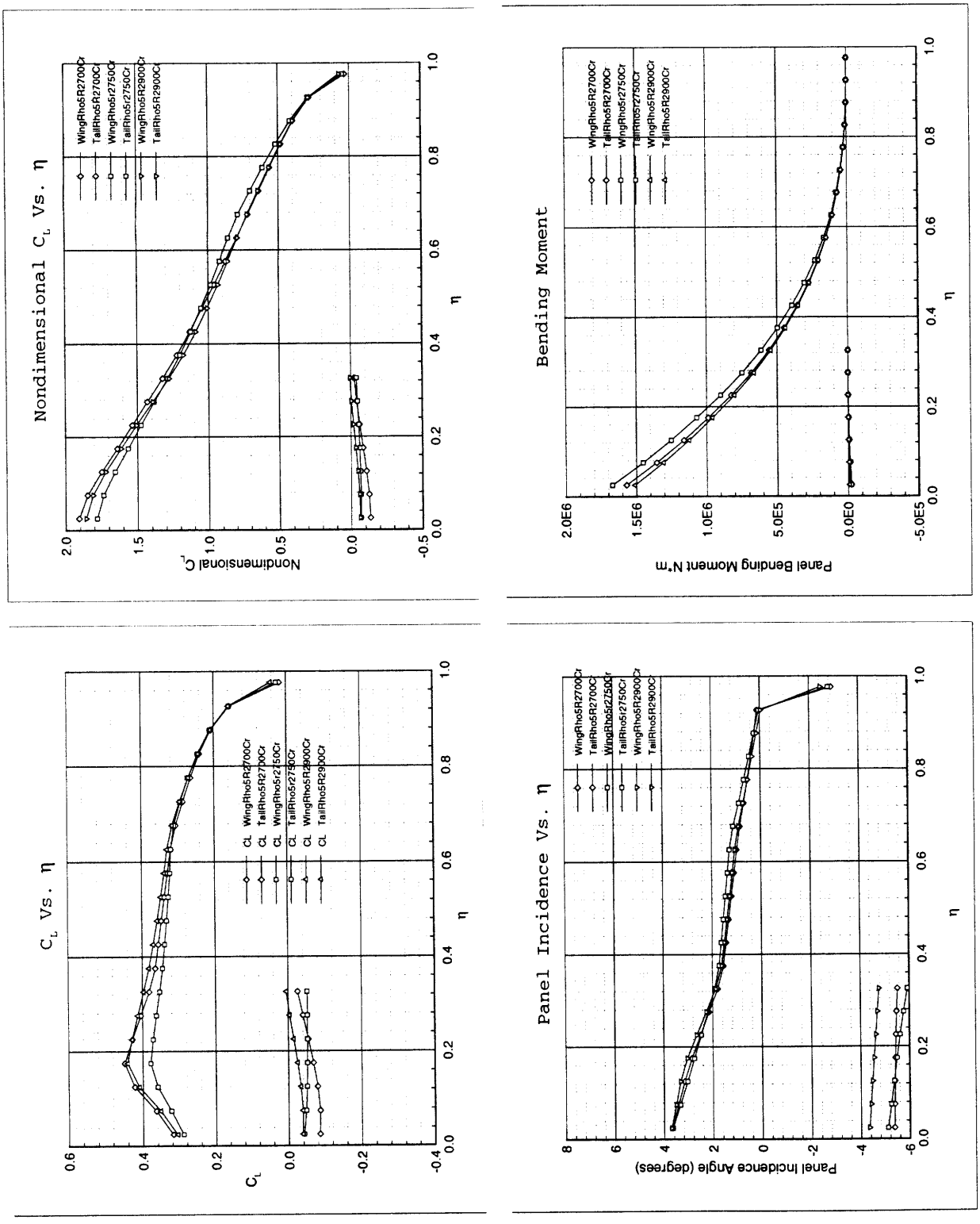

Figure 6-19: Aerodynamic data, long span, material density as independent variable

Data for:	Kcf 0.98	Kcf 0.99	Kcf 1.01	Kcf 1.02	Kcf 1.03	Kcf 1.04
Convergence Error	8.69978e-02	9.26173e-02	0.10205	8.68890e-02	8.77257e-02	0.12940
Structural and Geometry Data						
Wing Span (m)	20.56	20.78	20.57	20.32	20.48	18.97
Wing Area (m^2)	72.06	71.23	71.27	72.27	70.82	77.62
Wing Aspect Ratio	11.73	12.13	11.87	11.43	11.85	9.27
Tail Volume	0.58	0.55	0.58	0.56	0.51	0.46
Spar Box Mass (kg)	2223.68	2165.38	1947.12	2054.40	1910.23	1527.08
Tail Spar Box Mass (kg)	110.00	281.86	189.23	231.93	161.60	85.19
Wing Root Sweep (deg)	33.88	34.60	32.61	29.57	28.99	38.77
Wing Tip Sweep (deg)	24.62	24.62	24.62	24.62	24.62	24.62
Performance Data						
Wing Loading (Pa)	3395.96	3435.48	3433.31	3386.08	3454.53	3152.46
Cruise C_L	0.32	0.32	0.32	0.32	0.32	0.30
Cruise C_D	1.42e-02	1.36e-02	1.43e-02	1.42e-02	1.38e-02	1.40e-02
Inviscid Cruise C_D	3.28e-03	3.23e-03	3.25e-03	3.27e-03	3.38e-03	3.62e-03
Viscous Cruise C_D	9.44e-03	9.02e-03	9.57e-03	9.40e-03	9.25e-03	9.10e-03
Cruise Wave Drag C_D	1.47e-03	1.33e-03	1.49e-03	1.58e-03	1.20e-03	1.32e-03
Cruise L/D	22.50	23.78	22.56	22.34	23.46	21.11
Range (km)	7085.10	7489.20	7103.70	7036.70	7389.20	6649.60
Takeoff speed (m/sec)	75.47	75.46	75.46	75.46	75.47	75.47
Landing speed (m/sec)	54.81	54.81	54.81	54.81	54.81	54.81
Performance Metrics						
Efficiency range/fuel Km/Kg	0.64	0.68	0.64	0.64	0.67	0.60
Wing M.F. (spar box/total)	0.06	0.06	0.05	0.05	0.05	0.04
(Fuel mass)/(wing mass)	4.96	5.09	5.66	5.37	5.77	7.22

Figure 6-20: Trade Data for variance of skin roughness parameter

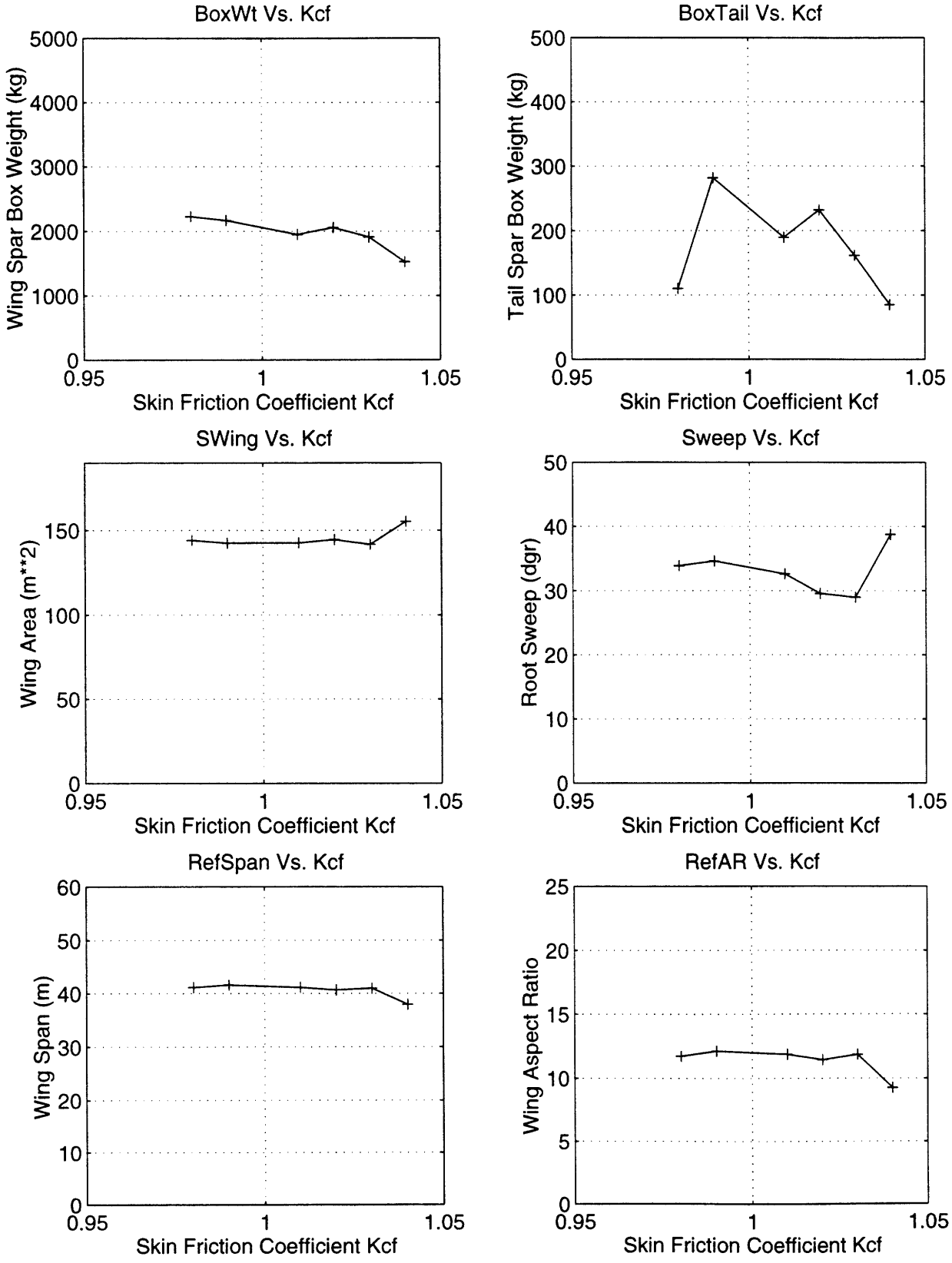

Figure 6-21: Trade Data for geometric parameters with variance of K_{cf}

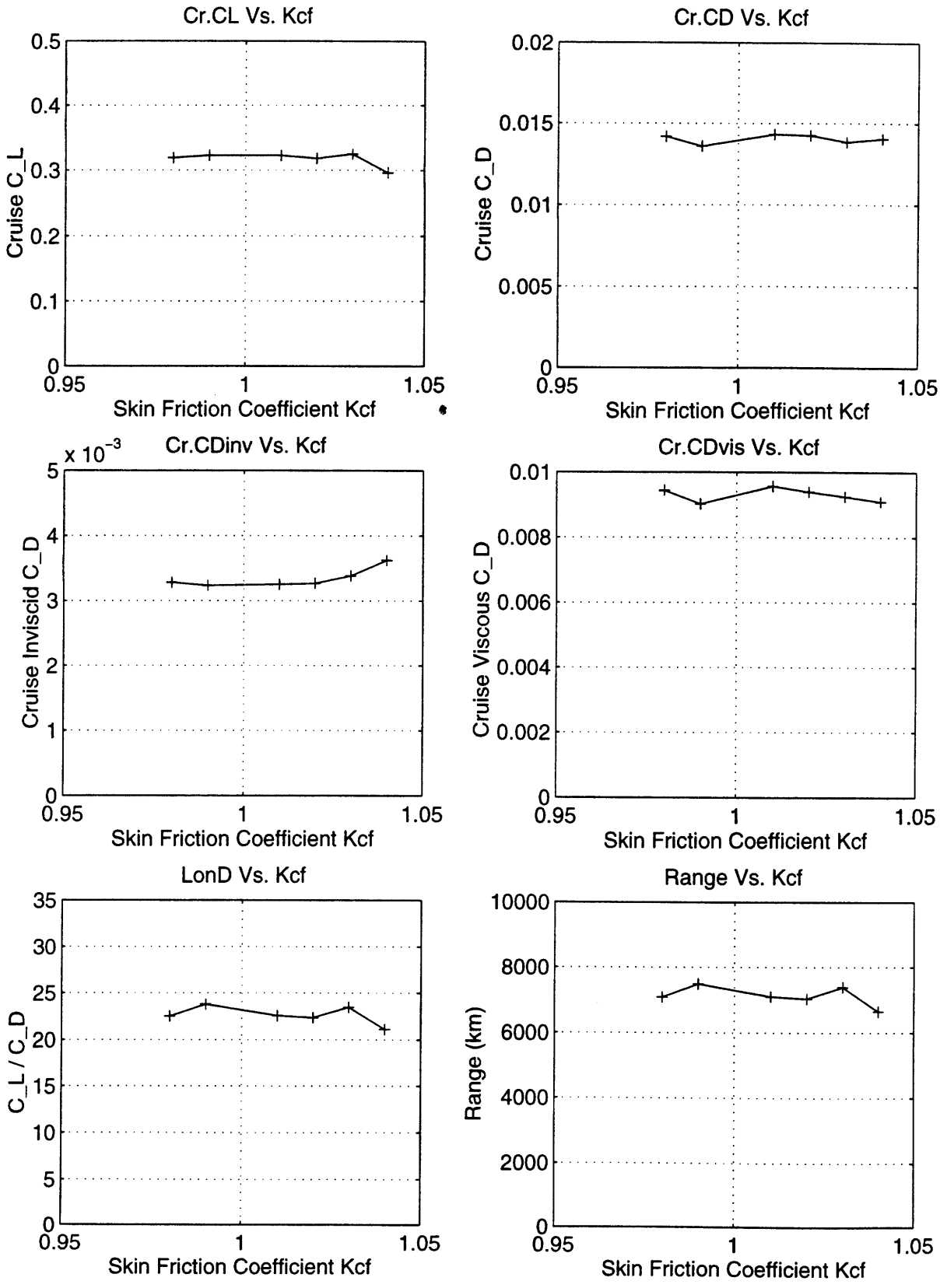

Figure 6-22: Trade Data for performance parameters with variance of K_{cf}

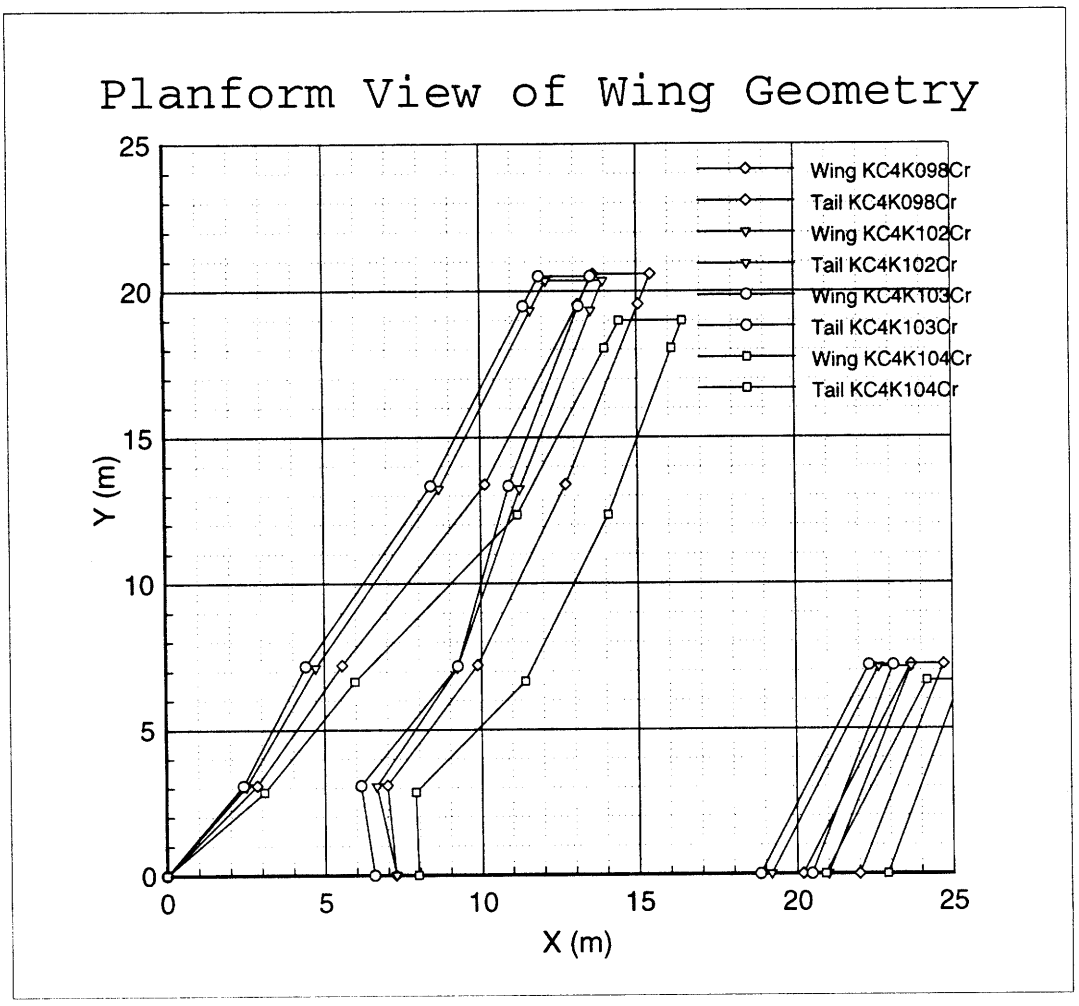

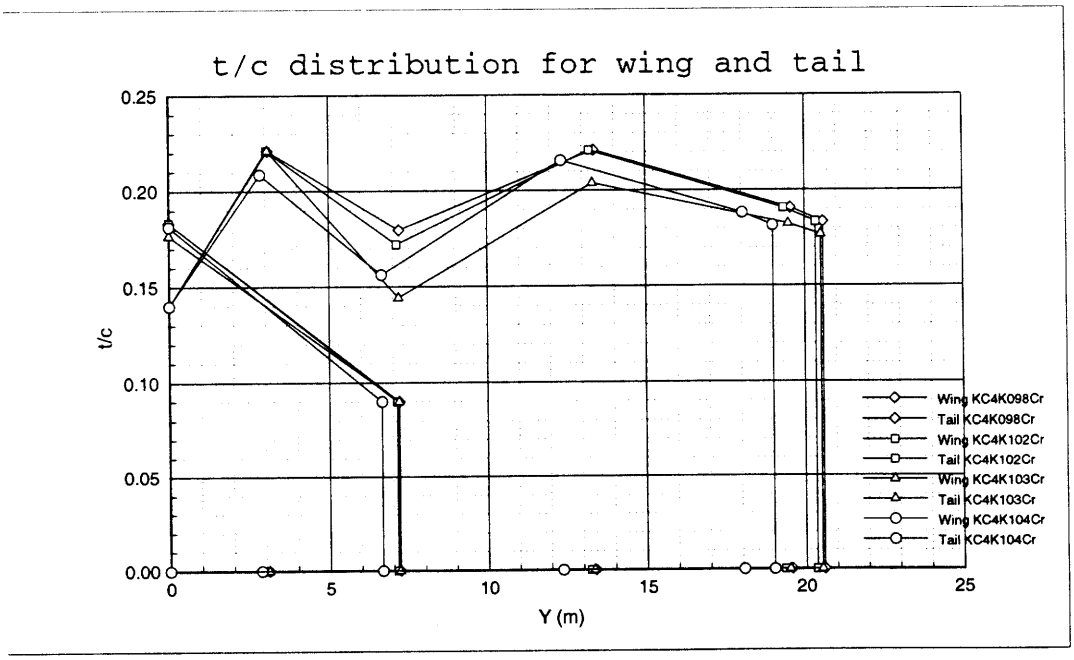

Figure 6-23: Planform data for K_{cf} = 0.98 , 1.02, 1.03 and 1.04

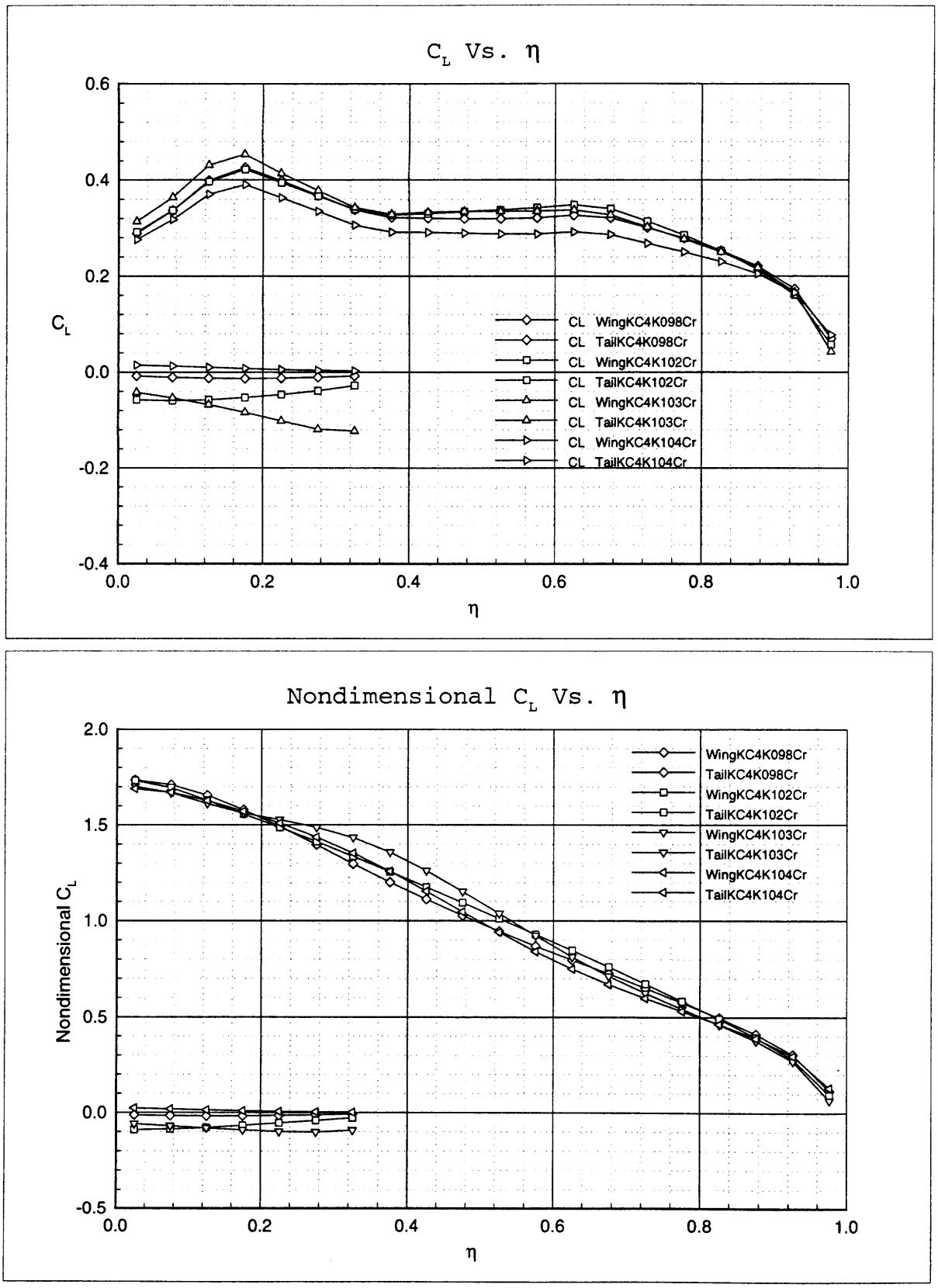

Figure 6-24: Planform data for $K_{cf} = 0.98$, 1.02, 1.03 and 1.04

Table 6.9: Trade Data for variance of crest critical Mach number offset

Data for:	Mcc5P0.out	Mcc5P03.out	Mcc5P06.out	Mcc5P12.out	Mcc5P14.out
Convergence Error	5.10913e-02	5.45624e-02	2.45211e-02	5.51291e-02	4.09190e-02
Structural and Geometry Data					
Wing Span (m)	17.76	18.84	18.93	25.56	26.51
Wing Area (m^2)	88.70	84.95	82.60	69.62	68.89
Wing Aspect Ratio	7.11	8.36	8.68	18.77	20.40
Tail Volume	0.29	0.34	0.28	0.61	0.65
Spar Box Mass (kg)	2086.44	2021.77	2932.98	4492.22	4299.05
Tail Spar Box Mass (kg)	80.02	82.02	72.84	147.49	179.51
Wing Root Sweep (deg)	46.92	40.49	46.38	33.48	26.74
Wing Tip Sweep (deg)	24.62	24.62	24.62	24.62	24.62
Performance Data					
Wing Loading (Pa)	2758.38	2880.61	2962.85	3515.16	3552.50
Cruise C_L	0.26	0.27	0.28	0.33	0.33
Cruise C_D	1.91e-02	1.51e-02	1.16e-02	1.26e-02	1.28e-02
Inviscid Cruise C_D	3.86e-03	3.58e-03	3.44e-03	2.11e-03	2.12e-03
Viscous Cruise C_D	7.65e-03	8.09e-03	7.49e-03	9.42e-03	9.57e-03
Cruise Wave Drag C_D	7.57e-03	3.39e-03	6.99e-04	1.10e-03	1.12e-03
Cruise L/D	13.59	17.98	23.95	26.17	26.06
Range (km)	4280.20	5663.10	7542.80	8240.50	8206.20
Takeoff speed (m/sec)	75.46	75.46	75.46	75.46	70.00
Landing speed (m/sec)	54.81	54.81	54.81	54.81	54.81
Performance Metrics					
Efficiency range/fuel Km/Kg	0.39	0.51	0.68	0.75	0.74
Wing M.F. (spar box/total)	0.05	0.05	0.08	0.12	0.11
(Fuel mass)/(wing mass)	5.29	5.45	3.76	2.45	2.57

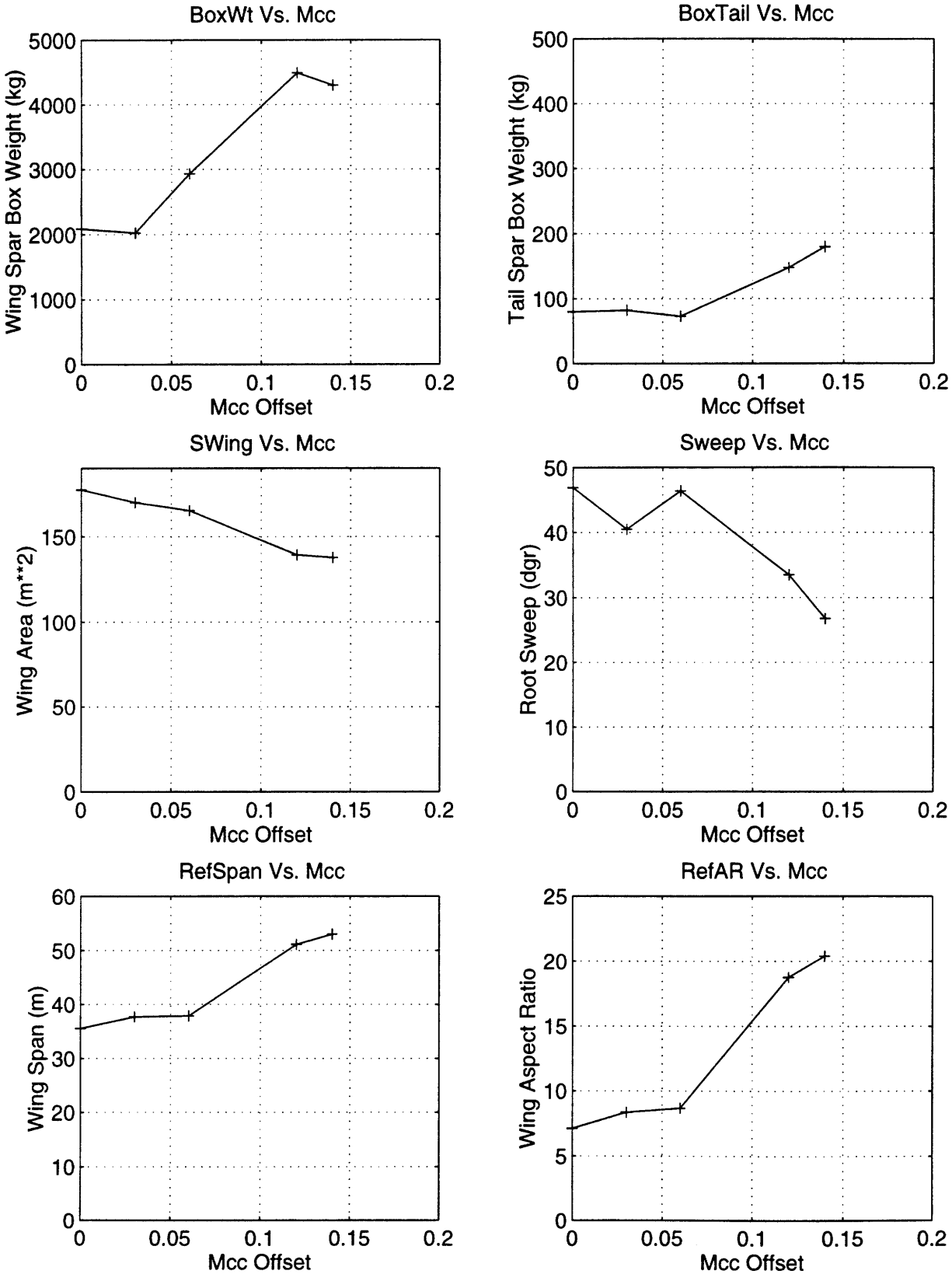

Figure 6-25: Trade Data of geometric parameters for variance of crest critical Mach number offset

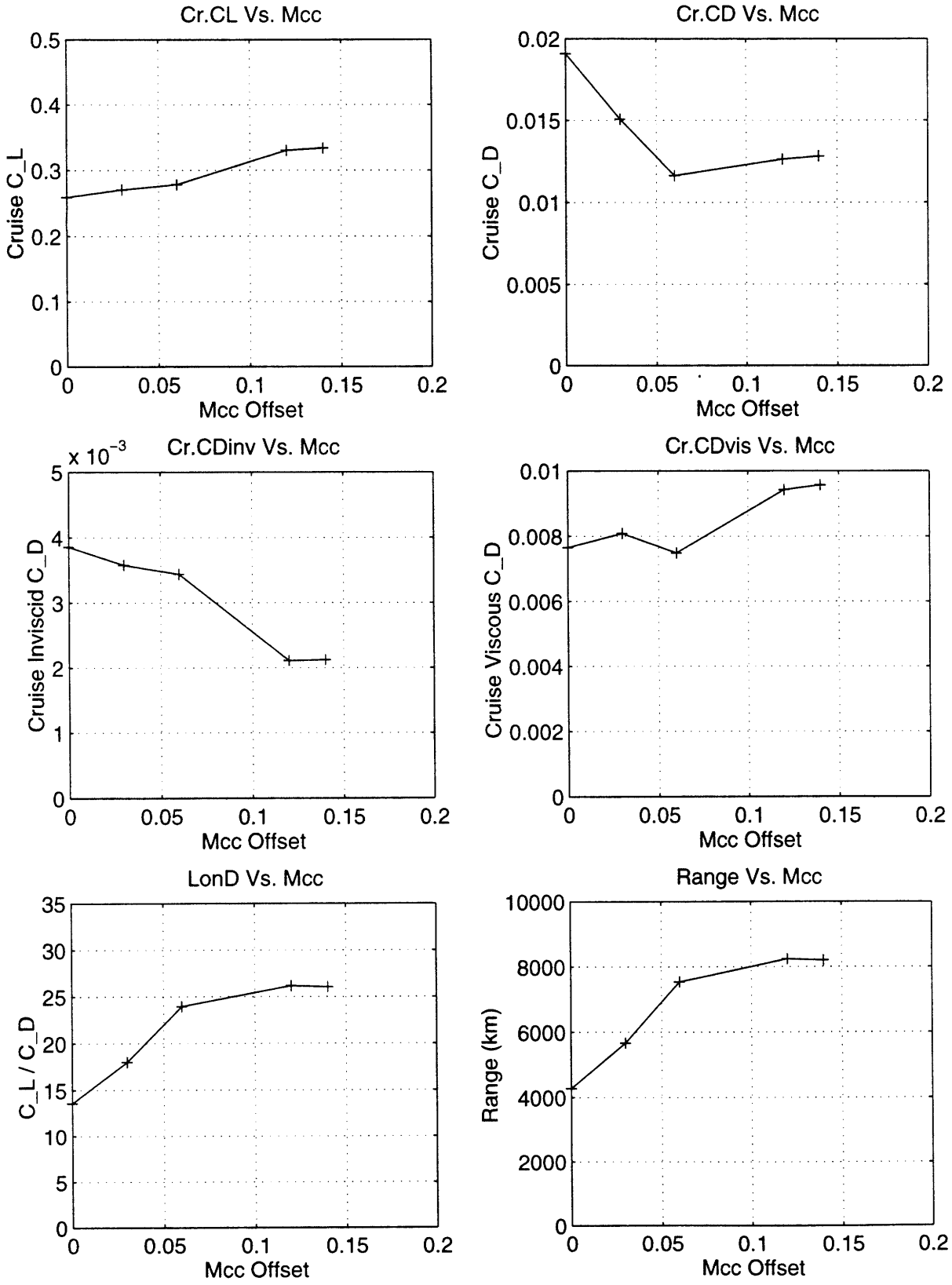

Figure 6-26: Trade Data of aerodynamic parameters for variance of crest critical Mach number offset

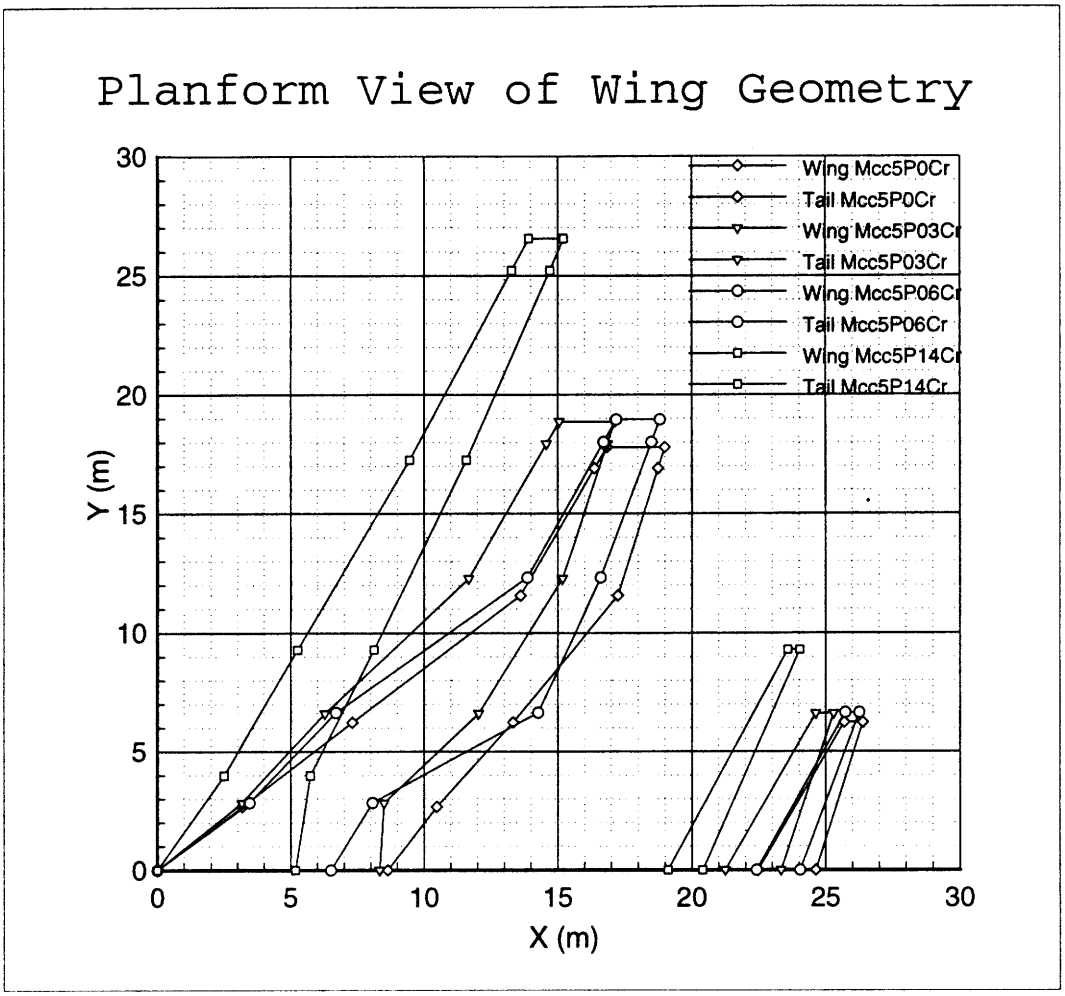

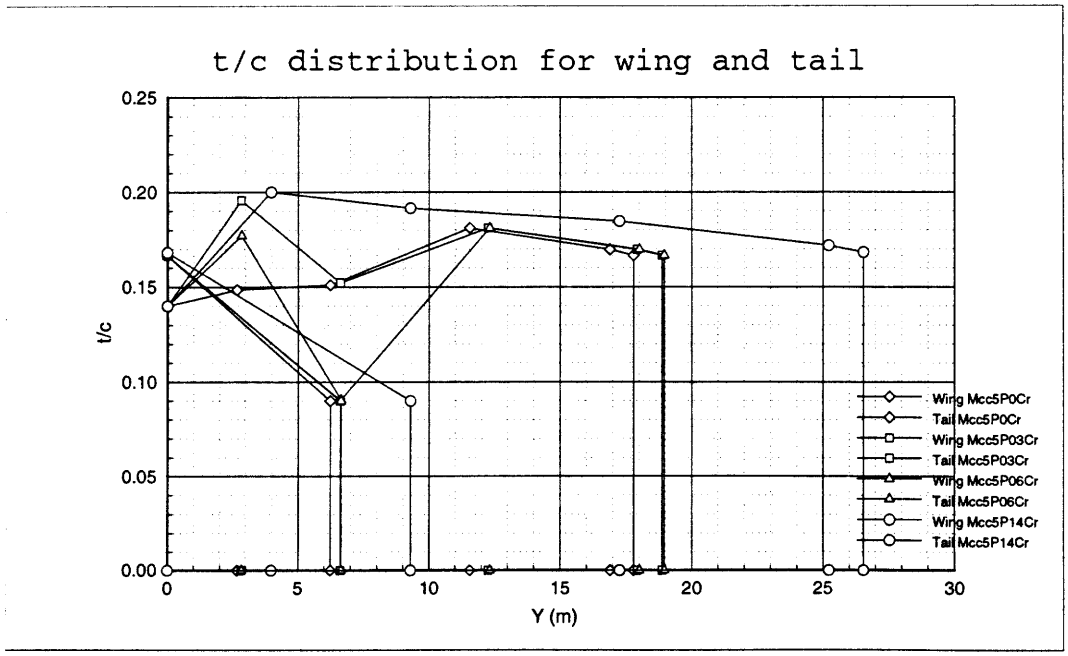

Figure 6-27: Planform data for Mcc = 0, 0.03, 0.06 and 0.14

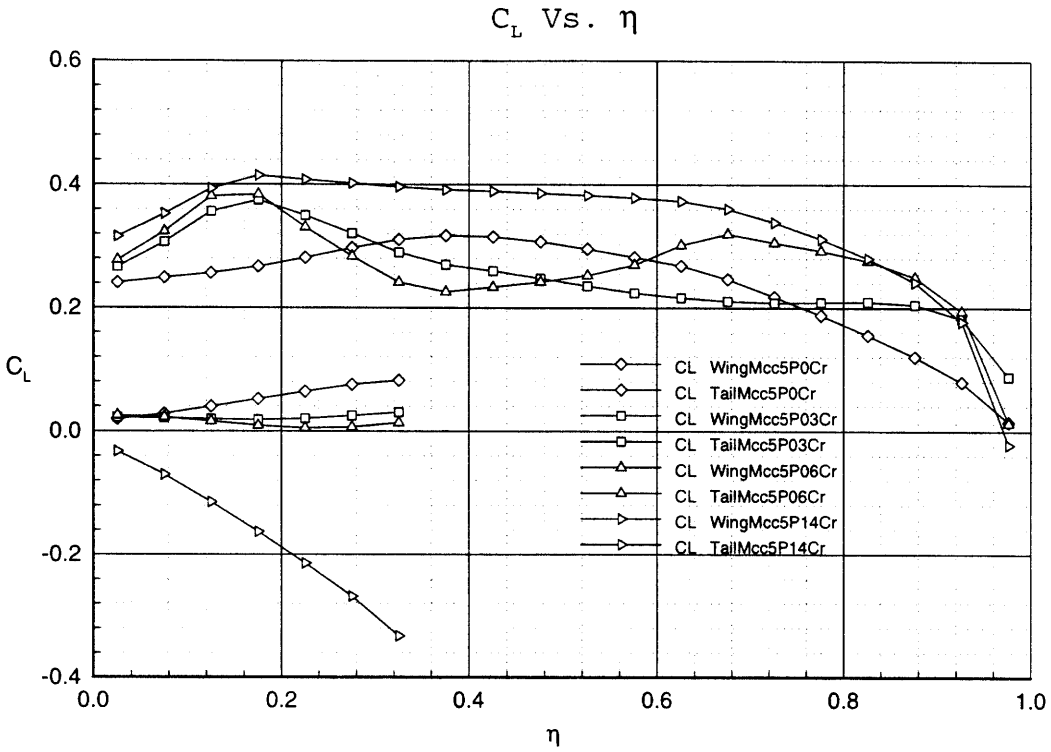

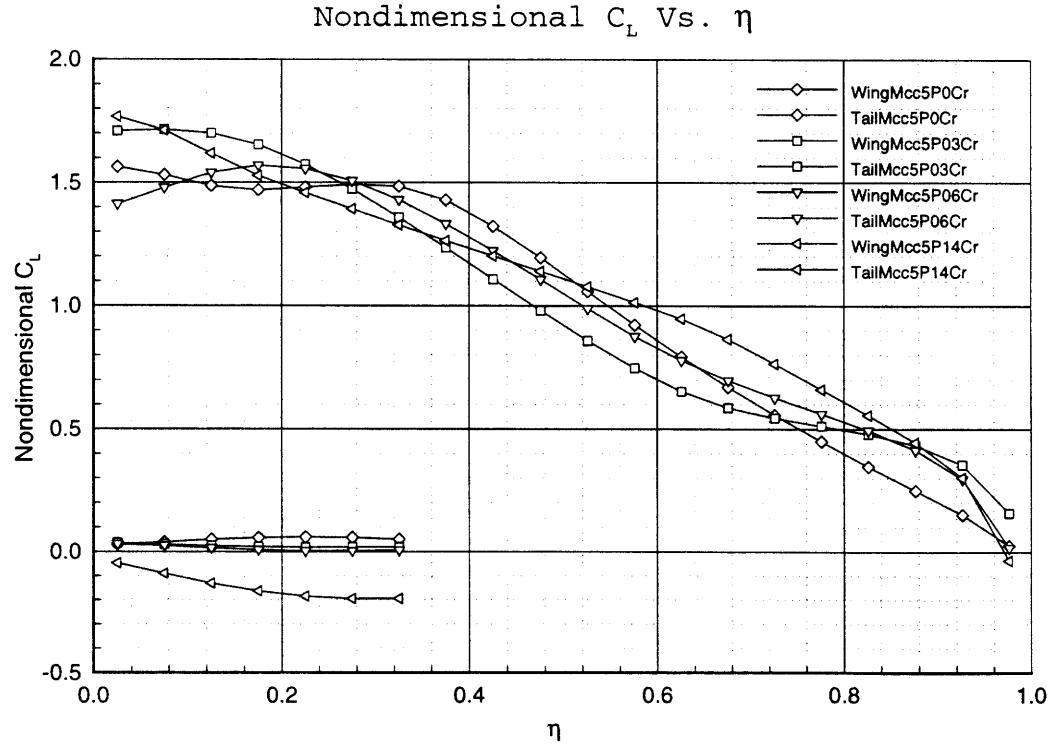

Figure 6-28: Planform data for Mcc = 0, 0.03, 0.06 and 0.14

Table 6.10: Trade Data for variance of Cruise Mach number

Data for:	Mach 0.675	Mach 0.7	Mach 0.725	Mach 0.775	Mach 0.8	Mach 0.85
Convergence Error	0.86959	2.39159e-02	2.30804e-02	3.87437e-02	0.61955	1.12778
Structural and Geometry Data						
Wing Span (m)	24.38	23.84	23.86	22.01	22.17	22.49
Wing Area (m^2)	84.55	82.05	80.40	72.09	71.43	85.35
Wing Aspect Ratio	14.06	13.85	14.16	13.44	13.77	11.86
Tail Volume	0.52	0.48	0.48	0.51	0.57	0.52
Spar Box Mass (kg)	2783.66	2823.42	2821.01	2977.67	2401.99	2220.42
Tail Spar Box Mass (kg)	220.03	150.42	148.51	106.25	139.14	304.67
Wing Root Sweep (deg)	27.62	25.68	25.45	35.39	26.29	28.18
Wing Tip Sweep (deg)	24.62	24.62	24.62	24.62	24.62	24.62
Performance Data						
Wing Loading (Pa)	2893.83	2982.43	3043.78	3394.51	3425.83	2867.12
Cruise C_L	0.40	0.38	0.37	0.36	0.34	0.25
Cruise C_D	1.36e-02	1.30e-02	1.24e-02	1.21e-02	1.18e-02	1.03e-02
Inviscid Cruise C_D	4.25e-03	3.95e-03	3.50e-03	3.58e-03	3.08e-03	2.05e-03
Viscous Cruise C_D	9.33e-03	9.06e-03	8.93e-03	8.50e-03	8.72e-03	8.28e-03
Cruise Wave Drag C_D	0.00000	0.00000	0.00000	0.00000	0.00000	0.00000
Cruise L/D	29.57	29.58	29.45	29.58	28.67	24.30
Range (km)	9160.90	9188.10	9172.30	9267.40	9008.80	7681.00
Takeoff speed (m/sec)	75.64	75.64	75.64	75.64	75.64	75.64
Landing speed (m/sec)	54.81	54.81	54.81	54.81	54.81	54.81
Performance Metrics						
Efficiency range/fuel Km/Kg	0.83	0.83	0.83	0.84	0.82	0.70
Wing M.F. (spar box/total)	0.07	0.07	0.07	0.08	0.06	0.06
(Fuel mass)/(wing mass)	3.96	3.91	3.91	3.70	4.59	4.97

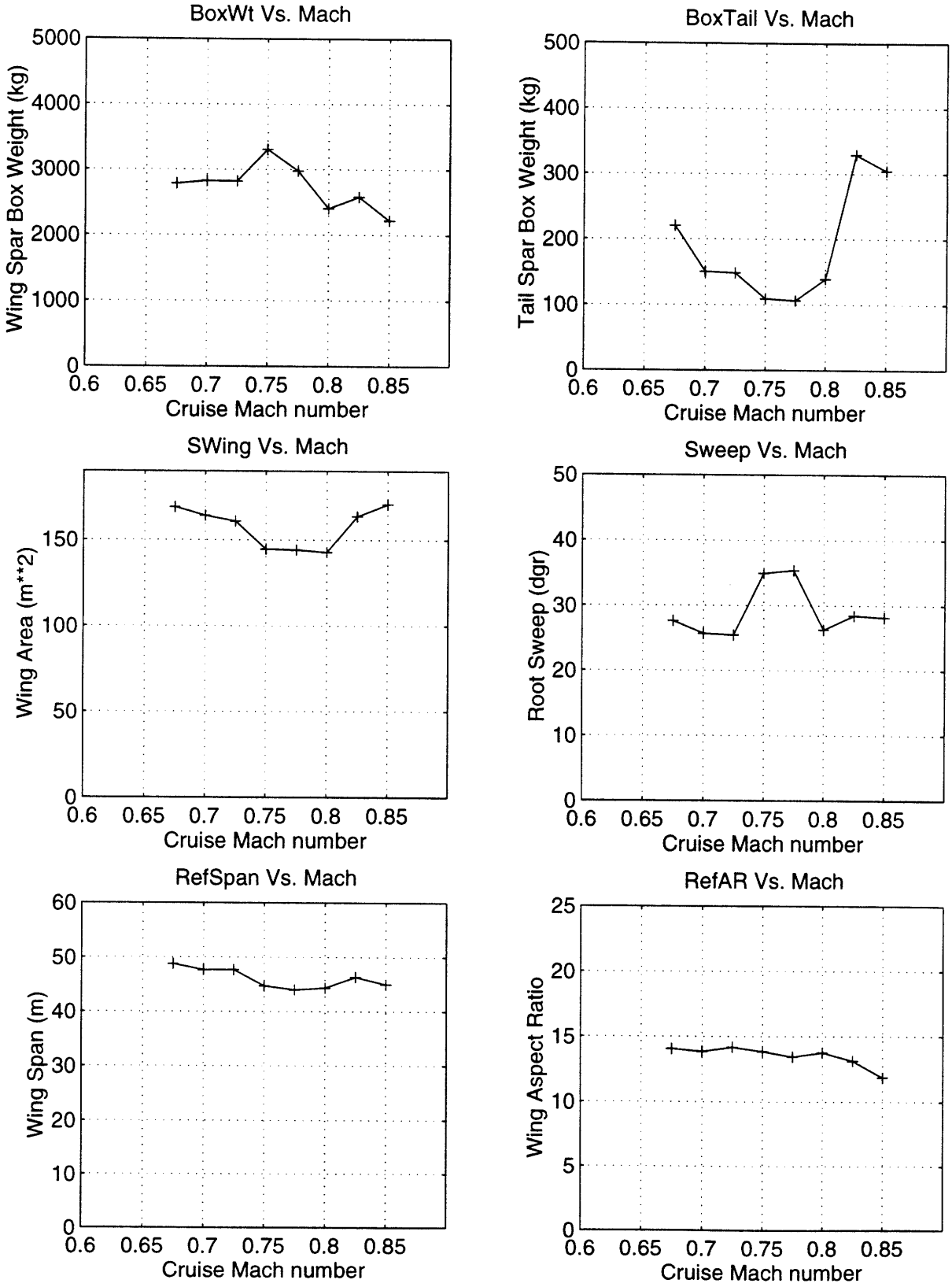

Figure 6-29: Trade Data of geometric parameters for variance of Cruise Mach number

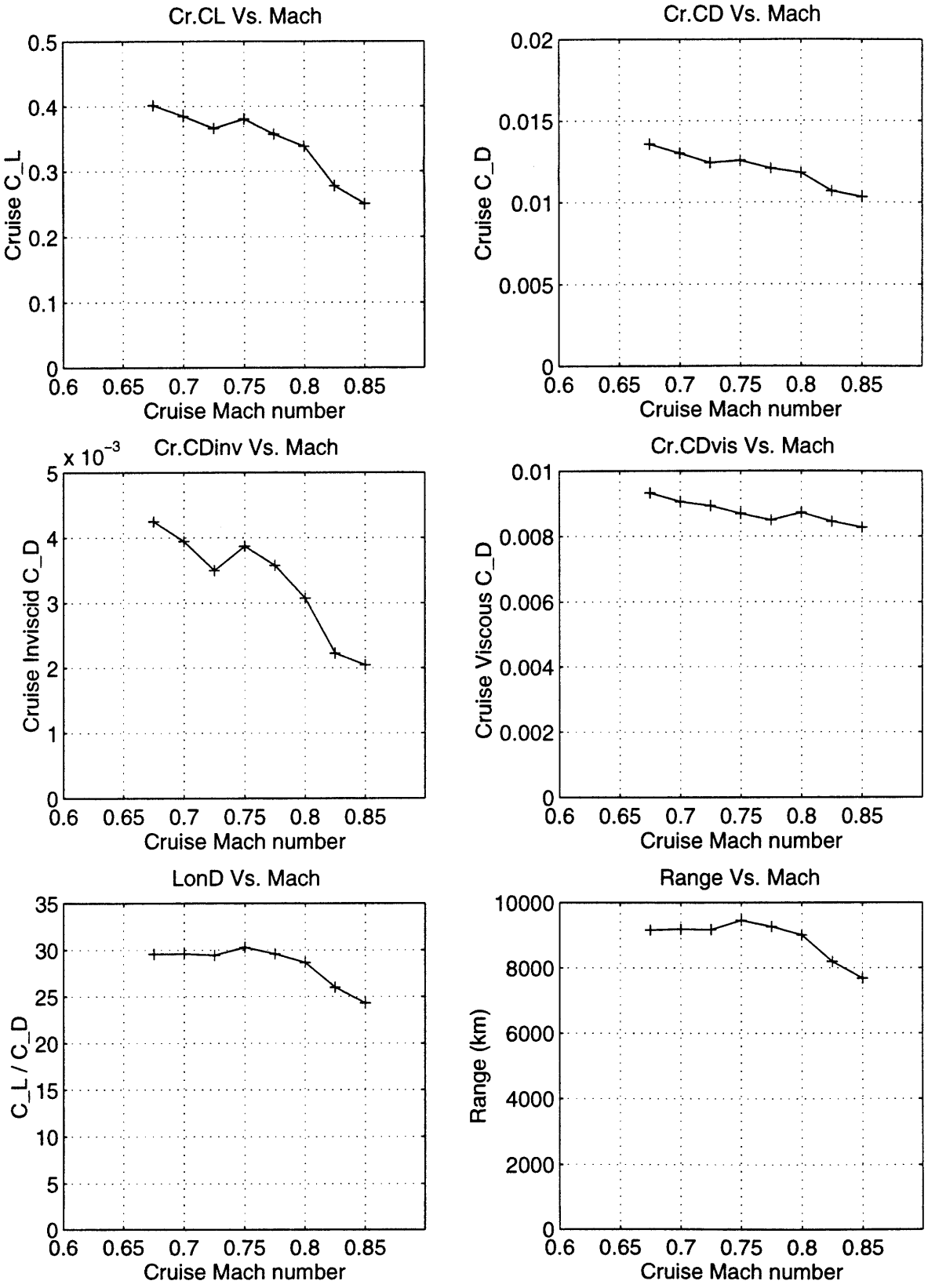

Figure 6-30: Trade Data of aerodynamic parameters for variance of Cruise Mach number

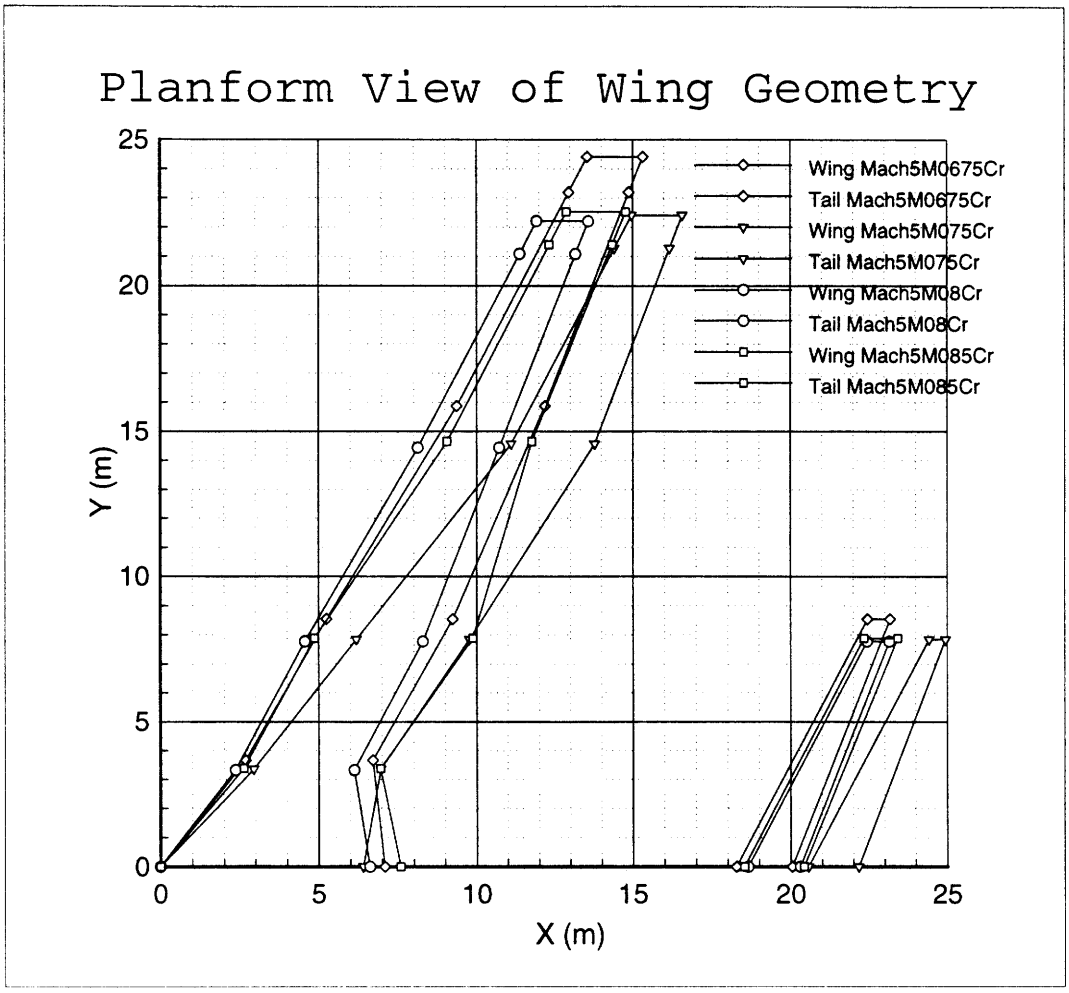

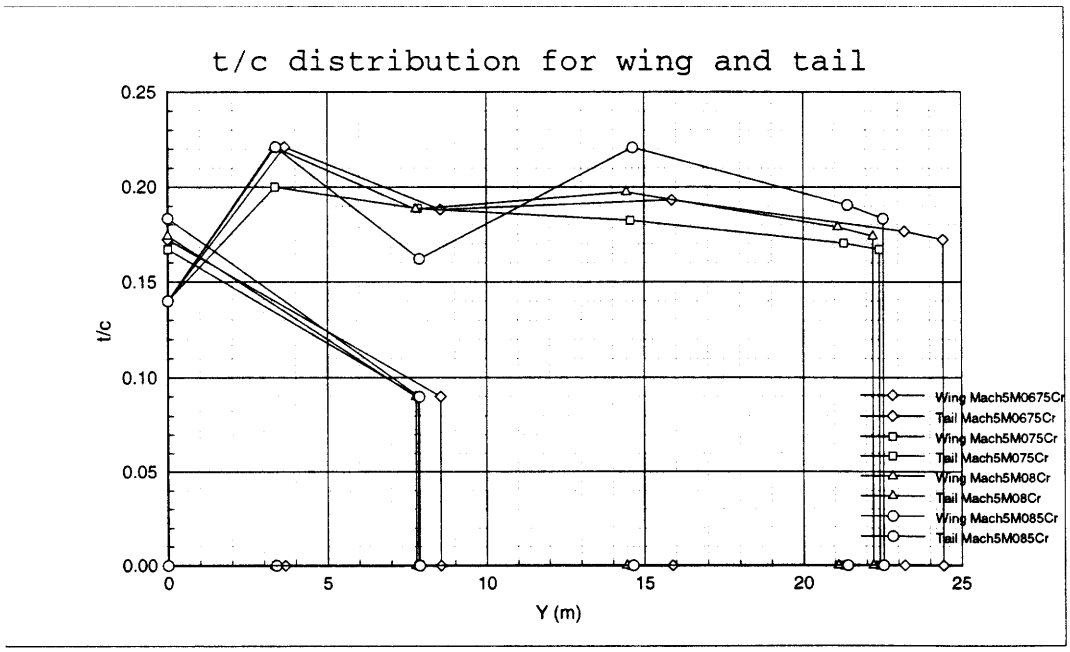

Figure 6-31: Planform data for Cruise Mach = 0.675, 0.7, 0.75 and 0.85

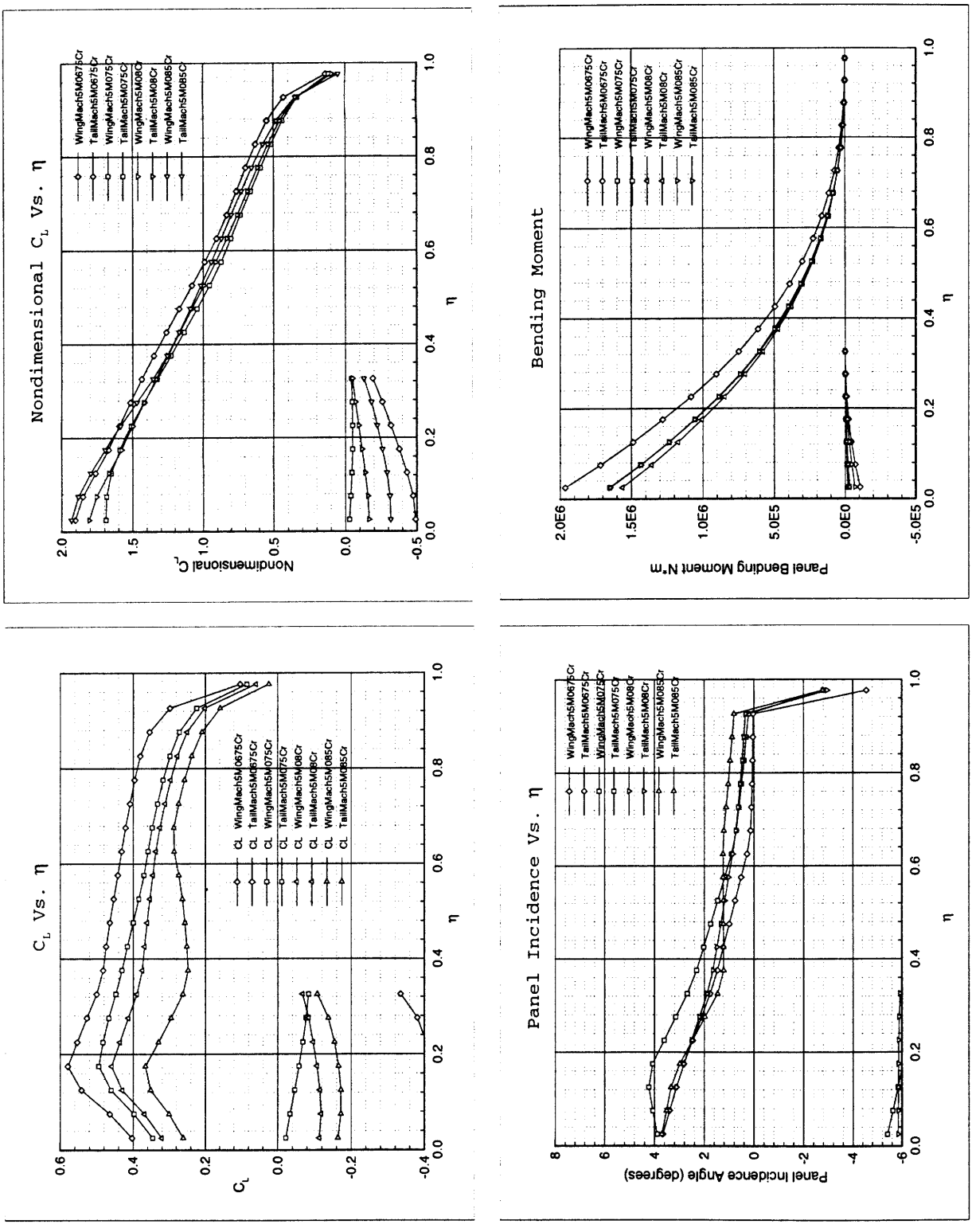

Figure 6-32: Planform data for Cruise Mach = 0.675, 0.7, 0.75 and 0.85

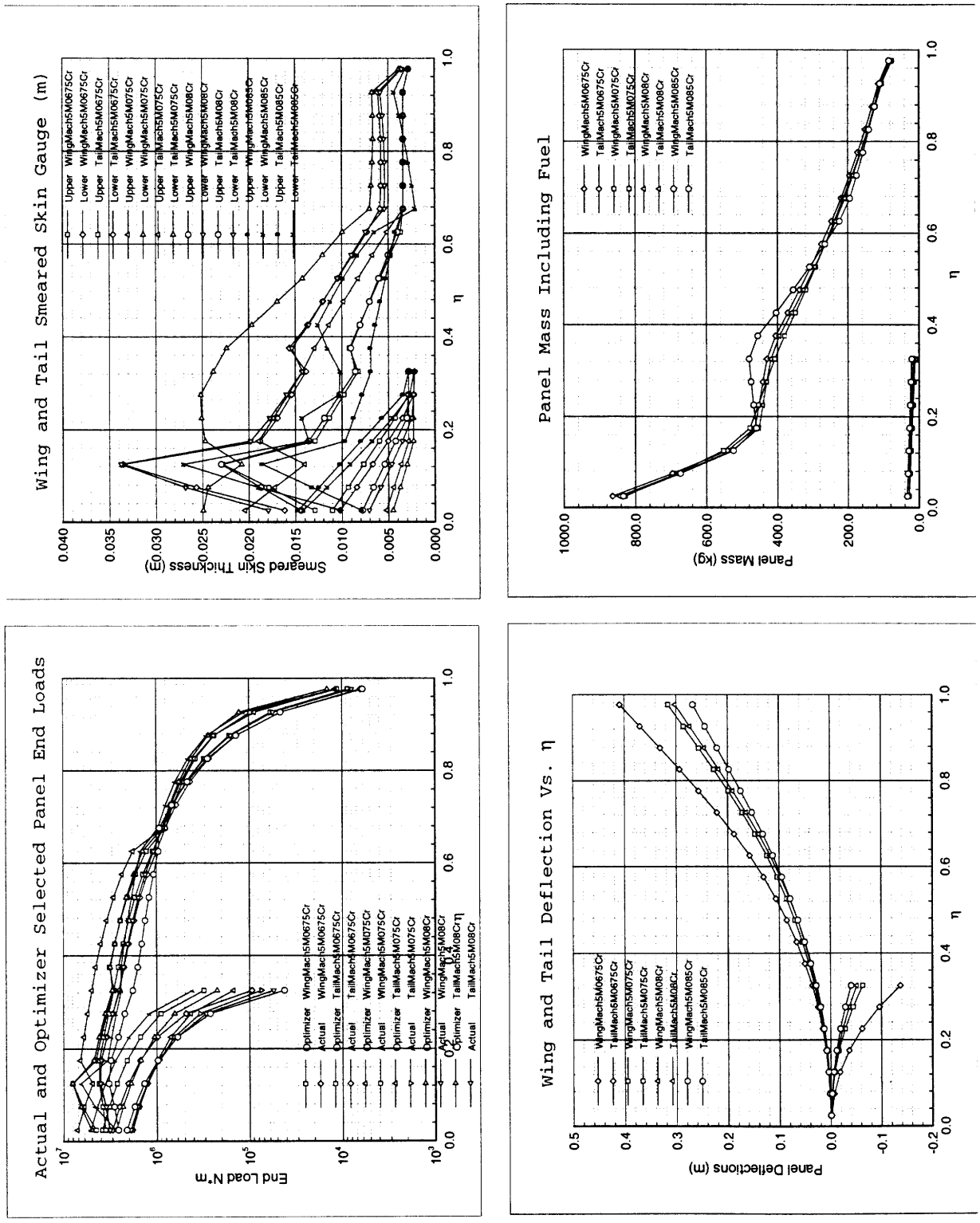

Figure 6-33: Planform data for Cruise Mach = 0.675, 0.7, 0.75 and 0.85

Chapter 7

Conclusions and Recommendations

When this project was first considered the goal seemed quite simple. The WASP code would be set up with a stable baseline case and trade studies would be run on this case by perturbing major design variables. The parameters were all major enough that their effects should be predictable and, presumably would yield smooth data with interesting trends. Perhaps more attention should have been given to the second to last sentence in the abstract of Sean Wakyama's thesis about the WASP Code:[1]

> "In many cases, the optimizer exploits physical effects, creating design features that are easy to interpret in hindsight but difficult to predict in advance."

This was certainly true in a number of the cases done for this study with the Cruise Mach number trade being a prime example. The expectations were that the optimizer would do the obvious and increase sweep with increasing Mach. However, what the optimizer found was that the higher the C_L, the higher the wave drag, and simultaneously, that minimizing wave drag would mean paying a very stiff penalty in C_{D_i}. Thus, with an approach that based on these these trends, the optimizer increased the wing area at high Mach numbers and kept the sweep nearly constant. The higher area was to reduce $C_L$and keep the wave drag reasonable, and the lack of increase in sweep was a consequence of trying to preserve the $C_{D_i}$with the already decreased aspect ratio. So this result was completely logical, but it is also not how wings are designed.

7.1 Summary of Trade Studies

As was mentioned in the problem statement, the goal of the exercise was to look at the effects of certain parameters on final optimized planforms instead of just in the vacuum of a fixed planform trade study. Looking back over the trade studies now, what have we learned and how might it be applied?

Airfoil C_{m_0} This study was very well behaved and the results even indicated a maximum performance at some finite value of C_{m_0}, possibly -0.10. However, by taking the planform from the C_{m_0}=-0.10 case and re-calculating the performance with the planform fixed and the C_{m_0}set to 0.0 again, this minimum was disproven. The structure was lighter for C_{m_0}=0 with a fixed geometry, so the "minimum" was purely function of

the optimizer finding a slightly better search path. However, all is not lost; despite the usual noise exhibited by the optimizer, this particular data set was quite well behaved. This indicates that the C_{m_0}has a relatively mild effect on the final planform and can most likely be left out of the initial optimization process.

The Skin Stress Ratio was the first of the two studies done using structural parameters as independent variables. This trade is in fact quite academic since in the real world the upper and lower skins should be sized independently. However, since this structural model used the stress ratio as a method for cutting the number of design variables in half (only the end loads on the upper surface of the wing), the study is of interest as a matter of checking the validity of the modeling. If the noise in the data is any indication, it would seem that a much better structural model with full resolution of upper and lower surface skin loads and thicknesses is necessary.

Wing Material Density was the second structural parameter and much more relevant to the real world problems. This parameter would indicate the type of changes in planform that might be feasible with a lighter alloy or even from composite structures. Unfortunately, it appears again that the current crude model is simply insufficient to produce useful information. There was significant bifurcation in the data set, on top of which there was wide variance in the parameters which were of the most interest, the spar box weights. Conclusions from this data set should be limited to emphasizing the need for a solid, stable structural model which takes into account the relevant physics including buckling near the wing tip. Possibly a model which included buckling would have been able to eliminate the family of longer wings from excess structural weight.

The Skin Roughness Parameter was the first of two attempts to break down the drag into components and examine the role of each component. The ultimate goal here would be to see if the research money should be spent on reducing skin friction or wave drag. As has been discussed at great length, this data set proved to be phenomenally un-cooperative and large amounts of data were thrown out as simply unusable. That which remains then becomes highly questionable. The indications so far have to be kept in the qualitative range, however it appears that $K_{cf}$is a considerably stronger factor in determining both sweep and aspect ratio than and been anticipated. The discovery that that calculation of wetted area is sweep and thickness dependent to a high degree may explain why this parameter was such a strong driver. The conclusions then are mixed with the first recommendation being to try the data set over again with a much simpler calculation of wetted area as simply 2.1 multiplied by the projected areas. Unfortunately there is insufficient time remaining to carry out this calculation.

The Mcc offset was the second attempt to modify the influence of a particular drag factor, in this case compressible drag. The results here showed this to be a very strong driving force behind the ultimate sweep and span of the wing. As the code is currently set up, it is not possible to extract the information necessary to convert the M_{cc} offset into a more relevant parameter such as shock strength reduction or shock location movement. However, if one were to judge from this data set and the previous "skin roughness parameter" data set, the research money would be handed first to the airfoil design team working on reducing compressible drag.

The Cruise Mach number is not a design parameter so much as a design consideration. As already discussed both in this chapter and in section 6.9 this trade study revealed

an interesting chain of logic for how the optimizer was trading the effects of C_{D_i} with C_{D_v}. This goes back to the physics of the problem and while the optimizer has found an interesting approach to the problem, it is not necessarily correct. The approach also indicates that the relationships between the three components of drag are highly critical and must be balanced properly in order to find an effective optimum. However, effective modeling is most likely only part of the problem, the other part being that the problem is not properly posed to get the more conventional results to increasing cruise Mach number. This question of how to pose the problem will be discussed in the section 7.3.1

7.2 Importance of Static Margin

During the course of this experiment, certain constraints would unexpectedly turn out to be the crucial shortcoming or sticking points in the optimization process. The most notable of these was the Static Margin constraint which was discussed in sections 3.3.2 and 6.1.0.1. Having a down load on the tail is a feature which is not fundamental to the physics because an unstable, lifting tail is without question more efficient than a down loaded tail. Historically, some degree of static stability has been necessary so that humans could fly the aircraft unaided. However, more recent designs, such as the *BOEING* 777 rely on fly-by-wire controls which have continuous computer feedback so that the aircraft can be flown in a statically unstable configuration while still feeling quite manageable to the human in the captain's seat. Since static stability is not something the optimizer will consider without an enforced constraint equation 3.2 was used to calculate the static margin which was constrained to some minimum value. However, there is no set method for choosing this minimum. As the Mach and Kcf trades clearly showed, this parameter can have large effects on the sweep of the final wing (see figure 6-4 for a good example). The variation in the constraint between these cases was in the range of 2.5 to 3.0, with the 2.5 being the baseline number. This relatively small range makes selection of the parameter considerably more difficult. Is the SM to be chosen based on some minimum tail down load at either cruise or take off? Or chosen to provide a "reasonable" loading distribution? There is no clear feedback metric for adjusting the constraint.

Since an excessive constraint can push the optimizer into finding a much higher wing sweep than usual, this can rapidly deteriorate into a case of the tail wagging the dog. To make matters worse, there were several cases where the only SM values which could provide a proper down load on the tail in cruise also produced completely infeasible wing planforms. In cases of high wave drag the natural response of the optimizer is to increase wing sweep. This effectively increases the streamwise chord, and barring a significant reduction in span, the area will increase and the MAC will increase. A higher MAC means that for the same set of slopes the static margin will be easier to meet. Eventually, if the MAC is large enough, most of the SM constraint is met by this multiplication, not by the ratio of slopes. The optimizer still doesn't care if the tail is lifting or not from a stability standpoint and somewhere in the middle of this cycle the tail can in fact cross over and become lifting. Since the SM is still being met, the optimizer is happy even if the user is not.

Ultimately this indicates that the problem needs to either be bounded to a region where the SM is an effective and proper method to indicate stability, or another stability indicator must be found. The full configuration was already constrained to be < 0 however this also seems to be inadequate. Also, as was discussed in section 6.1.0.1, the way the CG and center

of pressure for the aircraft are chosen *should* enforce a down loaded tail no matter what the static margin. Again, this did not appear to be the case, and is possibly a mis-understanding of the code book-keeping where CG is concerned.

7.3 Problem Modeling

As has been mentioned several times already, nonlinear wing planform optimization is *not* a simple problem. The WASP codes uses the most basic of models for computing the structural and aerodynamic parameters, but even then a standard optimization case has over fifty design variables and several hundred constraints. At points in the optimization, the search path could hinge on any one of these variables or constraints, and, if the variable is not correctly scaled, the results could end up very different from what is expected. Yet, the problem with the code seems more likely to be too few variables than too many, or at least, that the models are too simple.

The optimization design space can be thought of as an n-dimensional "surface" which the optimizer tracks along looking for a minimum while avoiding constraints. Evaluation of the models is what builds the surface. If the first order information from the models is not correct, that is, if the slope of the performance parameters is too shallow or too steep, the minimum will be shifted or cease to exist entirely. For example, the weight of the wing does not increase fast enough with increasing span because there is no buckling considerations on the outboard wingtip. The optimizer will quickly take advantage of this to add extra span on the wing to increase the aspect ratio and reduce the C_{D_i}. Likewise, the Mach drag rise curve of an airfoil is a very precise measure of the performance of the airfoil with the location and the slope of the rise being considered important down to 0.01 Mach. It is simply impossible to get this detailed information into a simple wave drag calculation, but the drag rise point should be a major driving factor in amount of sweep in the wing.

Clearly then, having models which accurately represent the physics to a high precision over the entire operating range of the optimizer is key to finding a detailed and accurate design space to search for an optimum in. In addition, being able to parameterize geometry and aerodynamic models to reduce the number of design variables and constraints will also increase the chances of finding a good search path. This makes the optimization an all-or-nothing proposition. A quick and dirty test code can not be run with simple models to check the concepts since as soon as the iterations start the optimizer will take advantage of the first weakness in the models it finds to produce an unreasonable planform.

At the current time, the models are still too simple. There are two ways to try to patch up the models to account for this; model enhancement and application of constraints. Both of these approaches have undesirable side effects. Model enhancement means adding empirical or otherwise self-contained data adjustments to the original model. For example, the flaps and slat data which is needed for the low speed calculations are empirical factors tacked onto the basic lifting line model. This approach will tend to introduce problems with the second order information not being smooth, which makes finding a search path very difficult. Most constraints should be taken as an indication of areas where the model needs work and then the model fixed before trying to get lots of data out of an over constrained case. To picture this problem better, imagine the "trough" in design space which is a result of increasing AR and decreasing C_{D_i}. With an appropriate structural model, this trough quickly grows shallow and disappears as the wing grows and gets heavier faster than performance increases. Now, with a simple model, the trough does not get shallower, so

a "wall" is placed across the trough to keep the optimizer from tracking too far in that direction. But this leaves the current design point backed against a wall in a trough and a good push might be needed to be able to find a new search direction.

Thus it seems clear that in order to produce a consistent, stable and accurate optimization space, the models to build the space must also be of considerable accuracy and fully comprehensive over the desired range of flight conditions.

7.3.1 The other half of the issue: posing the optimization problem

The previous section discussed at great lengths the merits and necessities of having thorough and consistent models. However, there is another issue which is perhaps just as important and this is in how the problem is posed. The optimizations done here were run at a fixed weight with a goal of maximum $\frac{C_L}{C_D}$. This puts a strong emphasis on reducing drag, but not so much on keeping weights reasonable. This approach is quite consistent with the problems experienced with noisy spar box weight results. This approach perhaps also allowed the drag trade studies to over-emphasize the impact of the drag parameter, especially the M_{cc}which produced huge changes in wing spar box weights. Thus, when testing for a particular parameter it is important to consider what effect that parameter has on the specific optimization goal, not just on the overall planform.

On a more positive note, optimization for wing span usually experiences problems with run-away spans. This optimizer deserves some credit for finding mostly reasonable spans and aspect ratios. This is especially surprising considering that the structural model did not include buckling constraints at the tip which is usually what cuts the span down.

7.4 Future Work

In section 7.3, the problems with having insufficient models was discussed with the ultimate conclusion that it would be very difficult to make a solid, stable optimization space without considerably more comprehensive models. Yet, as also mentioned in the problem statement, fully functional and complex models require hours to run a single example, so that an optimization case with several thousand model evaluations would be running for weeks on end. Ultimately we have arrived at another set of compromises, and the trade off is speed against accuracy and performance.

A possible approach to building a better version of this optimizer is to start with all of the superfluous constraints in the current optimization runs and try to remove them through model improvement. This will should lead to a considerably easier optimization path. However, this also leads down a slippery path to making the optimizer and models specific to one problem. Again, it is a fine line between being too general and having enough information to actually be functional.

7.5 Conclusions

In conclusion, the current state of the optimization technology makes this type of trade study at best an unstable task, and at worst a nightmare method of finding as many optimizer and model weaknesses in as short a time as possible. The results of these trades would serve far better as clues as to what needs improvements in the modeling than for revelations about the effects of airfoil C_{m_0}or other parameter effects on wing planforms.

Appendix A

Range Calculation

The aerdynamic portion of the code optimizes the planform for maximum Range. As already explained in section 3.4, the standard Breguet range equation 3.3 is used. Since all factors are constant except $\frac{C_L}{C_D}$, this is really just a performance $\frac{C_L}{C_D}$optimization.

Actually altering the code to optimize real range by varying the amount of fuel and the cruise velocity would have been very difficult. Even letting the code vary the amount of fuel available for range as a function of wing vollume tended to lead to long thin wings with well distributed fuel to take advantage of inertial fuel bending relief and a higher aspect ratio as more and more of the flight could be conducted in cruise.

However, using the simple Breguet range equation as a metric for code results can also be misleading because it does not account for altitude differences or climb fuel necessary. Therefore, the following set of equations were derived for calculating range as a post-processing tool.

To start with, the $\frac{V}{TSFC}$ terms can be replaced with the heating value of the fuel and the engine efficiencies η_t and η_t. Velocity dependance will now depend on η_t, the expression for which(A) uses the Mach number. This is most easily seen through a dimensional analysis of these two terms (all other terms are nondimensional)

$$V \times \frac{1}{TSFC} = V\frac{\dot{w_f}}{F} = \frac{m}{sec}\frac{Nsec}{N} \tag{A.1}$$

Where $\dot{w_f}$ is the fuel flow and F is the thrust. Using the following Definitions: $N = \frac{Kgm}{sec^2}$ and $joule = Nm = \frac{Kgm^2}{sec^2}$ We can express A.1 as:

$$V \times \frac{1}{TSFC} = \frac{j}{kg}\frac{sec^2}{m} \tag{A.2}$$

Introducing the fuel heating parameter h_r which has units of $\frac{j}{kg}$ and gravitational acceleration which is assumed constant at $g = 9.8\frac{m}{sec^2}$ we can finally express A.1 as:

$$V \times \frac{1}{TSFC} = \frac{h_r}{g} \tag{A.3}$$

The heating value of the fuel is subject to reduction by both the thermal and the propulsive efficiency values for the engine. The thermal efficiency can be directly related to the total temperature ratio across the engine, the theoretical limit to which can be expressed

as a function of Mach number and γ

$$\eta_t = 1 - \frac{1}{\pi^{\frac{\gamma-1}{\gamma}}\left(1+\frac{\gamma-1}{2}M_\infty^2\right)} \tag{A.4}$$

And the full efficiency is the produce of $\eta_t\eta_p\eta_f$ where the other two efficiencis are propulsive and fan, respectively. The net product of these terms should be approximately 0.30 or less.

A.1 Fuel used in climb

The range was also adjusted for the extra fuel needed in climb. This adjustment is done by finding the increase in potential energy necessary to increase the altitude from take off to cruise, convert this energy to a mass in fuel, and divide the appropriate efficiencies. The total energy required is:

$$E_{climb} = W_{take\,off}\Delta altitude \tag{A.5}$$

That is, simply $mg\Delta h$, the potential energy increase. The take off altitude is 0 m and the cruise altitude was set at 11,000m and initial weight is Maximum aircraft take off weight. Convert this value to actual fuel burned with:

$$W_{fuel} = \frac{E_{climb}}{h_r}\frac{g}{\eta_t\eta_p} \tag{A.6}$$

Depending on the efficiencies, this results in a take off fuel burn on the order of 5000 N

Appendix B

Foil Properties Scaling Derivations

As mentioned in section 2.2, the code calculates the area moments of inertia and the parabolic skin coefficients for a unit foil. When used to calculate stress, these values must be scaled to the local conditions. There are three scaling factors which need to be considered:

1. Scaling to local $\frac{t}{c}$. This is a fairly simple multiplication of (Generic Foil)*$\left(\frac{\frac{t}{c_{local}}}{\frac{t}{c_0}}\right)$
2. Scaling the spar box from being a streamwise cut of the wing to being perpendicular to the elastic axis. Since the generic foil has a chord of 1.0, and the maximum thickness does not change, this means an effective $\frac{t}{c}$change as : $\frac{t}{c}_{\perp} = \frac{\left(\frac{t}{c}\right)_{fs}}{cos(sweep)}$
3. Scaling to the local chord length, which, since the generic foil is of unit chord, simply involves multiplying by the local chord.

The order (exponent) of the scaling factor is different for the spars and the skins. For example,

$$I_{xx_{spar}} = t_{spar} \int_{z_{lower}}^{z_{upper}} z^2 dz \Rightarrow \tag{B.1}$$

$$I_{xx_{spar}} = \frac{t_{spar}}{3} z^3 |_{z_{upper} - z_{lower}} \tag{B.2}$$

Where t_{spar} is the smeared gauge for the spar in question and the limits of integration are the upper and lower z coordinates of the spar.

To simplify this discussion, the symbol T will be the actual thickness of the spar and C will be the actual chord. Looking at the previous equation we can see that $I_{xx_{spar}}$ is a function of T^3 and skin thickness. Since the skin thickness is not scaled, this factor will be left out. T is a direct function of $\frac{t}{c}$. Therefore, to scale the foil for local $\frac{t}{c}$will require the first scale factor cubed, to scale for a change in chord will require multiplying by the third scale factor cubed and to adjust to the elastic axis will require the second scale factor cubed. In math:

$$I_{xx_{spar_{local}}} = I_{xx_0} \left(\frac{chord_{local} \left(\frac{t}{c_{local}}\right)}{\left(\frac{t}{c_0}\right) cos(sweep)} \right)^3 \tag{B.3}$$

When Evaluating I_{xx} for the skins, the skin is represented by a parabola

$$z = A + Bx + Cx^2 \tag{B.4}$$

The basic I_{xx} formula is

$$I_{xx} = t_s \int_{x_{front\ spar}}^{x_{rear\ spar}} z^2 ds \tag{B.5}$$

That is, the Skin area times the z distance from the centroid integrated along the length of the skin. Area is (length*thickness) and z is a function of x which gives:

$$I_{xx_{skin}} = t_{skin} \int_{x_{front\ spar}}^{x_{rear\ spar}} \sqrt{1 + f'(x)^2} z^2 dx \tag{B.6}$$

Where $f'(x)^2$ gives the length of the skin. However, the assumption is usually made that $f'(x)^2 \approx 0$ (skin length is the straight distance between front and rear spars) greatly simplifying the integral. The resulting integral requires squaring and integrating the formula for the parabola, which is left to the reader as a miscellaneous exercise. The result is that $I_{xx_{skin}}$ depends on T^2C. As with the spars, all three scale factors affect the T so all three are squared, but the Chord is only affected by the third factor so the final scaling looks like:

$$I_{xx_{skin_{local}}} = I_{xx_0} \left(\frac{chord_{local}^3 \left(\frac{t}{c_{local}}\right)^2}{\left(\frac{t}{c_0}\right)^2 (cos(sweep))^2} \right) \tag{B.7}$$

That should clarify the process of which scale factor is applied how many times. The cross term basic equation is

$$I_{xz} = t_{skin} \int_a^b xz ds \tag{B.8}$$

Applying this to the spars:

$$I_{xz_{spar}} = t_{spar} \int_{z_{lower}}^{z_{upper}} zx dz \tag{B.9}$$

which results in:

$$I_{xz_{spar}} = t_{spar} x_{spar} \frac{z^2}{2} \Big|_{z_{lower}}^{z_{upper}} \tag{B.10}$$

And since x depends on chord and z depends on T , which also depends on Chord, the scale factor is again a function of chord cubed and the first two scale factors squared.

$$I_{xz_{spar_L}} = I_{xz_{spar_0}} \left(\frac{chord_{local}^3 \left(\frac{t}{c_{local}}\right)^2}{\left(\frac{t}{c_0}\right)^2 (cos(sweep))^2} \right) \tag{B.11}$$

Where $I_{xz_{spar_L}}$ is the local spar I_{xz} For the skins:

$$I_{xz_{skin}} = t_{skin} \int_{front\ spar}^{rear\ spar} \sqrt{1}(A + Bx + Cx^2) x dz \tag{B.12}$$

Again, I'll skip the full integration and boil the results down to:

$I_{xz_{spar}}$ is a function of TC^2 so that again the chord scaling is a cube, the other scalings are first order.

$$I_{xz_{skin_L}} = I_{xz_{skin_0}} \left(\frac{chord_{local}^3 \left(\frac{t}{c_{local}}\right)}{\left(\frac{t}{c_0}\right) (cos(sweep))} \right) \tag{B.13}$$

And finally for the I_{zz} parameters the basic equation is:

$$I_{zz} = t_{skin} \int_a^b x^2 ds \tag{B.14}$$

For the spars:

$$I_{zz_{spar}} = t_{spar} \int_{z_{lower}}^{z_{upper}} x^2 dz \tag{B.15}$$

which results in:

$$I_{zz_{spar}} = t_{spar} x_{spar}^2 z|_{z_{lower}}^{z_{upper}} \tag{B.16}$$

So the scaling is chord cubed and first order on the first two scaling parameters, see equation B.13 and substitute "spar" for "skin" .

For the skins it is simply:

$$I_{zz_{skin}} = t_{skin} \int_{front\ spar}^{rear\ spar} x^2 dx \tag{B.17}$$

So that the only scaling factor is $chord^3$

$$I_{zz_{skin_L}} = I_{xz_{skin_0}} chord_{local}^3 \tag{B.18}$$

These scalings are applied at the beginning of the Oracle function in order to calculate the Ixx, Izz and Ixz parameters for the local foil.

B.1 Parabola scaling factors

Now that all of the inertial terms have been properly scaled to the local foil, it is necessary to find the locations of maximum and minimum shear. The (x,z) coordinates of the spar corners are already known, but to find a the z coordinate of the skin for some x requires pulling out the parabolic coefficients from Fprop. These coefficients were calculated for a unit foil, which means the equation really looked like:

$$\frac{z}{c} = A + B\left(\frac{x}{c}\right) + C\left(\frac{x}{c}\right)^2 \tag{B.19}$$

If we need to scale the coefficients for a new $\frac{t}{c}$then all of the coefficients can be multiplied through by the $\frac{t}{c}$ratio. Likewise the cos(sweep) scaling is applied to all of the coefficients. However, if we want to change the chord, the result of multiplying through by the local chord, c gives:

$$z = Ac + Bx + C\left(\frac{x_2}{c}\right) \tag{B.20}$$

Which physically makes sense because the offset, A needs to be shifted, the slope is the same but the acceleration needs to be flattened out. So now we should be all set to apply the bending moments to the fully scaled section and scaled sectional properties.

Bibliography

[1] Wakayama, Sean *Lifting Surface Design Using Multidisciplinary Optimization* Ph.D. Thesis, Stanford, December 1994, SUDAAR 661

[2] Gill Philip E, Walter Murray and Margaret H. Wright *Practical Optimization* Academic Press 1981

[3] Kroo Professor Ilan, Stanford University, personal communication.

[4] McLean, J. D. and Elliott, J.K. *Exploratory use of the t_{eff} Concept in Airfoil Design BOEING* AERO-B1B1B-C94-005, July 11,1994

[5] McLean, J. D. *Theory for WINGOP: Spanload Optimization with structural weight penalty BOEING*D6-54742, Cage code 81205

[6] Rivello, Robert M. *Theory and Analysis of Flight Structures* McGraw-Hill 1969

[7] McLean, J. D. Personal Communication

[8] Press, William H, Flannery, Brian P, Teukolsky, Saul A, Vetterling, William T. *NUMERICAL RECIPES in C* Cambridge University Press, 1990

[9] Proprietary Data used during an Internship with the *BOEING*company between 6/19/95 and 12/19/95

[10] Josephs, H.J. and Brook, V.S. *The Probable Error of the Mean of a Small Sample* Research Report No. 13801, Post Office Research Station 519. 241.5: 519. 215.9, 20 November 1953